UNIVERSIDADE FEDERAL DO PARANÁ

FELIPE PEREIRA DINIZ

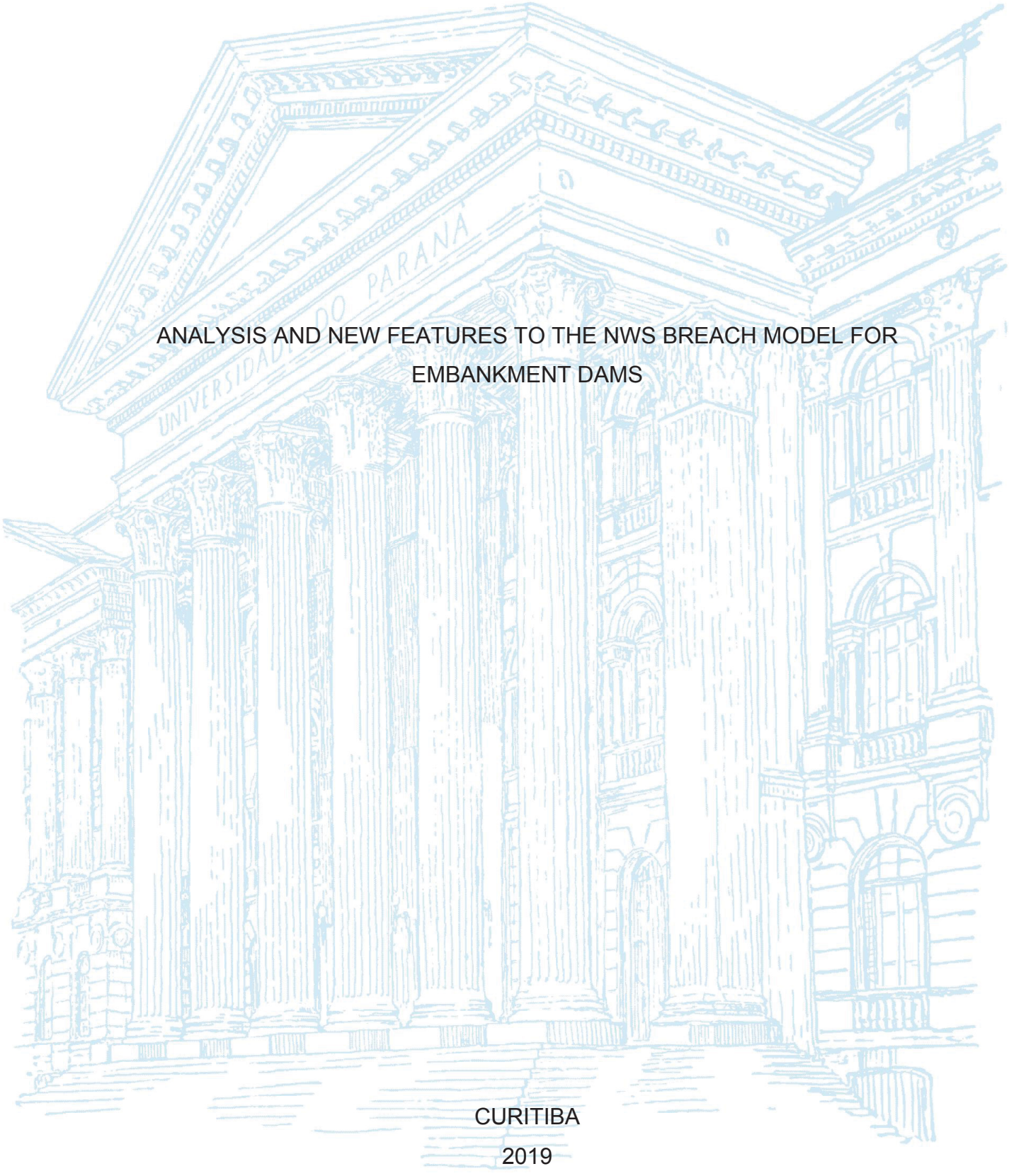

ANALYSIS AND NEW FEATURES TO THE NWS BREACH MODEL FOR EMBANKMENT DAMS

CURITIBA

2019

FELIPE PEREIRA DINIZ

ANALYSIS AND NEW FEATURES TO THE NWS BREACH MODEL FOR EMBANKMENT DAMS

Dissertação apresentada ao curso de Pós-Graduação em Engenharia de Recursos Hídricos e Ambiental, Setor de Tecnologia, da Universidade Federal do Paraná, como requisito parcial à obtenção do título de Mestre em Engenharia de Recursos Hídricos e Ambiental.

Orientador: Prof. Dr. André Luiz Tonso Fabiani

CURITIBA

2019

Catalogação na Fonte: Sistema de Bibliotecas, UFPR
Biblioteca de Ciência e Tecnologia

D585a Diniz, Felipe Pereira
Analysis and new features to the NWS Breach model for embankment dams [recurso eletrônico] / Felipe Pereira Diniz – Curitiba, 2019.

Dissertação - Universidade Federal do Paraná, Setor de Tecnologia, Programa de Pós-graduação em Recursos Hídricos e Ambiental
Orientador: André Luiz Tonso Fabiani,

1. Barragens -segurança. 2. Barragem- ruptura. 3 Barragem de terra e enrocamento. I. Universidade Federal do Paraná. II. Fabiani, André Luiz Tonso. III. Título.

CDD: 627.80289

Bibliotecária: Roseny Rivelini Morciani CRB-9/1585

MINISTÉRIO DA EDUCAÇÃO
SETOR SETOR DE TECNOLOGIA
UNIVERSIDADE FEDERAL DO PARANÁ
PRÓ-REITORIA DE PESQUISA E PÓS-GRADUAÇÃO
PROGRAMA DE PÓS-GRADUAÇÃO ENGENHARIA DE RECURSOS HÍDRICOS E AMBIENTAL - 40001016021P0

TERMO DE APROVAÇÃO

Os membros da Banca Examinadora designada pelo Colegiado do Programa de Pós-Graduação em ENGENHARIA DE RECURSOS HÍDRICOS E AMBIENTAL da Universidade Federal do Paraná foram convocados para realizar a arguição da Dissertação de Mestrado de **FELIPE PEREIRA DINIZ**, intitulada: **"ANALYSIS AND NEW FEATURES TO THE NWS BREACH MODEL FOR EMBANKMENT DAMS"**, após terem inquirido o aluno e realizado a avaliação do trabalho, são de parecer pela sua Aprovação no rito de defesa.
A outorga do título de Mestre está sujeita à homologação pelo colegiado, ao atendimento de todas as indicações e correções solicitadas pela banca e ao pleno atendimento das demandas regimentais do Programa de Pós-Graduação.

Curitiba, 25 de Fevereiro de 2019.

ANDRE LUIZ TONSO FABIANI
Presidente da Banca Examinadora

p/ JOSÉ RODOLFO SCARATI MARTINS
Avaliador Externo (USP)

ELOY KAVISKI
Avaliador Interno (UFPR)

JOSÉ JUNJI OTA
Avaliador Interno (UFPR)

ACKNOWLEDGEMENTS

To my family that is always by my side and is the base of my existence - source of support and energy in my ventures.

To my old friends that the university gave me - the notorious "Descolados" group - and that always find a way to remain in touch, even though each one of us have parted ours ways to follow our dreams.

A special thanks to Bado, Cezar, "Salto", Ramon, Paulo and Vini who, along with me, faced the challenge of a master degree. We could always count on each other for support and a laugh, shared in strictly academic encounters.

To all the colleagues I met in PPGERHA, who shared with me the hardships of the courses and their personal life and academic experiences. It was a pleasure to know such distinctive people.

A special thanks to Laís, Ledi, Liege, Luzi, Lucas and Jéssica who shared the study room and endured me for two years. I can't express how lucky I was to be around you every single day. You are amazing. All the laughs and advises made a huge difference and I will sure miss our time together in the study room, including you guys messing with my stuff and unattended computer.

To the professors from the Department of Hydraulics and Sanitation and the Graduate Program in Water Resources and Environmental Engineering and all the employees. Your dedication and competence in what you do is a reference for high quality in our university and in our country. This is something that makes me very proud and I thank you for all the teachings.

A special thanks to my supervisor professor André for all the support and patience during these years, you were always friendly and ready to help when needed. I see you as an example of academic and professional excellence and I thank you for seeing this journey to the end with me.

At last, I thank the National Counsel of Cientific and Technological Development (CNPq) for the financial support through a master scholarship.

RESUMO

Em estudos de impacto sócio-econômico e ambiental existe a preocupação em simular o rompimento da barragem e a propagação da onda sobre o vale a jusante. As técnicas de propagação da onda de cheia já são bem consolidadas enquanto que ainda se realizam muitos estudos para melhor representar a ruptura de barragens, em especial para barragens de terra e enrocamento em que a ruptura ocorre progressivamente. A maioria dos modelos existentes para esses casos se aplicam para barragens homogêneas ou com núcleo de argila e simulam apenas o galgamento. O modelo *BREACH* do *National Weather Service*, USA, tornou-se popular por simular tanto galgamento quanto *piping* e ser de uso livre, além de código aberto. Assim, estudou-se este modelo para compreender como ele simula uma barragem de enrocamento com núcleo de argila e constatou-se que se ponderam as propriedades dos materiais a cada passo de tempo, homogeneizando toda a barragem. Assim, implementou-se uma rotina semelhante para simular barragens zonadas, com um núcleo (zona) não central à barragem a exemplo de uma ensecadeira, avaliou-se a sensibilidade da rotina alterando o D_{50}, D_{90}/D_{30}, a porosidade e a altura da zona e observou-se o impacto sobre a vazão de pico, tempo de pico e dimensões da brecha. Dois testes foram realizados, um com a barragem natural de terra no rio Mantaro no Peru, galgada, e outro com a barragem de Teton, USA, rompida por *piping*. Para este caso, modelou-se uma zona com D_{50} de 25 mm e uma altura de 60% da própria barragem, reduzindo em 20% a vazão de pico e aumentando seu o tempo em 76%. Uma ensecadeira rompida por *piping* foi modelada com o modelo *BREACH* original em que os *inputs* foram consideravelmente alterados para obter resultados próximos dos dados de campo. Assim, para validação, com o modelo *BREACH* e a nova rotina para barragens zonadas remodelou-se este acidente, sendo preciso mudanças sutis menores que 10% à declividade do leito do rio e propriedades dos materiais para obter uma simulação ótima com uma vazão de pico 5.37% maior.

Palavras-chaves: Barragem de terra e enrocamento. Segurança de barragens. Ruptura de barragem. Modelagem. NWS BREACH.

ABSTRACT

Dam breaching and the determination of flood maps are the concern of social-economical and environmental studies when analyzing the potential risks of any dam. There are well consolidated techniques for assessing flood maps, but many studies are still going on for better modeling of dam breaching, specially regarding embankment dams in which the failure occurs in a long time period. Most existing models for dam breach are suitable for homogeneous or composite dam (central inner cored) and for overtopping. As for the BREACH model from the National Weather Service, USA, it is suitable for both overtopping and piping, aside from being free of use and open source. Through examination of this model it was observed that it models composite dams by pondering the materials properties thus, creating a so called equivalent homogeneous dam. A similar routine was created to model zoned dams, with a non-central inner core such as in a coffedam, and it was tested changing the D_{50}, D_{90}/D_{30}, porosity and height of the inner zone while observing the impacts on the peak outflow, time to peak and breach dimensions. Two test cases were performed: one with the overtopped landslide dam on Mantaro river, Peru, and another with the Teton dam, USA, failed due to piping. For this last test, the peak outflow was reduced in 20% and the time to peak increased in 76% when modeling a zone with a D_{50} of 25 mm and a height of 60% of the dam. A cofferdam breached by piping was modeled using the original BREACH model and it resorted to great changes to the inputs to obtain a best fit to the actual event. For validation, this accident was remodeled by the new BREACH with the zoned dam routine, needing only slight variations of less than 10% to the slope of the river bed and the properties of the materials to obtain a best fit simulation with a peak outflow 5.37% higher.

Key-words: Embankment dams. Dam safety. Dam-break. Modeling. NWS BREACH.

LIST OF FIGURES

LIST OF TABLES

SUMMARY

1 INTRODUCTION

1.1 GENERAL

Dams are of great importance to mankind since they provide water storage for different purposes such as irrigation, recreation, energy generation, flow regularization and others. Even though such structures have many benefits and are meant to last, they are susceptible to failures from diverse causes (e.g. earthquakes, piping, overtopping, human errors, etc.). These failures may be catastrophic like the case of Teton dam in the United States with numerous deaths and a prejudice of one billion dollars in 1976 (LUO et al., 2011).

Because of such high associated risks to property and life, it is necessary to devise programs and measures to predict and analyze potential failure modes and to assess the dams' current integrity, as well as implementing actions to correct it. But such preventive actions can never be 100% effective and so, warning systems and procedures for evacuation of individuals from hazardous areas are also developed (WAHL, 2010).

On this scope, it was created in 1968 the first European law on dam-break risk analysis in France, right after the failure of Malpasset dam in 1959 with over 400 injuries. This law, according to M. MORRIS, J.-C. e BALABANIS (1999), made mandatory the creation of emergency plans including the simulation of the flood wave, flood maps and estimation of wave arrival time. Similar laws were right after implemented in other European countries; meetings and conferences were arranged along the years to discuss and assemble the many technologies in use in Europe, such as the Concert Action on Dam-Break Modeling - CADAM and Investigation of Extreme Flood Processes and Uncertainty - IMPACT.

In the United States, after numerous dam failures in the 70's the Federal Guidelines for Dam Safety were created in 1979 demanding the inclusion of inundation maps in projects as well, according to WAHL (2010), and in 1996 the National Dam Safety Program was created and renewed in 2006. Even with all this care, in accordance with the FEMA (2012) there are registered 83,987 dams in the USA with an averaged age of 52.7 years, from which 10,000 will reach this mark in the next 10 years and 16% poses already a potential hazard.

In Brazil, the rising of such laws and regulations came only recently. The Federal Law 12.334/2010, entitled National Policy of Dam Safety, wishes to ensure the observance of safety standards, to regulate and promote the monitoring of dams providing guidelines to classify them according to a risk category and associated potential damage (BRASIL, 2010). According to ANA (2018), the latest Dam Safety Report, there are 24,092 registered dams and in 76% of them it remains unknown in what state they are and how high of a risk they may impose. From those who were analyzed, 723 present a high potential hazard associated with a high risk category, this number corresponding to 12.5% from the classified dams and 3% of the total.

These numbers raise great concern and shows how important and urgent it is to assess the associated risk of these structures, thus why dam-break studies must be done. In such studies we are concerned with the prediction of the outflow hydrograph and its routing through the downstream valley, as explained by WAHL (1997). From them, the breaching process, related to the determination of outflow hydrograph, is still the main source of uncertainties in contrast to the flood routing that has already its own well-consolidated techniques, as discussed by AMARAL (2017).

For the dam breaching, several computational models have been developed along the years for many failure modes and diverse types of dams, and even though there are so many, some limitations remain. For instance, how the dam structure is represented, whether if it is a homogeneous or composite dam, how the breaching starts and develops over time, for what sort of failure it is suitable and some models even predetermine the final size and shape of the breach (M. MORRIS, 2011). Moreover, the majority of models are not free of use and, according to WEST, M. MORRIS e HASSAN (2018), those solving differential equations demand high computational cost .

WEST, M. MORRIS e HASSAN (2018) presented a resume of the state of art around dam breaching models and according to them, no model simulates a dam with a core adjacent ("attached") to its upstream face, i.e. a zoned dam, as example of a cofferdam. The only exception to this is the HR BREACH, a commercial model, which works also with zoned dams but measures the erosion rate through the concept of erodibility, instead of using sediment transport equations as more usual (M. MORRIS, 2011).

We observe from all of this that there is a need for tackling the zoned dams modeling and, ideally, that it is free-of-use, of low computational cost and, naturally, reliable.

1.2 OBJECTIVES

The NWS BREACH is a model developed in the National Weather Service in 1988 and revised in 1991 (FREAD, 1991). It is an open-source and free-of-use model for embankment dams breached due to piping or overtopping, therefore chosen as object of study to fill in the addressed gap in modeling. To do so, the following goals are set:

- To study both the manual and source code of the BREACH, looking specially at how composite dams are modeled;
- To develop a routine for zoned dams based in the modeling of composite dams;
- To test the new routine against the test cases of Teton dam in USA and Mantaro landslide dam in Peru, both used for validation of the original model;
- To validate the model with a case study of a breached cofferdam.

1.3 STRUCTURE

This dissertation begins by presenting the main aspects circling the theme of dam-break. Section 2.1 shows usual designs or layouts of man-made embankment dams. Section 2.2 discusses the strategies behind dam-breach modeling with its pros and cons. Then, it is discussed in Section 2.3 the usual uncertainties involved in each modeling and how they may affect the analyzes.

Right after, Section 2.4 shows some of the relevant studies composing the state of art in dam-break. For example, experimental studies in small-scaled models for better understanding of breaching processes and computational models that are either of public use, have unique features or show themselves to be a future benchmark.

The NWS BREACH is detailed through analyzes of its manual and source code in Chapter 3. Then, in Chapter 4 the new feature for zoned dams is described along with a sensibility test to the D_{50}, D_{90}/D_{30}, porosity and height of the zone. Next in Chapter 5, the model is validated to a case study of a cofferdam breached by piping. Finally in Chapter 6, some conclusions are drawn and recommendations for future works are given.

The Appendix A presents a general flowchart of how the original BREACH model works and which sequence of measurements it performs. A description of inputs and outputs of the model with its new routine for zoned dams is, respectively, in Appendices B and C. The percentage variations caused by a modeled zone over the peak outflow, time to peak and breach dimensions are presented in Appendices D and E for Mantaro landslide dam and Teton dam, respectively.

2 BIBLIOGRAPHIC REVIEW

2.1 EMBANKMENT DAMS

According to BUREAU (1987), embankment dams were the first type constructed since old civilizations for water supply purposes. Nowadays, around 75% of the existing dams belong to this category, which are further divided in earth- and rockfill dams (ICOLD, 2008).

The selection of which type of dam best suits a given site depends on several factors. For embankment dams, a narrow stream with high rocky walls usually calls for a rockfill dams, while low smooth plains are good for earthfill ones. Looking the foundation, gravel ones are suitable for embankment dams when well compacted and a good seepage control is provided. Silt or fine sand foundations are not recommended for rockfill dams and should be even extra care when an earthfill dam is concerned. In clay foundations, earthfill dams can be used if the river slope is relative flat, while rockfill dams are normally not economical for this situation (BUREAU, 1987).

Another dictating factor is the spillway. When the excavated material for the spillway can be used for dam construction, embankment dams are usually selected. Small spillways and those separated of the dam's main body are also a good fit with embankment dams. Other considerations such as the hydrology and the availability of material at the site are important to consider as well (BUREAU, 1987).

Once the earthfill dam is chosen, it is only left to choose what sort. Earthfill dams can be divided into three types according to its structure, which will be described bellow. A fourth and additional type, which is actually a specific application for this sort of dam, is also included and presented.

- Diaphragm embankment

Diaphragm embankments have, in general, most of the dam's body made of a pervious material (e.g. sand, gravel or rock) and a thin diaphragm or membrane of impermeable material acting as a water barrier. The impermeable material can be of asphaltic or reinforced concrete, metal, compacted earthfill or geomembrane. Moreover, this diaphragm is either positioned at the upstream face of the dam or in the middle of it (ENGEMOEN, 2012).

The BUREAU (1987) specifies further that the diaphragm width at any elevation must be less than 10 feet (3.0 m) or at any elevation must be less than the dam height above the considered elevation. Otherwise, this type of dam is classified rather as a composite dam. Figure 1 shows examples of this type of dam.

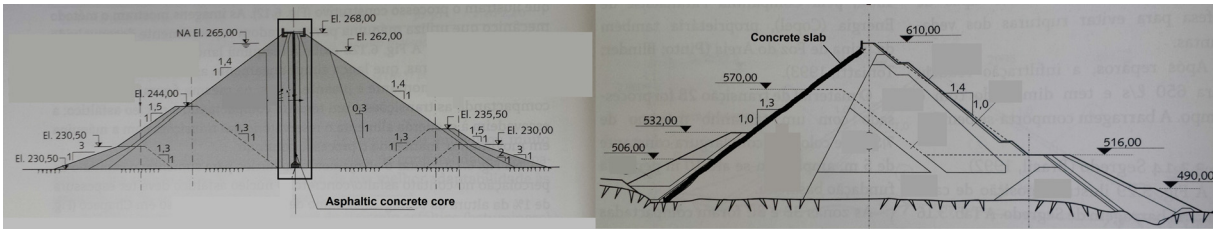

FIGURE 1 – Foz do Chapecó dam with asphaltic concrete core on the left, adapted from MAGELA (2015), and Segredo dam with concrete slab on the right, adapted from CRUZ, MATERÓN e FREITAS (2014), in Brazil.

- Homogeneous embankment

As the name implies, in this sort of embankment only one material is used for the dam's body, which must be impervious enough to serve as a water barrier. Furthermore, the upstream slope must be flat enough to provide stability during reservoir's level variations, as well the downstream slope when the reservoir is full and the dam's body becomes saturated (ENGEMOEN, 2012).

Despite choosing a material impervious enough, the occurrence of seepage is unavoidable resulting in a seepage's depth at downstream around a third of the dam's height, as shown in Figure 2. For this reason, the use of a completely homogeneous dam is out of use, replaced instead for a modified homogeneous dam. According to ENGEMOEN (2012), it is recommended the construction of a rock toe at the downstream face to act as a drainage, as demonstrated in Figure 3. Another option is the construction of inclined drains with a horizontal blanket or the installation of pipe drains, as shown in Figure 4.

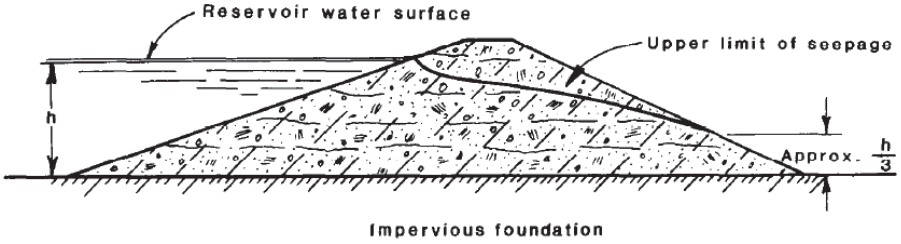

FIGURE 2 – Example of a homogeneous dam with seepage (BUREAU, 1987).

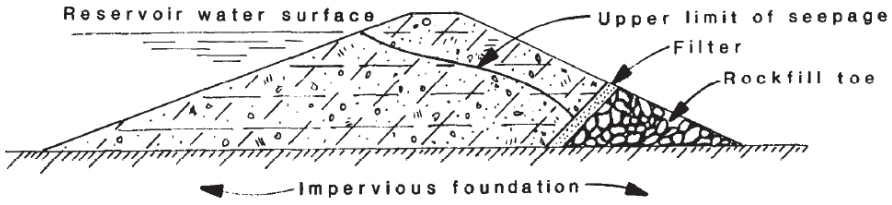

FIGURE 3 – Example of a homogeneous dam with a rock toe (BUREAU, 1987).

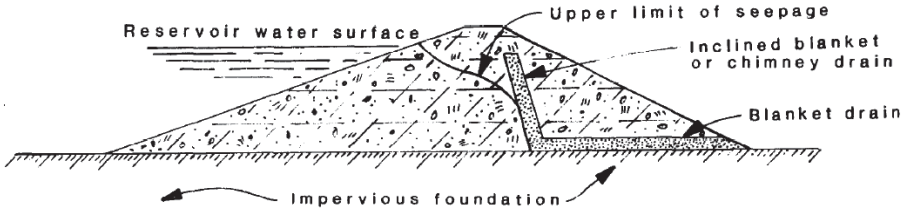

FIGURE 4 – Example of a homogeneous dam with inclined drains and horizontal blanket (BUREAU, 1987).

- Composite embankment

This type is the most commonly used for embankment dams and is also known as zoned dam. However, this term is reserved to a specific embankment dam that will be later presented. Composite embankment takes advantage of combining different materials that may be present at the site, resulting in more stable and impervious structures with even steeper slopes depending on the materials combination (ENGEMOEN, 2012).

Usually, the structure is composed of an impervious core (fine soils such as silts, clays, sandy silts and gravelly clays) are surrounded by a transition zone at upstream (sand or pebble) and a filter zone at downstream (sand or gravel), which in turn are surrounded by outer zones of more pervious but more resistant materials as well (cobbles, gravel or rock). ENGEMOEN (2012) comments further that depending on the granulometry of the employed materials, no transition zone is needed. A example of such structure is shown in Figure 5.

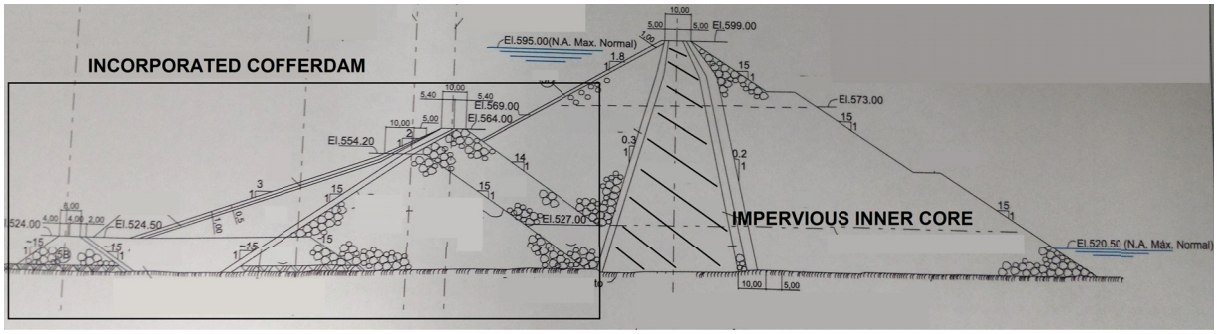

FIGURE 5 – Cross-section of Corumbá I powerplant, Brazil, with hightlight of the inner core and cofferdam. Adapted from CBDB (2009).

- Cofferdam

As mentioned before, this classification is actually more a specific application of embankment dams. According to COSTA (2012), cofferdams are river deviation structures that allow the dam construction in dry conditions. Moreover, there are two methods for construction of such structures: partial or total river closure.

Regarding the total closure, its structure is similar to the composite dams and it is constructed by launching uncompacted material (gravel or cobble) during periods of low flow, followed by a transition zone (sand or peeble) and a more impervious material, building in upstream direction each layer (COSTA, 2012). On the sequence, the cofferdam is further elevated by repeating the process at its downstream face, which happens in part submerged. When in dry conditions, each launched layer is compacted.

In total river closure, the cofferdam is constructed both up- and downstream of the dam's site. Sometimes for economical reasons, both cofferdams, or at least the one at upstream, are incorporated into the dam's body as can be observed in the previous Figure 5. Another important detail about cofferdams is that the usual material's granulometry is bigger than one used for the dam's main body, since cofferdams must be heavier enough to divert the river while not being eroded (CBDB, 2009).

2.2 MODELING METHODS

All developed models can be grouped according to their modeling approach and this varies little from author to author. In this section, the existing approaches will be described with its main characteristics, pros and cons and some examples. The classification presented here was based in KAHAWITA (2007).

2.2.1 Empirical models

The empirical models are based on documented data of breach events. From statistical regression analysis of these data, a set of equations for peak discharge, breach final width and time of failure are obtained (M. MORRIS, 2011). The advantage of such models is that they are easy to use since no computation is required, but that should be done with care. According to the author, their performance is entirely depended on the users' previous knowledge of their applicability. Furthermore, the number of cases from which these equations are derived is small and does not represent the entire variety of dam types. For instance, the majority of data is from small dams with less than 15 m according to WAHL (1998).

2.2.2 Parametric models

As discussed earlier, empirical models make use of data sets of dam failures to predict parameters such as the final breach width, but due to the dubious quality of these data the estimations accuracy is compromised. In order to correct this, parametric models were developed to use some hydraulic equations, although simplified so not to demand much computation. Thus, these models can assess the time to failure and final breach shape based on their record of historical dam failures as the empirical models do and then measure the breach growth along time and the outflow hydrograph through hydraulic equations (WAHL, 1998).

According to ZHU, VISSER e VRIJLING (2004), they can use as well breach shape and its formation time as inputs and reproduce their development in time. M. MORRIS (2011) commented that some of the simplifications in these cases are adopting a linear growth rate for the breach, using the weir equation for the flow over the dam. Another usual simplification is that the breach channel is not modeled and so, no erosion can be assessed as stated by KAHAWITA (2007).

Some examples are the NWS DAMBRK developed by Fread in 1984, the HEC-RAS by U.S. Army Corps of Engineers - USACE and MIKE11 by the Danish Hydraulics Institute in 2009. KAHAWITA (2007) listed these ones as examples because they require certain parameters like the time to failure as inputs for breaching assessment. Even though they provide a detailed analysis of the flood maps and regarding only the breaching process, fully physical models do not require such parameters as inputs.

One important detail to be clear is that these models are as good as the quality of their inputs, thus relying strongly on the user's choices for some of applied equations' coefficients (M. MORRIS, 2011).

2.2.3 Physically based models

These models differ from the two others for combining the concepts of hydraulics, sediment transport and soil mechanics for predicting the breach growth rate and the resulting outflow hydrograph. Therefore, they provide more insights and are more accurate, but there is even today a lack of complete understanding of the interaction between hydraulic and geotechnical aspects. Some simplifications due to this lack are the only applicability to homogeneous dams and the neglect of initial breach formation (ZHU; VISSER; VRIJLING, 2004).

According to M. MORRIS (2011), besides the consideration of hydraulics, sediment transport and soil mechanics as mentioned, another great advantage of these models are that few parameters must be predefined and uncertainty analyses can be performed. However, the disadvantages are that the simulation runtime may be long depending on the model's choice and, usually, the models apply 1D or 2D equations which require already considerable computational effort. The use of 3D equations is still not practical.

2.3 MODELING UNCERTAINTIES

On the previous section the modeling approaches for dam-break were presented, being the best the physically-based ones for applying hydraulics, sediment transport and soil mechanics all together and thus, performing a more realistic simulation. Therefore, it is convenient to discuss now the modeling uncertainties.

A first source of error is the predefinition of the breach shape. As it is noticed in the models listed in the report of WEST, M. MORRIS e HASSAN (2018), the assumption is usually

trapezoidal or triangular and, in some cases, even rectangular or combining different formats. However, as concluded by IMPACT (2004b), the breach is in reality rectangular for many cases of cohesive and non-cohesive dams. For the non-cohesives the trapezoidal assumption may be valid although not entirely accurate, because that is the final format seen in a dam-break scenario for embankment dams, after the breach ceased to erode and its side slopes slumped after being dried (M. W. MORRIS et al., 2008).

Another issue mentioned by M. MORRIS (2011) is concerning the available study case data. The number of study cases is limited, specially when concerning large dams, and the data quality is dubious. Usually, some of the data (e.g. breach format and time to failure) is obtained from observers presented at the time of incident and that have no expertise on the matter thus, the informations provided are subjected to misinterpretations.

Another modeling problem is the considered erosion process, where most models simulate surface or hydraulic erosion with disregard to headcut or geotechnical erosion, both of these processes exemplified in Figure 6. However, for a model to be more accurate it is needed that both erosion types be accounted for.

According to XU e ZHANG (2009), headcut is an erosion process characteristic of cohesive dams where blocks of material are eroded in an instant creating step-like structures in the dam's body. As for surface erosion, it happens more often in non-cohesive dams where the dam is eroded gradually layer by layer. These processes can be observed in Figure 7 showing the range of observed erosion processes for each type of soil. According to M. MORRIS e HASSAN (2009), it was noticed even the occurrence of both erosion types for a composite dam.

FIGURE 6 – Example of surface (left) and headcut (right) erosions observed in field tests according to IMPACT (2004a) and HANSON, COOK e HUNT (2005), respectively.

Considering that, it is noticeable the need to assess the erodibility of dam's materials and some recent models turn to this approach usually by Equation (2.1):

$$E = \kappa(\tau - \tau_c)^{\alpha}, \tag{2.1}$$

where:

E is the erosion rate [m/s];

κ is the material erodibility [m^3/N.s];

τ is the shear stress [N/m^2];

τ_c is the critical shear stress [N/m^2];

α is an empirical coefficient [-].

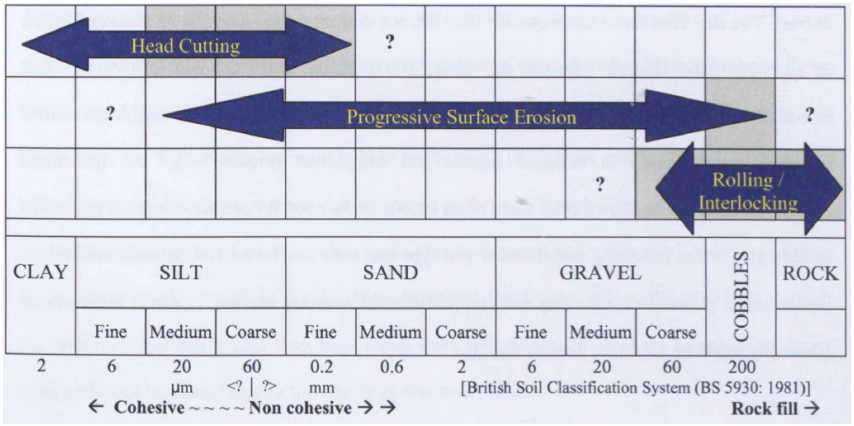

FIGURE 7 – Expected erosion process for each dam composed material (M. W. MORRIS et al., 2008).

On this matter, M. MORRIS (2011) criticizes the models that employ sediment transport equations, stating that they were derived from fully developed and steady river flows, not resembling at all the conditions observed in a dam breach. Critical shear stress, flow velocity on breach and others parameters incorporated by sediment transport equations do not represent well enough the water content and compaction of the material, which are very interlinked with the erodibility and have great impact on modeling. Even though this parameter should be considered, it is difficult for the modeler to estimate it and that explains why the sediment transport equations are the general approach.

VAN EMELEN, ZECH e SOARES-FRAZAO (2015) evaluated the influence of sediment transport equations. Their dam-breach model used the Saint-Venant equations coupled with the Exner equation and it was valid for overtopping. The modeling results were compared with experimental data performed for the analyses. It was concluded that the sediment transport equations of Meyer-Peter-Müller (1948) and Smart-Jäggi (1983), a variation of Meyer-Peter-Müller for slopes up to 20% according to SMART (1984), gave the most accurate peak outflow with 11% and 3% of deviation, respectively. Comparing all the tested equations, the ones that showed themselves comparable with one another revealed a root-mean-square-deviation inferior to 20%, with Meyer-Peter-Müller equation included in this group. Lastly, correction factors to adjust the equations for steeper slopes did not show relevant improvements.

A final point of uncertainty worth of mentioning is the breach initiation. Most models simulate the breach only after a initial one is introduced and have difficulty on determining the time to breach initiation, initial failure mode and transition between failure modes (WU, 2011).

It is left to emphasize that there are a wide variety of models to choose from and many uncertainties involved. When compared for the same case study, these models may result in quite different hydrographs, but for the flood routing it may not provoke the same degree of error. According to BRUNNER (2014), since the hydrographs have similar volumes for originating from the same reservoir, they will converge eventually and this may happen rather fast and at a relative short distance from the dam as exemplified in Figure 8. How fast this convergence will take depends on many factors from the valley (e.g. roughness and slope) and the outflow hydrograph (e.g. steepness of rising limb and volume).

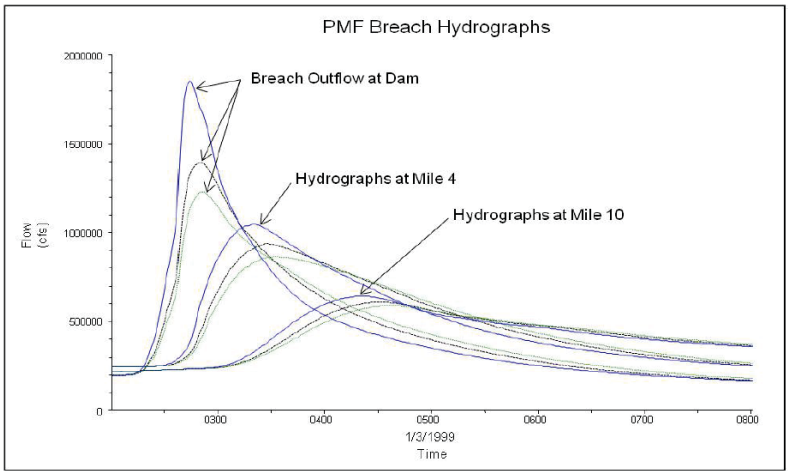

FIGURE 8 – Convergence of routing performed in HEC-RAS for different hydrographs (BRUNNER, 2014).

Being so, the closest regions at downstream of the dam must receive extra care when defining flood plains and dam safety procedures (BRUNNER, 2014). Although different hydrographs may convergence, it should not be interpreted that errors in breach modeling are irrelevant, that further improvements on modeling are not needed and that the model should not be chosen wisely.

2.4 RELEVANT SCIENTIFIC CONTRIBUTIONS

The models and researches presented herein were chosen for either having a particularity not seen in other works, being a reference for dam-break studies, possessing data for model validation or being known and reliable models.

2.4.1 A mathematical model of progressive earth dam failure

Despite its age, this model has unique features that make it stand out from the others. The following description is based on the PhD thesis of NOGUEIRA (1984) that created the model.

The model is applicable for earthfill dams failured due to overtopping. The equations used are the 1D-Saint-Venant equation coupled with the 1D-Exner equation for breach profile.

The sediment transport is evaluated with the Meyer-Peter-Müller equation. The equations are discretized by finite differences and a quadratic mesh is applied. The reservoir routing is done by mass conservation.

The breach format is defined by a cosine function and the initial breach may be positioned in any part of the dam's body. Both the breach enlargement and the slope stability analysis consider the condition of erodible and non-erodible abutments. The model was validated with the case of the Mantaro landslide dam in Peru.

2.4.2 NWS BREACH

This is the only model found to be both free of use and open-source, being these the reasons for its widely use. The following description is based on the manual written by FREAD (1991) and is further detailed in Chapter 3.

The NWS BREACH is a physically-based model developed by Danny Fread in 1988 at the National Weather Service, USA, and revised in 1991. It predicts the breach development with almost none pre-determined parameters and it is suitable for both piping and overtopping failures, simulating even the transition between them, in embankment dams either man-made or natural. For man-made dams, they may be homogeneous or composite. When composite, the model averages the materials properties in order to create an equivalent homogeneous dam.

When overtopping occurs, the flow over the crest is calculated by a broad-crested weir equation and the flow into the formed channel with a similar equation. If piping is being simulated, an orifice equation is used.

To measure the erosion, the model employs a modified Meyer-Peter-Müller sediment transport equation for steeper slopes and the reservoir's variation level is determined by mass conservation. A collapse due to the hydrostatic force is also considered. Moreover, the submergence effect due to the tailwater level is also considered.

Since it does not solve differential equations, the model is fast to obtain the final result.

2.4.3 BOSS DAMBRK

The BOSS DAMBRK is an improved version of the DAMBRK model from the National Weather Service developed in 1988. The following description is based upon the manual of BOSS (2003).

DAMBRK simulates the failure of a dam, computes the resultant outflow hydrograph and simulates movement of the dam-break flood wave through the downstream river valley, which may contain up to ten dams and/or bridges. Moreover, it can simulate both subcritical and supercritical (mixed) flow in the same routing, route any specified hydrograph using

dynamic routing without requiring data for the dam or reservoir, perform reservoir routing without failure of the dam as in spillway design studies and it considers backwater effects.

The flood routing, its main feature, is based on solving the 1D Saint-Venant equations in an open channel. In addition, the channel boundaries are rigid, i.e., cross sections do not change shape due to scour or deposition. As for the breach itself, the rate of development, shape, and final size of the breach must be specified by the user.

Concerning the breaching, the model is able to simulate both overtopping and piping. In overtopping failure the breach has a rectangular, triangular or trapezoidal shaped that grows progressively downward from the dam crest. The flow through the breach at any instant is calculated using a broad-crested weir equation. The final breach shape is specified by the side slope and the final width of the breach bottom. As for piping failure, it is simulated as a rectangular orifice breach that grows with time and is centered at any specified elevation. The flow through the breach is calculated with either orifice or weir equations depending on the relation between pool elevation and the top of the orifice.

The approach for the breaching is parametric as explained in Section 2.2 and the manual recommends the use of the NWS BREACH model for a more detailed analysis.

2.4.4 CADAM project

The Concerted Action on Dam-Break Modeling project - CADAM was a followed up of a larger project that started with the publication of a french law, which demanded the performance of dam-break studies from dam owners. With this law, a meeting was organized in Chatou, France, in March 1996 with scope of modeling validation. The next meeting happened in Lisbon, Portugal, in November 1996 and analytical test cases were shared and discussed. The third meeting was in Brussels, Belgium in June 1997 and this time laboratory tests were discussed (M. MORRIS; J.-C.; BALABANIS, 1999).

From these three meetings and the support of Europe Commission is that the CADAM project was born, which started in February of 1998 and lasted two years. The first meeting was in Wallingford, UK, in March of 1998 and it was reviewed and discussed all the information from the previous three meetings. Moreover, gaps in dam-break knowledge were identified and selected for future research. In total, five topics emerged from it and they were: the need to perform tests with realistic dimensions, to gather data of real dam failures and check the applicability of modeling equations to them, to differentiate breaching processes and to perform 2D modelings (M. MORRIS; J.-C.; BALABANIS, 1999).

The second meeting took place in Munich, Germany, in October of 1998 and it had breach and erosion modeling as topics. Some of the conclusions were that the models accuracy for peak discharge was around 50%, for more or less depending on the model, and most of them showed problems in modeling non-cohesive homogeneous dams. Regarding field tests, it was

noticed the lack of reliable data, since many of these informations are from eye-witnesses that have no expertise on the matter. As for laboratory tests, they are not completely trust-worthy since it is difficult to properly instrument the small-scaled models. Moreover, there is a great deal of subjectivity on every analysis due the modeler's assumptions (M. MORRIS; GALLAND; BALABANIS, 1999).

The third meeting was in Milan, Italy, in May of 1999 and it concerned the modeling performance of the Toce river flood and discussions on breach processes, social-economic impacts from dam-break and risk mitigation. The performance analyses was a special occasion and main event of this meeting, because the modeling results were compared against small-scaled model of a real valley. Some conclusions were that there is a difficulty in scaling the roughness in small-scaled models. Regarding social-economical aspects, there is a need to better evaluate if the infrastructures will colapse due to flood waves. Furthermore, it was discussed that the public should be aware of potential flood risks and kept always informed, making emergency plans work better (M. MORRIS; GALLAND; BALABANIS, 2000a).

The final meeting was in Zaragoza, Spain, in November of 1999. Similar to the previous meeting, this one was focused on the modeling performance of Malpasset dam failure, together with discussions over breach formation, flood routing and sediment processes from several works. The analyses of Malpasset dam marked the final step of CADAM project for modeling a real life failure. Some conclusions were that there is a great impact of user's assumptions, specially on 1D modeling. Concerning concrete dams, there was a questioning on how to better model failures of such structures. It was questioned as well the accuracy of available data for modeling (M. MORRIS; GALLAND; BALABANIS, 2000b).

Right after, a document was elaborated which summarized all the knowledge gathered from the four meetings. Concerning breach formation, it was recognized that the uncertainties of breach modeling may be the greatest cause of all uncertainties in dam-break analyses. The accuracy at the time of such models was around 50% for peak discharges with no model being identified as the best possible choice for use. The breaching mechanics should be better studied as well (M. MORRIS; SAMUELS, 2000).

2.4.5 IMPACT project

The following informations were mainly taken from IMPACT (2005). The IMPACT project - Investigation of Extreme Flood Processes and Uncertainty was a project developed from 2001 to 2004 in Europe that continued the work started by CADAM. The project was composed of five reports which addressed the following themes: breach formation, flood propagation, sediment movement, uncertainty analysis and geophysics and data collection.

The first report focused on breach prediction and it involved five field tests of 40 m wide and 22 small-scaled tests mostly at a scale of 1:10 to the field test as follows. The main goals were to obtain reliable data for future modeling validation, understand better the

breaching processes and assess the uncertainties of models available at the time.

- Field tests:
  - 6 m high cohesive embankment (25% clay and less than 15% sand) submitted to overtopping;
  - 5 m high non-cohesive embankment (less then 5% fines) submitted to overtopping;
  - 6 m high composite embankment (rockfill and moraine) submitted to overtopping;
  - 6 m high composite embankment (rockfill and moraine) submitted to piping;
  - 4.5 m high homogeneous embankment (moraine) submitted to piping.
- Small-scaled tests:
  - 9 tests with non-cohesive homogeneous embankment dams submitted to overtopping;
  - 8 tests with cohesive homogeneous embankment dams submitted to overtopping;
  - 5 tests with cohesive homogeneous embankment dams submitted to piping failure.

The second report was about flood propagation composed of small-scaled tests and field researches on actual flood incidents. The aim was to obtain knowledge on flow characteristics, to possess reliable data for modeling validation and perceive the differences between the effects observed in real and laboratory simulated floods.

Another report was on sediment movement and small-scaled tests were run for the purpose of analyzing two aspects. The intense erosion resulted by the wave propagation and the changes on the valley resulted after the wave.

One of the reports focused on the matter of uncertainty (IMPACT, 2004c). More precisely, how each uncertainty contributed for the overall uncertainty and how they could affect the predictions.

The last report was a research on available data of real dam-break events in Hungary and Czech Republic. Then, the collected data were put through statistical analyses.

Concerning the breaching, some conclusions were already commented in Section 2.3 . Others worth mentioning is that the peak discharge prediction may vary around 30% depending on the model and inputs. Location of the breach plays a great role on the results. Finally, when choosing a model the user should consider what type of dam is being simulated, if a uncertainty analysis is required (some models provide this option), if headcut erosion is likely to occur and if an approximated or detailed prediction is necessary.

2.4.6 SPHysics

The model to be described here is based on the papers of GÓMEZ-GESTEIRA et al. (2012b) and GÓMEZ-GESTEIRA et al. (2012a). SPHysics is an open-source model developed by a partnership among several researches with the objective to study free-surface flows. SPH stands for Smooth Particle Hydrodynamics that is the core method in which the model is based. In general, this method is a Lagrangian meshless method and it consists in dividing the application domain in a number of particles defined by the user, considering the interaction among the particles according to the influence region around each particle. All equations implemented on the model (e.g. conservation and motion equation) are discretized according to this method.

SPHysics is usually applied in coastal studies, but also for dam-break. However, its use in practical applications is very limited. For example, it took six hours for a computer with a Intel X5500 using all its eight cores to run a simple dam-break case, in which the flood wave faced a pilar in the center of the domain. This simulation was performed with the DualSPHysics and it used over 26,000 steps and one million particles for the method, resulting in 1.5 seconds of physical time. Further comparisons among computer capabilities for this example is presented in CRESPO et al. (2015).

2.4.7 HR BREACH

The original HR BREACH model was developed in 2002 at the HR Wallingford, an independent civil engineering and environmental hydraulics organization. Later in 2011, Mark Morris wrote his thesis at the same organization, reviewing the concepts of dam-breach and improving the HR BREACH capabilities. The comments on the model are all based on the thesis of M. MORRIS (2011).

HR BREACH is a commercial model suitable for homogeneous and composite embankment dams failured either by overtopping or piping. For overtopping, an initial channel is assumed and discretized in nodes. The model determines the critical section that separates super- and subcritical flows and measures the flow profile through one of the methods: 1D/2D Saint-Venant, steady uniform flow or steady non-uniform flow. A weir equation is used on the determined critical section. For piping, a orifice equation is applied instead.

Several options of sediment transport and erosion equations are available for the user's choice, hence modeling both surface and headcut erosion. The breach format is assumed rectangular for both failure modes and for overtopping it is considered, at first, the existence of vortexes near the toes of the breach side walls. These vortexes erode and undercut the breach cross-section while the slope stability is checked by equilibrium of forces.

The main new feature to the second version of HR BREACH is the modeling of zones with different erodibilities. Several simulations were performed with different erodibilities

and zone configurations, revealing the changes to the outflow hydrograph that, in general, were smoothed and extended for cases of low erodibility. This was the only model found that performed such analysis, similar to the main objective to be reached in this dissertation.

2.4.8 Numerical modeling of earth dam breaching by overtopping

STAV-2D (Strong Transients over Alluvial Valleys) is a model developed in the Technical Institute of Lisbon and is based on the Saint-Venant equations featuring dynamic bed geometries and sediment transport, all of that based in the model of FERREIRA et al. (2009). Later LOPES (2015) reproduced the STAV-2D in MATLAB, named then as STAVBreach, focusing on modeling of embankment dam failures due to overtopping.

According to the author, essentially, the model uses the 2D Shallow-Water equations coupled with the Exner equation and discretized by Finite Volume Method.

The sediment transport happens whenever the frictional and collisional stresses of the particles are not in equilibrium. The collapse of the breach side slope happens if the slope angle becomes steeper than a certain critical angle, assuming then a residual slope angle.

The model was validated against analytical solutions like Stoker's and Ritter's and against four data of small-scaled models from the National Laboratory of Civil Engineering (LNEC) in Lisbon, Portugal. The model showed good agreement and behavior for all the comparisons.

2.4.9 DLBreach

The DLBreach is a model available for 1D, 2D and 3D analyses for either embankment dams or levees. The 2D version to be presented in this section was developed by WU (2016) and all the information is based on his work.

The model is, as commented earlier, suitable for embankment dams and levees (homogeneous or composite) submitted to either overtopping or piping, this one either on the main body or the foundation. A transition between them is also possible.

The piping is taken as a horizontal rectangular channel which is eroded uniformly in all directions. The piping may be considered to be full of water or partially full. When overtopping is simulated, the initial breach format is trapezoidal and it can change to rectangular or not, depending on the soil properties.

The model considers both surface and headcut erosions. For non-cohesive soils, the model uses a non-equilibrium transport equations, i.e. the sediment concentration is not equal to the transport capacity of the flow. When dealing with cohesive soils, the model accounts for the erodibility that can be either informed or taken from reference values in the own model.

Other capabilities are the use of mass conservation for reservoir routing in case of

dams, a time series of water level in case of levees and the consideration of submergence effect, which is done in the same manner as in the NWS BREACH model. If applicable, a spillway can be accounted for and the wind influence on generating waves that may overtop the structure.

The validation was done with data from the IMPACT project and some real dam-break cases.

2.4.10 HEC-RAS

HEC-RAS (Hydrological Engineering Center - River analysis System) is a free of use model developed by the U.S. Corps of Engineers. It possesses many applications, being one of them for dam-break and the following will be a description based on the guide's manual of BRUNNER (2014) for this specific application. Nowadays, the model possesses, for the first time, a 2D-modeling capability.

The model is able to simulate overtopping, piping and even the transition between them. For estimating the breach parameters, the user may choose one of two approaches. The first, to inform the parameters on the breach, such as final dimensions and time to full development, which may be based on empirical equations mentioned in Section 2.2.1. The second approach is to inform the flow velocity on the breach channel versus the widening and vertical erosion of the breach channel, along with the breach's maximum bottom width, minimum bottom elevation and initial diameter (piping) or channel width (overtopping). The breach position is also an user's choice.

For overtopping, HEC-RAS considers headcut at the toe of the dam which grows towards the upstream. The flow into the formed channel is measured by a broad-crested weir equation. For piping, an orifice equation is used and as the piping grows mass blocks are displaced near the dam's toe due to headcut erosion, culminating to the transition to overtopping.

The reservoir routing is measured by either the Saint-Venant equations or by a mass conservation balance. HEC-RAS suggests that the latter is better suited for small reservoirs, but it depends from the valley (rugosity, shape and slope) as well.

Aside from performing the breaching and obtaining the outflow hydrograph, the model is able to do its routing through the downstream valley. Three approaches are commonly chosen: modeling the rivers with 1D Saint-Venant equations plus storage areas; modeling the rivers entirely with 2D Saint-Venant equations; combining the two approaches using the 2D equations for a more detailed analysis upon need. The Puls routing method is also available for choice.

The first approach requires less computational time thanks to the simplification of Saint-Venant equations to 1D. The second allows a better resolution of the flood areas, but it has a high computational time. Because of the pros and cons of both previous methods, it is interesting to combine them by using the 1D equations for a general flood mapping

and eventually the 2D for a better analysis of areas of interest. As for the Puls method, it is based in the principle of mass conservation where it is evaluated the inflow and the outflow is determined based in the storage capacity of the basin, being more suitable for cases with a single outlet. Therefore, this is a more simplified method, less robust than the approach with !D Saint-Venant equations.

As commented in Section 2.2.2 and it is here observed, HEC-RAS does not perform a actual breach prediction since it predefines, or rather limits, certain breach parameters. Its focus and strength is the flood routing when concerning dam-break modeling. Thus, the model allows the user to inform the outflow hydrograph from the breach and recommends even the use of the NWS BREACH model for obtaining it.

2.4.11 Retro-analysis of the mud wave of Fundão dam-break with different models and simulation hypothesis

The recent work of MACHADO (2017) shows a interesting contribution to dam-break studies in general, even though it was focused in tailing dams failures. In performing a analysis of flood wave from Fundão dam in Brazil, one of the used models was HEC-RAS which is suitable only for Newtonian fluids. Thus, it was proposed to adapt the Manning's coefficient according to the fluid concentration. Moreover, the contraction and expansion coefficients were adapt as well according to the same methodology, which it is only possible for the 1D simulations.

Thus, this pseudo-Manning as it was called showed good agreement to the field data from accident and to the simulations done with the FLO-2D, a commercial software able to simulate Non-Newtonian fluids. This methodology may also be used for dam-break of water storage or hydroelectric dams where the materials of the embankment dams will create a hyper-concentrate fluid that will not behave as a Newtonian fluid, changing the resulting flood map.

2.4.12 Experimental characterization of failure by overtopping of embankment dams

This recent thesis is a benchmark in experimental studies of dam-break for performing small-scaled models with cohesive soils, assessing the influence of compaction and water content, taking measurements with state-of-art equipment, studying the influence of structural collapse in the overall breaching process and defining procedures for performing such experiments. The main details and conclusions to be described are based on AMARAL (2017).

The total of six small-scaled models consisted of homogeneous dams that ruptured due to overtopping, all of it conducted in the National Laboratory of Civil Engineering (LNEC) in Lisbon, Portugal. The dams had a height around 0.45 m, a crest length around 1.2 m and width of 0.17 m and the up- and downstream slopes were 1:2 and 1:2.5, respectively. The reservoir volume was of 60 m^3.

The soils for the experiments were chosen to represent the most common types of homogeneous dams constructed in Portugal and, based on a pilot test, it was concluded that the optimal soil for such experiments would consist of a maximum fines content of 30% - on the experiments they were around 27%. Moreover, the soils were used in their natural state to assure homogeneity on the dams body.

It was wished to evaluate the compaction regarding the used method for it, the water content and the erodibility, besides the hydraulics of the breaching, and it was found out that using vibratory instead of percussive compaction was better. Regarding the scaling method, it was proved that it was not necessary to do it for the soil's granulometry, thus assuring that erosion observed in the model would match the one in a real dam. However, the compaction done in the model needed to be lower due to lower shear stresses from the scaling. For the experiments, it was adopted how low the compaction should be based on the pilot test, not defining a method for scaling the erodibility.

To evaluate the outflow and thus the hydrograph, two approaches were applied: local and non-local measurements. The latter was done, as well, by two approaches: using the mass conservation law, accounting for the reservoir's level variations, and a spillway, with a calibrated rating discharge curve, placed at a distance downstream of the dam. The local measurements were done, in turn, by three innovative procedures and made use of a Large Scale Particle Image Velocimetry (LSPIV), for estimating the surface velocity field, and a Particle Tracking Velocimetry (PTV) for the velocity vector. Two of the three procedures measured the outflow in the entrance section of the breach, being the only difference the reference cross-section for measuring its area, which was planar and curved. The last procedure applied the principle of energy conservation in a control volume with its outlet corresponding to the breach cross-section.

The first two local measurements showed themselves reliable and in good agreement with the non-local measurements, while the one based in the energy conservation not so much. It was commented in the thesis that local methods are very precise but demand expensive equipments and in large quantity, being an obstacle to their application.

Regarding specifically the measurements with LSPIV, the quantification of the hydrograph was done by a simple method. The outflow was calculated as the normal velocity to the breach cross-section, measured by the LSPIV, plus the estimated area of the cross-section. This procedure showed good agreement with other measurements and it was able to reproduce the main aspects of the breaching. For more detailed information about this LSPIV method, the article of BENTO et al. (2017) should be consulted.

The main type of erosion observed on the experiments was headcut. In addition, taking a closer look to the slope instability of the breach it was concluded that if such event happens downstream of the control section of the breach flow, the hydrograph suffers no impact. But, if the collapse happens at the control section or before, it is felt by the outflow. On this cases,

the sudden increase of the cross-section does not translate in an abrupt rise of the hydrograph, which is actually smooth and gradual. For better observation of such collapses, it was needed to take local measurements and analyze the data in a large time window.

3 NWS BREACH

In this section, the NWS BREACH will be presented stating its main features and differences between the manual and source code. In case of need for further information, the manual should be consulted in FREAD (1991). All subroutines from the model are presented in the end of this section and a flowchart is found in Appendix **??**.

All that is described herein is based on manual and the source code. The choice of used variables are according to the ones presented on the model to easy the understanding and correlation between this section and source code. A list of inputs and outputs can be found in the Appendices B and C, respectively.

Originally, the model works entirely in the Imperial System of Units and to make it more user friendly, two routines were written in the source code. One reads the inputs in the International System and converts them to the Imperial one, while the other takes the outputs and converts them back to the International System. It was done so to avoid mistakes in changing all the empirical coefficients of the equations and that is why they are presented in this section as written in the source code or the manual, in imperial units.

3.1 DESCRIPTION

The program was developed by Danny Fread in 1988 at the National Weather Service, USA, and revised in 1991. The model was written in Fortran, has around 2,000 lines and simulates the breaching in man-made and landslide (natural) dams, either homogeneous or composite, and provides its resulting outflow hydrograph.

The BREACH program computes two types of failures, overtopping and piping, with the breach assumed to be rectangular, at first, with the rate of width to flow depth informed by the user. The shape may change to trapezoidal in overtopping from case to case and a collapse of the dam's structure is possible as well. According to FREAD (1991), in case of overtopping the reservoir's water level must be higher than the top of the dam, causing a small channel along the downstream face as seen in Figure 9 where H_y is the water elevation, H_i is the initial water elevation in reservoir, H_u the dam's top elevation, H_l the dam's bottom elevation, H_{sp} the spillway elevation, W_{cr} is the dam's crest width, ZU and ZD are, respectively, the up- and downstream slopes and $D50_c$ and $D50_s$ are, respectively, the D_{50} of the inner and outer materials. These parameters are all in the Imperial System of Units with exception to the mean diameters, in millimeters.

In overtopping, the erosion begins if the flow velocity on the breach channel, measured by Manning's equation, exceeds a maximum permissible velocity which is a function of the cover over the downstream face. When it occurs, the slope erodes in parallel to the downstream

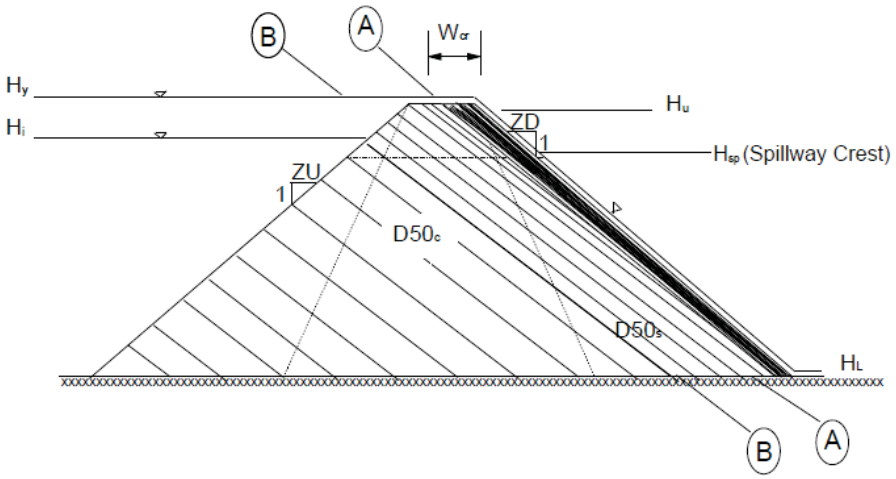

FIGURE 9 – Example of a dam's side view in NWS BREACH (FREAD, 1991).

face and towards the upstream face of the dam as signaled by the line A-A in Figure 9. As soon the line A-A reaches the upstream face, the erosion happens along the line B-B and, this time, also downward. The flow Q_b through the breach, which is firstly rectangular, is calculated by Equation (3.1) that is a broad-crested weir equation:

$$Q_b = 3B_o(H_y - H_c)^{1.5}, \tag{3.1}$$

Q_b is the breach outflow [cfs];

H_y is the water elevation in the reservoir [ft];

H_c is the bottom elevation of the breach [ft];

B_o is the breach width [ft].

As the breach channel erodes, it may collapse sideways resulting in a trapezoidal breach. For this to happen, the breach depth has to reach a critical value $H_k^{'}$ as shown in Figure 10 and determined by Equations (3.2) to (3.9):

$$\alpha = 0.5\pi - \theta, \tag{3.2}$$

$$\theta_0^{'} = 0.5\pi, \tag{3.3}$$

$$\theta_k^{'} = \frac{(\theta_{k-1}^{'} + \phi)}{2}, \tag{3.4}$$

$$H_k = H_c^{'} - \frac{y}{3}, \tag{3.5}$$

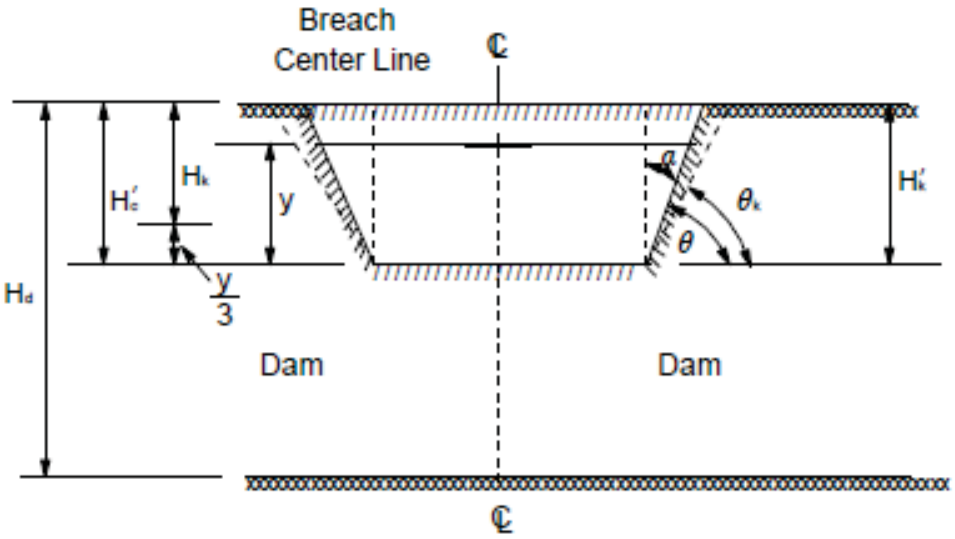

FIGURE 10 – Configuration of the possible slope collapses of a breach (FREAD, 1991).

$$H_k^{'} = \frac{4C\cos\phi\sin\theta_{k-1}^{'}}{\gamma_s}[1-\cos(\theta_{k-1}^{'}-\phi)]. \tag{3.6}$$

When $H_k \leq H_k^{'}$:

$$\theta = \theta_{k-1}^{'}. \tag{3.7}$$

When $H_k > H_k^{'}$:

$$\theta = \theta_k^{'}. \tag{3.8}$$

When k=1:

$$B_o = B_r y. \tag{3.9}$$

Where:

$H_k^{'}$ is the critical depth of the breach [ft];

$H_c^{'}$ is the depth of the breach [ft];

H_k is the depth of breach accounting the water influence on side-slope stability [ft];

H_d is the height of dam [ft];

y is the flow depth on the breach [ft];

B_o is the bottom width of breach [ft];

B_r is the ratio of breach width to flow depth [-];

γ_s is the specific weight of the soil [lbf/ft^3];

C is the material's cohesion [lbf/ft^2];

θ_k is the critical angle of the collapses [°];

θ is the side-slope angle [°].

Only three collapses, denoted by the index *k*, are computed by the program and after each collapse the breach may grow further in parallel to its cross-section. Once it reaches the river bed, the breach may continue to enlarge laterally until it reaches the abutments or the limit defined in the inputs.

An important detail is that once the breach collapses, the erosion will only progress after the removal of the collapsed material. Moreover, the breach's channel height is decreased by a third of the water depth in order to account for the water contribution to the slope stability, also shown in Figure 10.

This procedure described so far, based on the program's manual, does not reflect entirely what the program is actually doing. When analyzing the code relative to the breach's slope stability, it was noticed that the first collapse is computed with the critical breach depth determined only by the inner material properties in Equation 3.6. When the second collapse takes place both materials are considered, the inner and outer materials' cohesion, friction angle and unit weight are all simple-averaged and then the critical depth is calculated. The final collapse occurs in the same way as the first, but with use of only the outer material's properties.

According to the source code, the side-slope collapses does not occur instantly but rather along time. Through the subroutine SLUMP, to be explained in Section 3.2.6, once the collapse occurs it is measured the time to remove the material and how many time-steps it is required. Then, it is measured the increment of the side-slope angle based on that number of time-steps and this increment is added while the collapsed material is not entirely removed. Furthermore, the breach enlargement is measured by Equations (3.10) and (3.11):

$$B_o = B_o + 2\frac{DH}{\cos\alpha}, \tag{3.10}$$

$$B_t = B_o + 2(H_u - H_l)\tan\alpha. \tag{3.11}$$

Where:

B_o is the bottom width of the breach [ft];

B_t is the top width of the breach [ft];

H_u is the top elevation of the dam [ft];

H_c is the breach elevation [ft];

DH is the erosion [ft];

α is the side-slope angle to the vertical [rad].

Another matter not described in the manual, and is similar to what was done to the breach's slope stability, concerns when a dam with an inner core is simulated. Looking at the Figure 9, together with the lack of explanation in the manual, the user may imagine that the model designs the dam with an inner core of exact same crest's width as informed in the inputs. However, when turning to the code it is verified that the entire dam's structure is homogenized, i.e. made of only one material, and is treated that way through all the calculations. This procedure is done depending on the region or stage of failure (KG or KREG as denoted in the source code), defined as follows:

- Reservoir filling (KG=-1)
- No erosion on grass (KG=0)
- Erosion of downstream face (KG=1)
- Erosion of upstream face (KG=2)
- Drainage of reservoir with breach size fixed at maximum (KG=3)
- Piping mode (KG=4)
- Collapse mode (KG=5)

Then, geometric relations are determined accordingly to these stages, thus estimating two weighting factors FK1 and FK2 ranging from 0 to 1. With these factors, all the properties of the materials (porosity, friction angle, unit weight, cohesion and D_{90}/D_{30} ratio) are pondered.

When accounting the breach side slopes, Equation (3.1) becomes the Equation (3.12). To measure the normal flow depth on a rectangular channel the Manning equation is used and on a trapezoidal channel the Newton-Raphson method. However, once again there is a conflict

between the manual and the source code concerning the trapezoidal channel determination, which will be addressed later on Section 3.2.3.

$$Q_b = 3B_o(H_y - H_c)^{1.5} + 2\tan\alpha(H_y - H_c)^{2.5}. \tag{3.12}$$

Where:

Q_b is the breach outflow [cfs];

H_c is the breach's bottom elevation [ft];

B_o is the breach's bottom width [ft];

α is the breach's side slope with the vertical [rad].

Now if piping is the failure mode, an initial elevation must be informed. In this case, the breach outflow is defined by Equation (3.13) and the formed channel erodes both up- and downwards. The erosion is actually measured at the bottom channel, as if in overtopping, and mirrored to the channel top. At a certain point, the portion above the pipe collapses and the flow changes to weir type. This transition to overtopping occurs when the reservoir's water elevation is equal to or lower than the piping's top elevation plus half of its height.

$$Q_b = A\left[\frac{2g(H_y - H_p)}{1 + \frac{fL}{D}}\right]^{0.5}, \tag{3.13}$$

$$Re = 83,333\frac{Q_b D}{A}. \tag{3.14}$$

$Re < 2,000$:

$$f = \frac{64}{Re}. \tag{3.15}$$

$Re \geq 2,000$:

$$f = 0.105\left(\frac{D_{50}}{D}\right)^{\frac{1}{6}}. \tag{3.16}$$

Where:

A is the piping area [ft^2];

g is the gravity [ft/s^2];

H_y is the reservoir water elevation [ft];

H_p is the initial piping elevation [ft];

f is the Darcy's friction factor [-];

L is the piping length [ft];

D is the piping diameter [ft];

Re is the Reynolds number [-].

Once this transition happens, the erosion ceases until the collapsed material is removed. This is evaluated by the sediment transport equation used by the model, Equation (3.18), with the exception that the Shields' parameter is not accounted for since the collapsed material is already loosed and thus, shows no resistance against the outflow.

The reservoir's level variation is determined by law of mass conservation represented by Equation (3.17), solving for DY which is the reservoir's level variation:

$$DY = \frac{0.0826\Delta t}{S_a}(\overline{Q_i} - \overline{Q_b} - \overline{Q_{sp}} - \overline{Q_o}), \tag{3.17}$$

DY is reservoir's level variation [ft];

Δt is the time interval [h];

S_a is the reservoir's surface area at a certain elevation [acres];

$\overline{Q_i}$ is the averaged reservoir inflow [cfs];

$\overline{Q_b}$ is the averaged breach outflow [cfs];

$\overline{Q_{sp}}$ is the averaged spillway outflow [cfs];

$\overline{Q_o}$ is the averaged crest overflow [cfs].

With respect to the sediment transport, it was used the Meyer-Peter-Müller equation modified by SMART (1984), which can be observed in Equation (3.18). SMART (1984) validated the Meyer-Peter-Müller equation to channels with slopes of 0.04% to 20%. Meanwhile, FREAD (1991) added, mostly, EquationS (3.19) and (3.20) to account for cohesive and non-cohesive materials, respectively. The Equation (3.20) was used because the Meyer-Peter-Müller equation is suitable for non-cohesive materials, otherwise Shields parameter can not be considered, according to Graf (1984).

$$Q_s = 3.64\left(\frac{D_{90}}{D_{30}}\right)^{0.2} P\left(\frac{R_h^{\frac{2}{3}}}{n}\right) S^{1.1}(R_h S - \Omega). \tag{3.18}$$

- For non-cohesive materials:

$$\Omega = 0.0054\tau_c D_{50}. \tag{3.19}$$

- For cohesive materials:

$$\Omega = \frac{b^{'}}{62.4} PI^{c^{'}}. \tag{3.20}$$

Where:

Q_s is the rate of sediment transport [cfs];

$\frac{D_{90}}{D_{30}}$ is the ratio of grain diameter for which 90% and 30% of the sample is finer [-];

R_h is the hydraulic depth [ft];

P is the breach perimeter [ft];

n is the Manning's coefficient;

S is the breach slope [-];

Ω is the Shields' critical parameter accounting the material cohesion and breach slope [-];

τ_c is the Shields' critical parameter accounting the breach slope [-];

PI is the material's plasticity index [-];

$b^{'}$ is an empirical coefficient [-];

$c^{'}$ is an empirical coefficient [-].

Here, as well, there is a difference between the manual and source code with regard to the measurements of Shields' parameters that will be explained later on this section, when commenting on the subroutine SHIELD in Section 3.2.5.

Regarding Manning's coefficient n, it is determined by Equation (3.21), Strickler's equation, when not informed. According to the manual, the coefficient of the equation should be 0.013 and the D_{50} powered by 0.67, which is a mistake. The correct form of the Strickler's equation is as in Equation (3.21) according to HENDERSON (1966) and it is so used in the source code, dividing however the mean diameter per 305 to convert it from millimeters, as informed in the inputs, to feet. This conversion of units turns the 0.034 coefficient to 0.013, as it is in the manual.

$$n = 0.034 D_{50}^{0.167}. \tag{3.21}$$

Where:

n is the roughness;

D_{50} is the mean diameter [ft].

Moreover, if n is informed as input and its value is greater than 0.35, it is corrected by Equations (3.22) to (3.25). These equations describe a Moody diagram as the manual informs, but it does not present the equations that are only in the source code to be seen. The manual also informs that this procedure should be done when Manning's coefficient is greater than 0.99 instead.

$$XF = \frac{D_{50}}{Y_n}. \tag{3.22}$$

- $XF < 0.005$:

$$DF = 0.113 XF^{0.251}. \tag{3.23}$$

- $XF \geq 0.005$:

$$DF = 0.03 + 1.4(XF - 0.005). \tag{3.24}$$

$$n = 0.0926 Y_n^{0.167} \sqrt{DF}. \tag{3.25}$$

Where:

D_{50} is the mean diameter [ft];

Y_n is the normal depth of flow [ft].

Another capable structure collapse is caused by the water pressure on the upstream face surpassing the material's resistive forces. According to the source code, it will happen only to man-made dams when in overtopping failure and with the erosion along the downstream face of the dam.

The following equations for this collapse analysis are shown as presented in the source code and the manual, all of them with errors. Right after introducing them, the correct form will be presented.

The hydrostatic force F_w acts upon a wedge of height Y_c, measured from the breach bottom, and the resistive forces are divided in four components as seen bellow. All the forces can be observed in Figure 11 and measured by Equations (3.26) to (3.30):

- Shear force F_{sb} along the bottom of the wedge;
- Shear force F_{ss} along both sides of the wedge;
- Cohesive force F_{cb} along the bottom of the wedge;
- Cohesive force F_{cs} along both sides of the wedge.

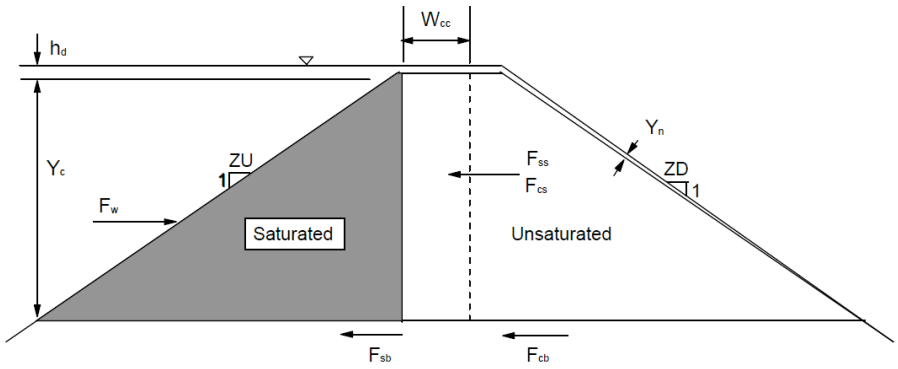

FIGURE 11 – Side view of dam with pressure force and resistive forces in collapse mode. Adapted from FREAD (1991).

$$F_w = 0.5\gamma_w(B_o + H_c \sin\alpha)(Y_c + 2h_d), \tag{3.26}$$

$$\begin{aligned} F_{sb} = \quad & \tan\phi[(\gamma_s - \gamma_w)0.5ZU(B_o + H_c \sin\alpha)Y_c^2 + \gamma_s B_o W_{cc} Y_c + \\ & + \gamma_s 0.5ZD(B_o + H_c \sin\alpha)Y_c^2 + 0.67h_d W_{cc} g + (1 + ZD^2)^{0.5} Y_c Y_n B_o \gamma_w], \end{aligned} \tag{3.27}$$

$$F_{ss} = \gamma_s \left(\frac{1 - \sin\phi}{1 + \sin\phi}\right) \tan\phi[W_{cc} + (ZU + ZD)Y_c]Y_c^2, \tag{3.28}$$

$$F_{cb} = CB_o[W_{cc} + (ZU + ZD)Y_c], \tag{3.29}$$

$$F_{cs} = 2C\left[W_{cc} + (ZU + ZD)Y_c\left((B_o + H_c \sin\alpha) + 2\frac{Y_c}{\cos\alpha}\right)\right]. \tag{3.30}$$

Where:

g is the gravitational acceleration [ft/s^2]

B_o is the breach bottom width [ft];

H_c is the breach's bottom elevation [ft];

γ_s is the material's specific weight [lbf/ft^3];

γ_w is the water's specific weight [lbf/ft^3];

α is the angle of breach's side slope with the vertical [rad];

ϕ is the material's friction angle [rad];

W_{cc} is the remaining crest width, still not eroded [ft];

ZU represents the upstream slope of the dam in 1:ZU [ft];

ZD represents the downstream slope of the dam in 1:ZD [ft];

h_d is the water elevation in the breach channel [ft];

Y_c is the height of the wedge to be collapsed, measured from the breach bottom and downwards [ft];

Y_n is the flow depth along the downstream face of the dam [ft];

C is the material cohesion [lb/ft^2].

It is always assumed that the downstream slope of the wedge is the same as the original dam, not considering the slope of the breach channel, from the analyzes of Equations (3.26) to (3.30).

Initially, Y_c is assumed to be 10 feet and the collapse is checked. If the water pressure is greater than the sum of all resistive forces, Y_c is increased by two feet and the program checks the collapse again. This procedure goes on until the water pressure is lower than the resistive forces and thus, the final computed height of the wedge is the determined value minus one feet. So, a volume for the collapsed material can be measured and the breach erosion stops until the complete removal of it.

To measure the volume of collapsed material, it is needed to know the rate of sediment transport which is done by Equation (3.31). It is not known the origin of this equation and no mention of it is present in the manual:

$$Q_s = 17,430B\left(\frac{A}{B}\right)^{1.67}\frac{S^2}{D_{50}^{1.67}}. \tag{3.31}$$

Where:

Q_s is the rate of sediment transport [cfs];

B is the bottom width of the breach before the collapse [ft];

A is the cross-sectional area of the breach before the collapse [ft^2];

S is the breach slope before the collapse [-];

D_{50} is the mean diameter of the material [mm].

In the source code, some differences exist to the manual in the collapse check. The initial height Y_c of the wedge is assumed as three feet instead of 10. The acting forces, with exception to F_{cb}, are also computed differently as shown bellow. The variables are the same as before with the addition of B_t as the breach's top width, expressed in feet:

$$F_w = 0.5\gamma_w Y_c(2Y_c + h_d)[0.5(B_o + B_t)], \tag{3.32}$$

$$F_{sb} = (\gamma_s - \gamma_w)Y_c \tan\phi\{[W_{cc} + 0.5(ZD + ZU)Y_c][0.5(B_o + B_t)]\}, \tag{3.33}$$

$$F_{ss} = 2(\gamma_s - \gamma_w)\tan\phi\left(\frac{1-\sin\phi}{1+\sin\phi}\right)\{[W_{cc} + 0.5(ZU + ZD)Y_c][0.5(B_o + B_t)]\}, \tag{3.34}$$

$$F_{cs} = 2C[0.5(B_o + B_t)][W_{cc} + (ZU + ZD)Y_c]. \tag{3.35}$$

The idea behind the measurement of the soil's resistive forces is the following. For the shear resistance, it is taken the volume of the analyzed section together with the weight of the soil to obtain the normal force and, in turn, the friction angle to obtain the horizontal component. For the cohesive resistance, it is taken the area of the rupture plane together with the cohesion to obtain the resistive strength. As for the hydrostatic pressure, it is taken the pressures at the top and bottom of the wedge together with the respective water volume to obtain the hydrostatic force.

The equations in the source code and the manual are similar in some aspects, but all present errors. For the hydrostatic force, Equation (3.32) is wrong due to the coefficient 2 and Equation (3.26) due to the absence of Y_c. To correctly account the hydrostatic force over the wedge of height Y_c, the pressure at the breach bottom and Y_c bellow must be taken. Thus, Equation (3.36) would be the correct one to measure the water force:

$$F_w = \gamma_w\{0.5Y_c[h_d + (Y_c + h_d)][0.5(B_o + B_t)]\}. \tag{3.36}$$

For the cohesive resistive force on the sides of the wedge, the rupture planes are on the sides and thus, Equation (3.37) measures correctly the area of these planes while the Equations (3.30) and (3.35) consider the horizontal plane instead:

$$F_{cs} = 2CY_c \left[W_{cc} + (ZU + ZD)\frac{Y_c}{2} \right]. \tag{3.37}$$

For the bottom shear resistance, the Equation (3.33) of the source code is incorrect because it does not consider that the wedge is only partially saturated, as shown in Figure 11, and does not account the water weight over the breach channel. As for the manual, Equation (3.27) is incorrect because the terms referring to the water weight do not consider the correct channel width of the breach to obtain this additional resistive force. The correct approach would be through Equation (3.38) that considers the saturation state as specified by Figure 11 and the water contribution:

$$\begin{aligned} F_{sb} = \quad & \tan\phi \left\{ Y_c[0.5(B_o + B_t)][\gamma_s(W_{cc} + 0.5Y_c ZD) + (\gamma_s - \gamma_w)0.5Y_c ZU] \right\} + \\ & + [0.5(B_o + B_t)][0.67\gamma_w h_d W_{cc} + (1 + ZD^2)^{0.5} Y_c Y_n \gamma_w]. \end{aligned} \tag{3.38}$$

Despite all of this, the approach of the source code is not entirely wrong, since it is in the safety side for not considering the buoyant force under the wedge and the water weight over the breach channel. In fact, the saturation state is an oversimplification, because the freatic line would extend itself to some point in the downstream face of the dam, making most of the soil saturated. As for the water weight, even though it would help on the stability, its contribution is small in comparison to the one from the soil.

Now for the side shear resistance, the correct approach would be to repeat the one for the bottom shear resistance and account the soil lateral pressure as expressed by Equation (3.39):

$$F_{ss} = 2\left(\frac{1 - \sin\phi}{1 + \sin\phi}\right) F_{sb}. \tag{3.39}$$

When testing the correct equations for the resistive forces, namely Equations (3.36), (3.38), (3.39), (3.37) and (3.29), with the validation tests of the original BREACH model, there were no differences in the results.

The flow submergence is also accounted for. After computing the parameters relative to the tailwater (Manning's coefficient, cross-section's area and top-width), a total outflow is estimated based on these conditions by Manning's equation. If this estimative is lower than the sum of spillway, breach and weir/overtopping outflow, the tailwater elevation *YTW* is increased in 0.5 feet and the tailwater conditions are estimated once again. This procedure repeats itself until the outflow determined by Manning's equation is greater the sum of spillway, breach

and weir/overtopping outflow. Then, the submergence factor is determined by the following equation:

$$SUB = 1.0 - 27.8\,[H_r - 0.67]^3\,. \tag{3.40}$$

In which:

$$H_r = \frac{YTW - H_c}{H_y - H_c}. \tag{3.41}$$

Where:

SUB is the submergence corrector factor [-];

H_c is the breach bottom elevation [ft];

H_y is the water elevation in the reservoir [ft].

According to the source code, the submergence factor is measured by Equation (3.40) if H_r is greater then 0.67. If H_r happens to be lower than 0.05, it is taken as 0.05. Comparing to the manual, this condition is not explained and the multiplier 27.8 in Equation (3.40) is actually 2.78.

Moreover, if SUB happens to be lower than its value from the previous time-step, SUB becomes equal to that previous value. The final value of SUB is safed in a secondary variable for comparison in the next time-step.

Only present in the source code as well, another factor is calculated right after SUB and it is used to further change/correct the breach outflow. This factor works similarly to SUB and is measured by Equation (3.42). Its origin is not known and it is not explained in the manual. The only explanation is a comment in the source code, stating that CV would be a submergence suppressor:

$$CV = 1 + 0.035\frac{Q_b^2}{(H_y - H_c)}CRL^2(H_y - H_l)^2. \tag{3.42}$$

Where:

CV is the submergence suppressor [-];

CRL is the crest length [ft];

H_c is the breach's bottom elevation [ft];

H_l is the river bed elevation [ft];

H_y is the water elevation in the reservoir [ft].

The order in which CV and SUB are used is the following. Right after the reservoir routing, the breach outflow is corrected by SUB. Close to ending the iterations at each time-step, CV and SUB are measured but only CV corrects the breach outflow.

Regarding the erosion measured at each time-step, named as DH, it is first estimated according to each case as shown in the flowchart in Appendix A. This estimate is used to measure the breach's outflow and geometry and sediment transport. Then, the erosion is actually measured with these informations by Equation (3.43), labeled as DHH in the source code, and compared with the estimate done previously:

$$DHH = \frac{3,600 Q_s DTH}{P(1 - POR)CL}. \tag{3.43}$$

Where:

DHH is the measured erosion [ft];

Q_s is the rate of sediment transport [cfs];

DTH is the time-step [h];

P is the breach perimeter [ft];

POR is the material porosity [-];

CL is the channel length [ft].

If the difference between them are within an acceptable error, provided as input, DH is incremented and the calculations go forward to the next time-step. Otherwise, the program returns to measure the breach and outflow after correcting the estimated erosion, initiating a new convergence-step. How the model checks this convergence is represented in the flowchart in Appendix A.

As for the time-step DTH, it is adjusted according to the stage of simulation. In general, if the erosion is great the time-step is reduced and vice-versa. Some of the recurrent adjustments are the following:

Piping:

$$DTH_i = 0.25 DTH_{i-1}. \tag{3.44}$$

Tailwater level above breach elevation:

$$DTH_i = 0.05DTH_{i-1}. \tag{3.45}$$

No convergence between estimated and measured erosions:

$$DTH_i = 0.5DTH_{i-1}. \tag{3.46}$$

$DH \geq 3$:

$$DTH_i = 0.5DTH_{i-1}. \tag{3.47}$$

$1.5 \leq DH < 3$:

$$DTH_i = \frac{DTH_{i-1}}{1.1}. \tag{3.48}$$

$DH \leq 0.5$:

$$DTH_i = 1.1DTH_{i-1}. \tag{3.49}$$

A final comment is done about how the model knows when to end the simulations. For this to happen and the results be plotted, one of the four conditions bellow must be met.

- Estimated simulation time (input) is reached;
- Reservoir is entirely depleted;
- Dam is entirely breached and breach outflow is less than 10% of its peak;
- Simulation surpassed the imposed limit of 5,000 iterations.

3.2 SUBROUTINES

When analyzing the source code, it is seen that 13 subroutines are presented that help the main program performs the simulations. These subroutines will be detailed in the sequence.

3.2.1 RDDATA

This subroutine reads all the inputs of the program and write them in the output file. All the inputs are listed in the Appendix B.

The values of time associated to the reservoir inflows are checked and the last value of time is defined as the maximum simulation time. If the informed estimated simulation time is greater than this maximum, the estimated time is equaled to it.

Furthermore, the area between consecutive top widths of tailwater is measured by averaging each consecutive pair and multiplying them by the difference between respective tailwater elevations. These calculated cross-section areas are later used in the modeling.

The maximum sediment concentration $SEDCON$ is converted to a sediment-water ratio $SWRM$ by Equation (3.50) and this ratio is used to determine a maximum acceptable sediment outflow:

$$SWRM = \frac{SEDCON}{1 - SEDCON}. \tag{3.50}$$

Whenever the ratio between the sediment and breach outflow is greater than $SWRM$, the sediment outflow is taken as a percentage of the breach outflow, this percentage defined by $SWRM$. Moreover, $SECON$ should range, usually, from 0.4 to 0.5 according to the source code.

Limits to the size of the breach are imposed as well. The maximum bottom width *BMX* is defined by Equation (3.51) which considers a trapezoidal cross-section with slopes of $40°$, divided per 57.2 to convert it to rad:

$$BMX = CRL - 2\frac{(H_u - H_l)}{\tan\frac{40}{57.2}}. \tag{3.51}$$

Where:

BMX is the maximum bottom width [ft];

CRL is the crest length [ft];

H_u is the initial reservoir water elevation [ft];

H_l is the dam bottom elevation [ft].

The maximum top width *BTMX* is set equal to the crest length if *BTMX* is not informed in the input file or equal to *BMX* if lower than *BMX*. Finally, this subroutine counts the number of provided data for head of spillway flow which is used in some calculations.

3.2.2 RECT

This subroutine computes the area, perimeter and hydraulic radius of a rectangular channel when in overtopping failure. The depth is also evaluated by Manning's equation and if it happens to be greater than two thirds of the difference between the reservoir water level and breach bottom elevations, the normal depth is set as the two thirds of the difference. This is executed because of the slope stability analysis described before on this section and represented in Figure 10.

3.2.3 TRAP

It is similar to the RECT subroutine, but now it is applied for determining the normal depth in a trapezoidal channel. As commented before, on this part of the model there is a difference between the procedure in the manual and in the code.

According to the manual, the normal depth y_n is assessed by Newton-Raphson method through the EquationS (3.52) to (3.57), reaching convergence when absolute error between y_n^{k+1} and y_n^k is equal to or less than 1%, with a first estimate for the depth done by Manning's equation and assuming the wetted perimeter approximately the bottom width.

Attention should be given to Equations (3.53), (3.54), (3.56) and (3.57) which contain an error to be corrected in the sequence:

$$y_n^{k+1} = y_n^k - \frac{f(y_n^k)}{f'(y_n^k)}, \tag{3.52}$$

$$f(y_n^k) = Q_b P^{0.67} - 1.49 S^{0.5} A^{1.67}, \tag{3.53}$$

$$f'(y_n^k) = 0.67 Q_b \left(\frac{\frac{1}{\cos\alpha}}{P^{0.333}} \right) - 1.67 \left(\frac{1.49}{n} \right) S^{0.5} A^{0.67} 0.5 (B_o + B_t), \tag{3.54}$$

$$A = 0.5 (B_o + B_t) y_n^k, \tag{3.55}$$

$$B_t = B_o + (y_n \tan\alpha), \tag{3.56}$$

$$P = B_o + \left(\frac{y_n}{\cos\alpha} \right). \tag{3.57}$$

Where:

y_n is the flow depth [ft];

Q_b is the breach outflow [cfs];

P is the wetted perimeter [ft];

B_o is the breach bottom width [ft];

B_t is the breach top width [ft];

A is the cross-sectional area [ft^2];

S is the channel slope [-];

$f(y_n^k)$ is the Manning's equation for the flow depth [ft];

$f'(y_n^k)$ is the derivative in flow depth of $f(y_n^k)$ [-];

α is the breach's slope angle with the vertical [rad] as in Figure 10;

k is an iteration counter.

The errors, as commented above, are the following. Equations (3.56) and (3.57) are without the multiplier 2 to consider both sidewalls of the breach's cross-section when determining the top width and wetted perimeter of the cross-section. The Equation (3.53) is missing the Manning's coefficient dividing the last term of the equation, but it is present in its derivative form in Equation (3.54). Still on this equation, it has missing a multiplier 2 in its first term due to the error previously found in Equation (3.57).

However, in the source code a different procedure is done. A maximum normal depth *YMAX* is set as two times the normal depth in the rectangular channel while a minimal depth *YMIN* is set as half of it and an auxiliary variable *YSV* is set equal to *YMAX*. Then, a first estimate is done by assuming that the normal depth *Y* is an average between *YMAX* and *YMIN*, what allows the measurement of breach's top width, area, perimeter and hydraulic radius by the same equations from the manual, which leads to the breach outflow through Manning's equation.

Right after, this computed outflow is compared to another estimated breach outflow obtained by the subroutine WEIR in Section 3.2.7, to be presented later on. In case the computed outflow is greater, *YMAX* becomes equal to *Y* and if it is lower, *YMIN* is equaled to *Y*. The convergence is verified by the absolute error between *Y* and *YSV*, which leads to two procedures.

If the error is greater than 1%, the computed normal depth becomes the new *YSV* and the calculations go back to the averaging between the maximum and minimum depths to find a new *Y* for the breach channel. If after 50 iterations there is still no convergence, *YMAX* is set as 10 times the normal depth in the rectangular channel and *YMIN* is set to zero, returning then to averaging *YMAX* and *YMIN* with a total of more 50 iterations for achieving

convergence. If after all this interactions the error is greater than 1%, a message is printed in the output informing of it and the depth in the trapezoidal channel is approximated as the depth in the rectangular channel.

If the error is lower than 1% or the depth was approximated as the depth in the rectangular channel, this obtained depth is compared to two thirds of the difference between reservoir water level and breach bottom elevations and it is set equal to the difference if greater. This analysis is due to the stability check of breach side slopes to account for the water contribution, seen in Figure 10.

Rewriten this subroutine to do the Newton-Raphson method as described in the manual and testing it, the model converged to the same answer. The only difference is that it took more iterations for the subroutine to find the correct normal depth.

3.2.4 TWSEC

The function of this subroutine is to compute some parameters relative to the tailwater. Before being called, if the program is on its third or previous iteration, the tailwater elevation *YTW* is assumed to be the first informed value from the input of elevations *HSTW* associated with the top widths of tailwater cross-sections. If not, the elevation is the own *YTW* minus two feet and if it happens to be inferior to the first *HSTW*, it is equaled to it plus 0.5 feet.

The measurements are done by a linear interpolation. In this subroutine, starting from the second informed value the inputs of tailwater elevation are scanned. If a value is equal to or greater than *YTW*, the subroutine keeps a track of the position/index *k* associated with it and the previous one (*k-1*). Then, the difference between the tailwater elevations *DH* relative to them are calculated along with the difference between the corresponding top widths *DB* and Manning's roughness *DC*. The difference between tailwater elevations *DY* is also measured. Thus, top width, area and Manning's rugosity for the tailwater are further estimated by interpolation as shown by Equations (3.58) to (3.60). The variables *YTW*, *DH*, *DB*, *DC* and *DY* are expressed in feet:

$$B = BSTW_{(k-1)} + \left(\frac{DB}{DH}\right) DY, \tag{3.58}$$

$$A = ASTW_{(k)} + 0.5(BSTW_{(k)} + B)DY, \tag{3.59}$$

$$CN = CMTW_{(k)} + \frac{DC}{DH} DY. \tag{3.60}$$

Where:

B is the top width of tailwater [ft];

BSTW is a input for top width of tailwater [ft];

A is the area of a tailwater cross-section [ft^2];

ASTW is a input for tailwater area [ft^2];

CN is the Manning's coefficient of the tailwater;

CMTW is the input of Manning's coefficient of each tailwater cross-section.

3.2.5 SHIELD

According to the manual, the particle's Reynolds number (Re^*) is measured by Equation (3.62) and, depending on its value, the critical dimensionless Shields parameter ($\tau_c^{'}$) is determined either by Equation (3.63), (3.64) or (3.65). The actual critical Shields parameter (τ_c) can be obtained then by Equation (3.61) which accounts for the breach slope:

$$\tau_c = [\cos(\arctan S)(1 - 1.54S)]\tau_c^{'}, \tag{3.61}$$

$$Re^* = 1,524 D_{50}(R_h S)^{0.5}. \tag{3.62}$$

$Re^* < 3$:

$$\tau_c^{'} = \frac{0.122}{(Re^*)^{0.97}}. \tag{3.63}$$

$3 \leq Re^* \leq 10$:

$$\tau_c^{'} = \frac{0.056}{(Re^*)^{0.266}}. \tag{3.64}$$

$Re^* > 10$:

$$\tau_c^{'} = 0.0205(Re^*)^{0.173}. \tag{3.65}$$

Where:

D_{50} is the particle diameter [mm];

R_h is the hydraulic radius of the flow [ft];

S is the channel slope [-].

The Equation (3.62) has an error in its coefficient, where it is 1,524 on the manual and 1,528 on the program. Looking further the source code, it is noticed another divergence from the manual regarding $\tau_c^{'}$ that is evaluated as follows:

$Re^* \leq 30$:

$$\tau_c^{'} = 10^{-1.208-0.194 \log Re^*}. \tag{3.66}$$

$30 < Re^* \leq 200$:

$$\tau_c^{'} = 10^{-1.49+0.35(\log Re^*-1.48)}. \tag{3.67}$$

$200 < Re^* \leq 25,000$:

$$\tau_c^{'} = 0.062. \tag{3.68}$$

$25,000 < Re^* \leq 90,000$:

$$\tau_c^{'} = 10^{-1.21+1.09(\log Re^*-4.4)}. \tag{3.69}$$

$Re^* > 90,000$:

$$\tau_c^{'} = 0.25. \tag{3.70}$$

To check if these limits are reached, it was written into the source code that the particle's Reynolds number and critical Shields' parameter should be plotted. From the cases for validation of the original BREACH, the one of Teton dam was selected as a test subject. The Figure 12 shows that the Shields' parameter dos not go beyond the limit of 0.062.

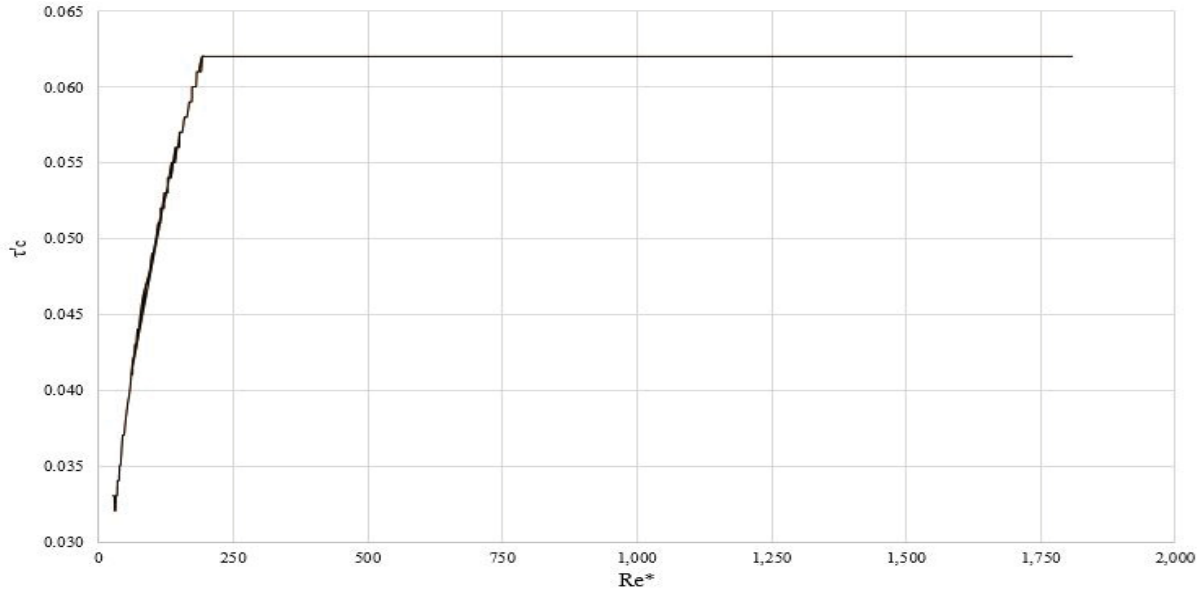

FIGURE 12 – Development of the critical Shields' parameter for the case of Teton dam (The author, 2019).

3.2.6 SLUMP

To check the occurrence of side slope collapse of the breach, this subroutine compares the breach's critical depths against the actual depth decreased by a third of the flow depth to account the water influence on the slope stability. These critical heights and others associated parameters are represented in Figure 10 and are measured by Equations (3.6) to (3.5).

When all three collapses are checked, the volume of collapsed material is computed together with the time to erode it based on the sediment outflow. This subroutine also measures the growth of the side slope per time-step based on the time-step at the first convergence-step.

3.2.7 WEIR

This subroutine computes the breach outflow through a broad-crested weir equation. According to the manual, Equation (3.12) is supposed to be used, but a different coefficient actually appears.

In the source code, the equation is presented as bellow in which the first term represents the outflow over the breach bottom and the second the outflow along the breach side slopes, which has the coefficient 2.2 instead of 2 as in Equation (3.12):

$$Q_b = 3B_o(H_y - H_c)^{1.5} + 2.2\tan\alpha(H_y - H_c)^{2.5}. \tag{3.71}$$

Where:

Q_b is the breach outflow [cfs];

B_o is the bottom width of the breach [ft];

H_y is the water elevation in the reservoir [ft];

H_c is the bottom elevation of the breach [ft];

α is the breach's side slope angle with the vertical [rad].

3.2.8 INTPPL

In order to write in the output file the total outflow associated, this subroutine performs a linear interpolation with each outflow in order to plot it in a time discretized by the same time-step.

3.2.9 INTPS

To determine the reservoir surface areas for each specific water elevation, this subroutine performs a linear interpolation with the given data in the inputs.

3.2.10 INTPSP

In order to measure the spillway outflows for each specific spillway head, a linear interpolations is done with the data on the spillway from the input.

3.2.11 INTPT

To obtain the reservoir inflows for each specific time, a linear interpolations is done with the data on the reservoir from the input.

3.2.12 PLOT

This subroutine is the last one used in the program and it organizes the total outflow data, thus plotting the hydrograph.

3.2.13 GRASSN

This subroutine measures the roughness of the grass cover. At the beginning, if it is checked that no grass erosion occurs, then the subroutine is ended. But if there is erosion or there is no grass cover, the next computational steps will occur based on the cover length provided in the input. The specific weir flow over the downstream face of the dam will determine, as well, the procedures done by the subroutine.

If the specific weir flow *QUW* is less than 10 cfs:

1. If cover length is greater than or equal to 30 inches, then factor FK1 is 0.15 and FK2 is -0.504;
2. If cover length is greater than or equal to 11 inches and lower than 30 inches, then factor FK1 is 0.082 and FK2 is -0.395;
3. If cover length is greater than or equal to 2 inches and lower than 11 inches, then factor FK1 is 0.06 and FK2 is -0.301;
4. If cover length lower than 2 inches, then factor FK1 is 0.037 and FK2 is -0.2065.

The Manning's coefficient *CNG* is thus measured by Equation (3.72):

$$CNG = FK1(QUW^{FK2}). \tag{3.72}$$

If the specific weir flow *QUW* is equal to or greater than 10 cfs:

1. If cover length is equal to or greater than 30 inches, then factor FK1 is 0.047 and FK2 is 1.818;
2. If cover length is equal to or greater than 11 inches and lower than 30 inches, then factor FK1 is 0.033 and FK2 is 6.667;
3. If cover length is equal to or greater than 2 inches and lower than 11 inches, then factor FK1 is 0.03 and FK2 is 10;
4. If cover length is lower than 2 inches, then factor FK1 is 0.023 inches and FK2 is 20.

The Manning's coefficient *CNG* is thus measured by Equation (3.73):

$$CNG = FK1 - \frac{QUW - 10}{FK2}. \tag{3.73}$$

4 ZONED DAM - NEW FEATURE

The BREACH model is a resourceful tool for dam-break modeling suitable for a wide range of applications, as observed in Chapter 3. However, it is not adequate for breaching of cofferdams, a common structure used for river deviations in hydropower plant projects as presented in Section 2.1. Despite this limitation, the BREACH model was used for analysis of a real cofferdam breached by piping, which has detailed informations omitted in this thesis due to legal reasons.

From the related works on dam-break described in Section 2.4, the HR BREACH model developed by M. MORRIS (2011) would be the best choice for this case. However, the zones that this model simulates differ from one another only by the erodibility, i.e. level of compaction, meaning that the material are all the same. Because of this, the HR BREACH would not be entirely suitable for modeling the breached cofferdam.

Thus, with the desire to better reproduce this event, taking advantage of the BREACH model being open-source and inspired by the feature of the HR BREACH for zoned dams, it was devised a new routine for zoned dams to the BREACH model. Instead of using the erodibility as in the HR BREACH, this routine models each zone with different materials (porosity, D_{90}/D_{30} and D_{50}), being a plus in comparison to the work of M. MORRIS (2011) and a new feature not seen in any other model.

To inform the standard BREACH model that a zone is simulated (new feature), the user must write in the input file the following data in the presented order:

MODE: Equal to 1 if a zone is within the dam, otherwise equal to 0;

ZD_{zone}: Slope of the downstream face of the zone [1 : ZD_{zone}];

WC_{zone}: Width of zone [m];

H_{zone}: Top elevation of the zone [m];

D_{50}: Grain size of zone material which 50% is finer [mm];

UW_{zone}: Unit weight of zone material [kg/m^3];

COH_{zone}: Cohesion of zone material [kg/m^2];

AFR_{zone}: Internal friction angle of zone material [°];

POR_{zone}: Porosity of zone material [%];

D_{90}/D_{30}: Ratio of D_{90} to D_{30} grain size of zone material [-];

CN_{zone}: Manning's coefficient of zone material. If left blank, it is measured as a function of grain size by Equation (3.21) as the standard model procedure.

These zones are always adjacent to the upstream face of the dam, thus not needing to provide the upstream slope which is the same as the dam's. The remaining necessary inputs are listed in Appendix B and the main outputs are in turn in Appendix C. Contrary to the original model, the inputs are informed in S.I and the outputs are given accordingly. However, in the source code the model works still in the Imperial System of Units, converting back and forth from each metric system, and it was done this way to avoid any error from adding or changing coefficients of the equations.

To account for a zone in the dam, the new routine checks the position of the breach channel relative to the zone and the dam itself. From it, geometric relations are taken to measure the influence of the zone at each time-step that is performed differently whether overtopping or piping is the failure mode. The material properties of the dam are then not considered anymore and the model works only with the pondered properties between the dam and the zone.

Recalling once again, the BREACH model is able to simulate a composite dam by averaging the materials properties based on geometric relations taken at each time-step. If the user wishes to insert a zone within such dam, the model will perform as usual until the breach reaches the zone, moment from which the model ceases to average the materials of the composite dam (outer and inner cores).

An important remark about the routine is that it was performed a modeling with a zone with the same properties as the dam, which was a homogeneous one. The results remained unaltered, as they were supposed to, showing that the routine presented no errors at first.

The analyses and results to be presented in this section were done modeling a zone with the same material properties as the dam, with exception of the D_{50}, D_{90}/D_{30} and the porosity. It was so in order to consider that the zone was build with materials presented at the dam site, the same used for the dam changing only the crushing of the material.

Furthermore, D_{50} and D_{90}/D_{30} are, respectively, indirectly and directly proportional to the rate of sediment transport defined by Equation (3.18) and the porosity is indirectly proportional to the erosion measurement by Equation (3.43). Thus, increasing the mean diameter makes the material "heavier", while reducing the D_{90}/D_{30} makes it more uniform and reducing the porosity reduces its pore size, all of this helping against the erosion.

For the analyses, the D_{50} were always fixed in 25, 50, 75 and 100 mm while the D_{90}/D_{30} and porosity were accordingly to each modeling test. Moreover, the analyses checked the influence of zones with heights of 30%, 40%, 50% and 60% of the dam height.

The effectiveness was measured by checking the peak outflow, time to peak and

breach dimensions.

4.1 OVERTOPPING

Once the breach channel reaches the zone, the routine measures the remaining non-eroded area of the zone according to the position of the breach channel, as shown in Figure 13.

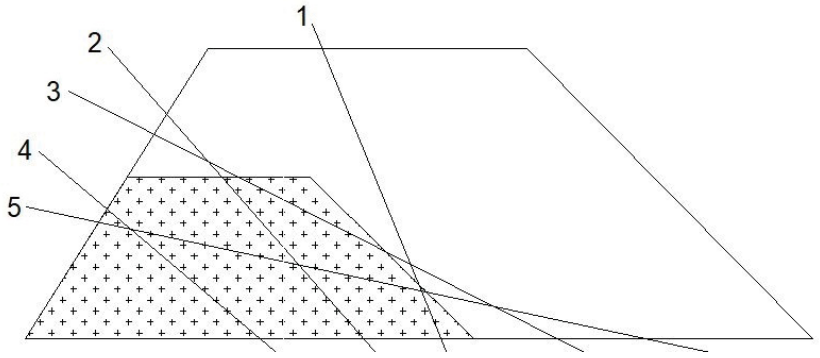

FIGURE 13 – Schematic of breach channel positions in overtopping (The author, 2019).

The position of the breach channel is measured by Equation (4.1) and its intersection with the downstream face of the zone by Equation (4.2):

$$x_{breach} = \frac{y_{breach} - (H_c - H_l)}{\tan(\pi - \arctan(S_{breach}))} + (WC - XP) + (H_c - H_l)ZU, \tag{4.1}$$

$$\begin{aligned} y_{intersection} = \quad & \tfrac{1}{1-\lambda}[(H_c - H_l) + \tan(\pi - \arctan(S_{breach}))(WC_{zone} + \\ & + H_{zone}(ZU + ZD_{zone}) - (WC - XP) - (H_c - H_l)ZU)], \end{aligned} \tag{4.2}$$

$$\lambda = \frac{\tan(\pi - \arctan(S_{breach}))}{\tan\left(\pi - \arctan\left(\frac{1}{ZD_{zone}}\right)\right)}. \tag{4.3}$$

The Equations (4.4) to (4.8) measure the non-eroded area of the zone for each breach position, lines 1 to 5 in Figure 13. The total zone area is also measured and by Equation (4.9):

- Position 1:

$$\begin{aligned} A_{zone} = \quad & \tfrac{(H_{zone} - H_l)}{2}[WC_{zone} + (WC_{zone} + H_{zone}(ZU + ZD_{zone}))] - \\ & - \left[\tfrac{y_{intersection}}{2}[(WC_{zone} + H_{zone}(ZU + ZD_{zone})) - x_{breach}(0)]\right]. \end{aligned} \tag{4.4}$$

- Position 2:

$$A_{zone} = \frac{H_{zone}}{2}[(x_{breach}(H_{breach}) - H_{zone}ZU) + x_{breach}(0)]. \tag{4.5}$$

- Position 3:

$$\begin{aligned} A_{zone} = & \frac{(H_{zone}-HL)-y_{intersection}}{2}[(x_{breach}(H_{zone}) - (H_{zone} - H_l)ZU) + \\ & +(x_{breach}(y_{intersection}) - y_{intersection}ZU)] + \frac{y_{intersection}}{2}[(x_{breach}(y_{intersection}) - \\ & -y_{intersection}ZU) + (x_{breach}(y_{intersection}) + y_{intersection}ZD_{zone})]. \end{aligned} \tag{4.6}$$

- Position 4:

$$A_{zone} = \frac{(H_c - H_l)x_{breach}(0)}{2}. \tag{4.7}$$

- Position 5:

$$\begin{aligned} A_{zone} = & \left(\frac{x_{breach}(0)(H_c-H_l)}{2}\right) - \frac{y_{intersection}}{2}[x_{breach}(0) - \\ & -(WC_{zone} + H_{zone}(ZU + ZD_{zone}))]. \end{aligned} \tag{4.8}$$

- Total area:

$$A_{zone}^{total} = \frac{(H_{zone} - H_l)}{2}[WC_{zone} + (H_{zone} - H_l)(ZU + ZD_{zone})]. \tag{4.9}$$

Where:

A_{zone} is the area of the non-eroded zone [ft^2];

x_{breach} is the position of the breach channel for any given elevation [ft];

y_{breach} is the elevation of the breach channel for any given position [ft];

$y_{intersection}$ is the intersection height between the breach channel and downstream face of the zone [ft];

S_{breach} is the slope of the breach channel [-];

H_{zone} is the top elevation of the zone [ft];

ZD_{zone} is the slope of the downstream face of the zone [1 : ZD_{zone}];

WC_{zone} is the width of the zone [ft];

WC is the width of the dam [ft];

XP is the eroded distance along the width of the dam [ft];

ZU is the slope of the upstream face of the dam [1 : ZU];

H_c is the bottom elevation of the breach [ft];

H_l is the river bed elevation [ft];

λ is an auxiliary variable [-].

Then, the influence factor of the zone is measured by the relation between A_{zone} and A_{zone}^{total} at each time-step and it is used to ponder each zone property. The factor over the rest of the dam is taken as one minus the zone factor. The sum of the pondered properties of all materials is used throughout the model.

The routine was first tested with the landslide dam located on Mantaro river, Peru. This dam was overtopped and it was modeled with the BREACH model using the main inputs of Table 1, containing the main outputs as well.

In all the analyses a zone was modeled with a downstream slope of 1:2 and a crest width of 1,500 m. Due to the great proportions of the dam, it was chosen such crest width in order to have a zone that could impact the breaching process.

The resulting percentage differences of the analyzed parameters are presented in Appendix D and some of these results are represented bellow. Since the total time for this breaching case are too long, Figures 14 to 17 show only the first 24 hours of the event, revealing already the points of interest for the analyses.

Figure 14 shows the impact of a zone with fixed height of 50% the dam height, a porosity of 55%, a D_{90}/D_{30} of 300 and a D_{50} of 25, 50, 75 and 100 mm. The routine was capable of reducing the peak outflow in 16.82%, the time to peak in 5.97% and the breach in 19.36% on average. Moreover, the behavior of the results was directly proportional to the D_{50} variation, with exception of the time to peak. However, even though the smoothing of the hydrograph was satisfactory, the sensibility to the D_{50} was poor showing differences smaller than 1.5 percentage points in the results from the mean diameter of 25 mm to 100 mm.

TABLE 1 – Main inputs and outputs of Mantaro landslide dam simulation (The author, 2019).

INPUT			
El. Water surface [m]	170.69	D_{50} [mm]	11
El. Top dam [m]	170.69	Unit weight [kg/m^3]	480.46
El. Bottom dam [m]	0	Internal friction angle [°]	38
El. Piping [m]	0	D_{90}/D_{30}	300
El. Spillway [m]	0	Crest width [m]	0
Upstr. face slope [1V:x]	17	Porosity [%]	55
Downstr. face slope [1V:x]	8	Cohesion [kg/m^2]	488.14
OUTPUT			
Total time [h]	122.66	Breach depth [m]	104.45
Peak outflow [m^3/s]	13,811.29	El. Bottom breach [m]	66.24
Time to peak [h]	5.92	El. Water surface [m]	70.52

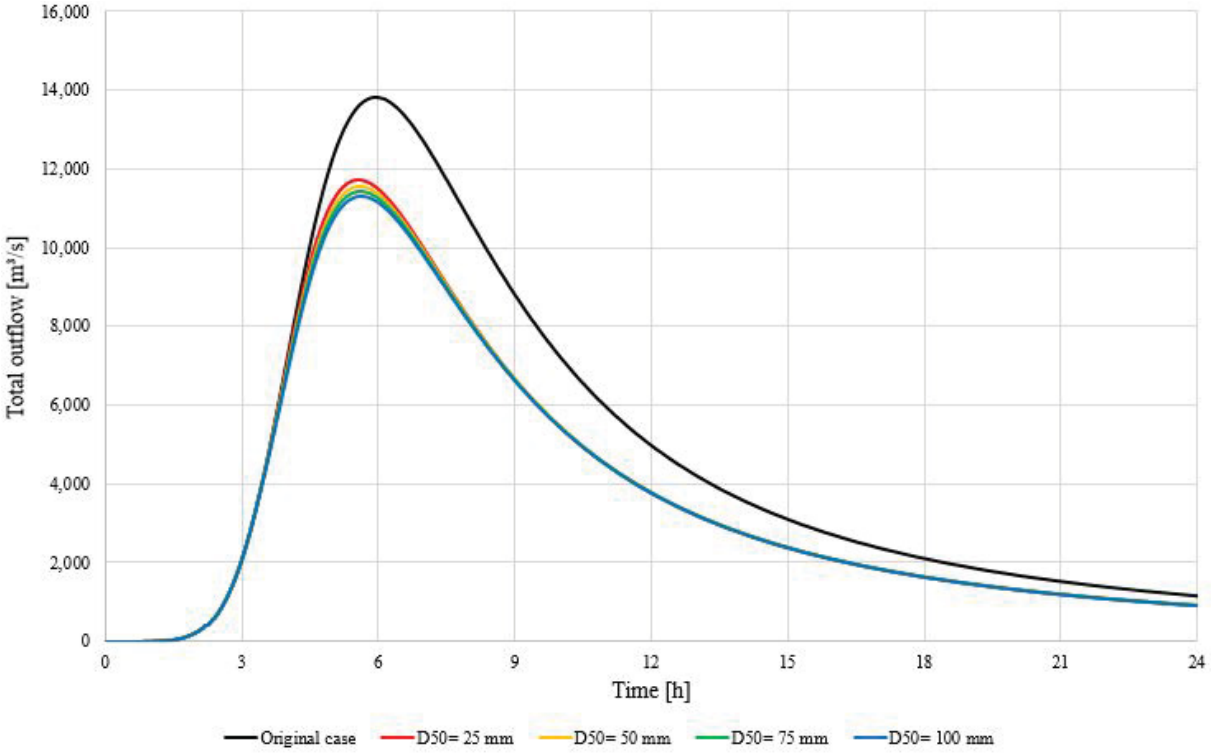

FIGURE 14 – Sensitivity analysis of Mantaro landslide dam for different D_{50} (The author, 2019).

Figure 15 shows the impact of a zone with fixed height of 50% the dam height, a porosity of 55%, a D_{50} of 25 mm and a D_{90}/D_{30} of 1, 100, 200, 300 and 400. Turning the zone material each time more uniform than the dam improved continuously the results. A zone with a D_{90}/D_{30} of 300, same as the dam, reduced the peak outflow in 15.07%, the time to peak in 6.58% and the breach in 18.78%. Even a less uniform zone of D_{90}/D_{30} equals to 400 was able to diminish the peak outflow in 10.48%, the time to peak in 7.17% and the breach in 17.1%. A theoretical zone with D_{90}/D_{30} of 1, in turn, reduced the peak outflow in 67.06%, the time to peak in 8.17% and the breach in 46.37%. Moreover, for the D_{90}/D_{30} of 1 it is noticeable an abrupt change in the outflow growth around time of 3.5 hours due to the zone starting to impact the breaching and causing great resistance against erosion, greater than in

the other simulations.

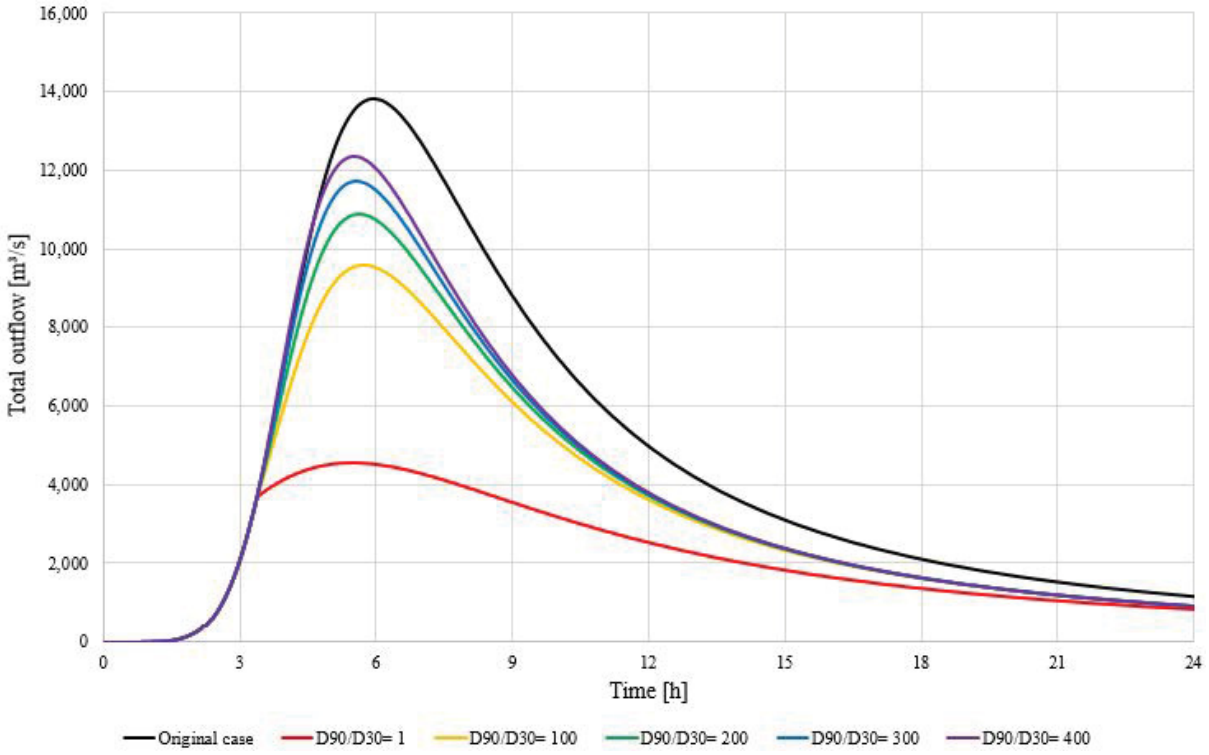

FIGURE 15 – Sensitivity analysis of Mantaro landslide dam for different D_{90}/D_{30} (The author, 2019).

In general, the reductions of the peak outflow and the breach are directly proportional to the D_{90}/D_{30} variations, while the time to peak is inversely. Concerning still the time to peak, it revealed a sudden increase in how much it was reduced.

Figure 16 shows the impact of a zone with fixed porosity of 55%, a D_{50} of 25 mm, a D_{90}/D_{30} of 300 and a height of 30%, 40%, 50% and 60% of the dam height. As the zone became higher the peak outflow and the breach reduced continuously. The reduction of time to peak was directly proportional to the increase of zone height except when it was 60% of the dam height.

The greatest impacts to the peak outflow and breach were for a zone height of 60% reducing the outflow in 27.18% and the breach in 23.03%. For the time to peak it was 6.58% the greatest reduction and for a zone height of 50% instead.

For a zone height of 30% the peak outflow remained the same while the breach decreased in 9.31%. Checking what happened at each time-step it was observed that the zone started being eroded around 5.75 hours after the beginning of simulation, while the peak outflow was reached around 5.93 hours after.

Figure 17 shows the impact of a zone with fixed height of 50% the dam height, a D_{90}/D_{30} of 300, a D_{50} of 25 mm and a porosity of 45%, 55% and 65%. As the zone material became less porous, the smoothing of the hydrograph was greater. For a porosity of 45% the

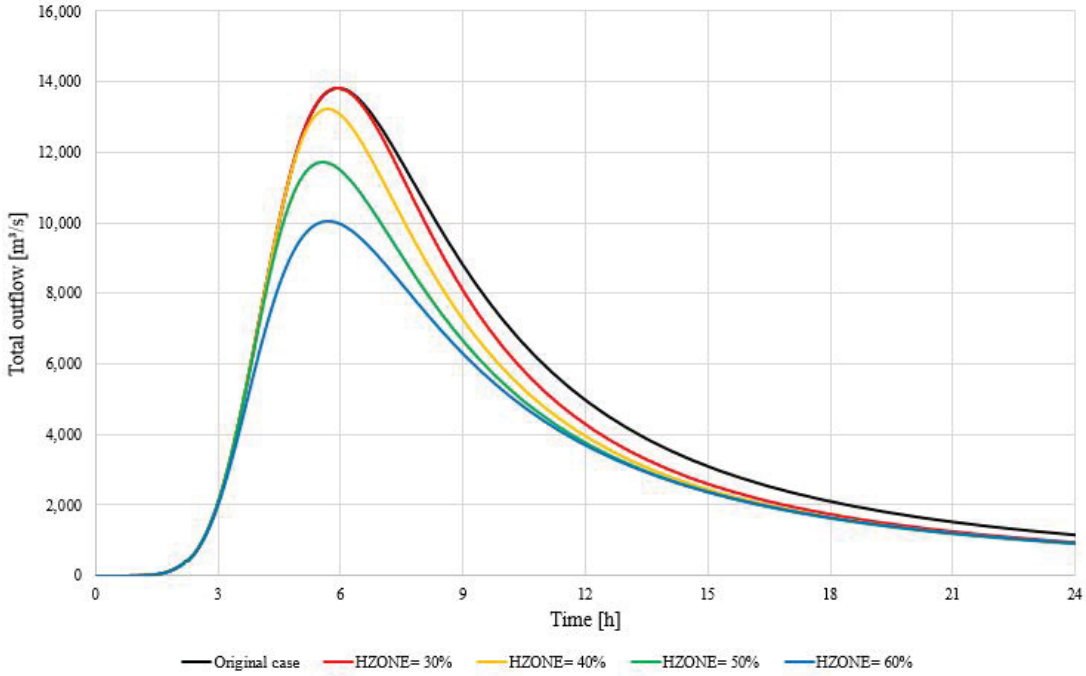

FIGURE 16 – Sensitivity analysis of Mantaro landslide dam for different zone heights (The author, 2019).

peak outflow was reduced in 27.51%, the time to peak in 1.51% and the breach in 21.86%. As for a material of 65%, i.e. more porous than the dam, the peak outflow was increased in 1.06% while the time to peak was decreased in 11.07% and the breach in 15.58%.

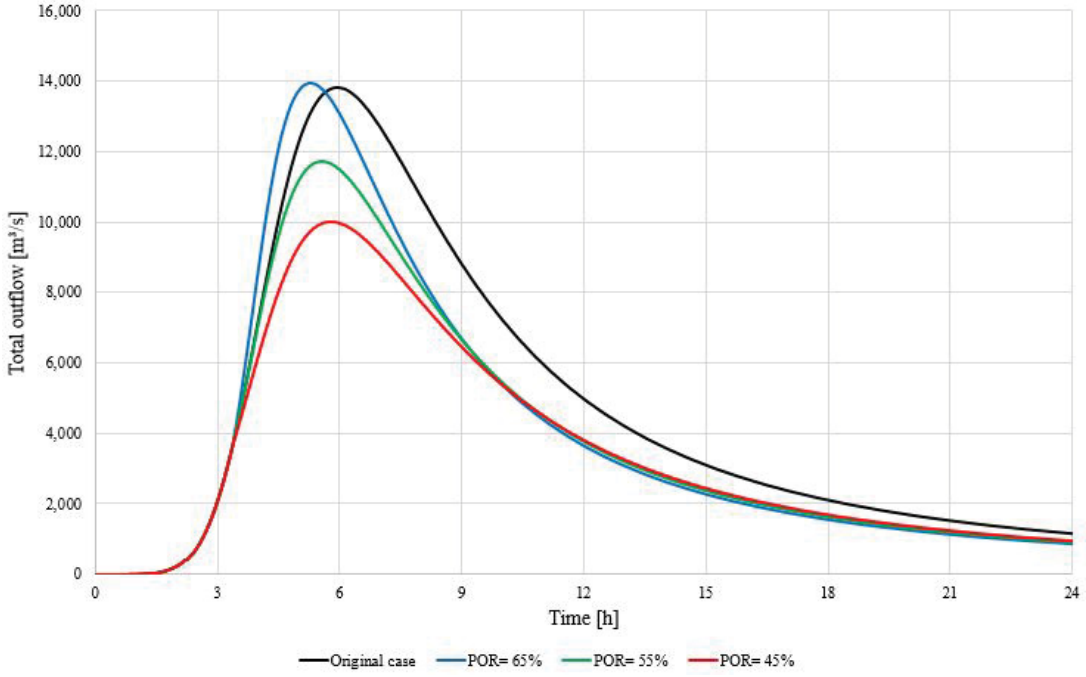

FIGURE 17 – Sensitivity analysis of Mantaro landslide dam for different porosities (The author, 2019).

4.2 PIPING

Once the breach channel reaches the implemented zone, the routine measures the distance of the horizontal projection of the breach channel within the zone and over the entirety of the dam, as shown in Figure 18.

The intersection point between the zone and the breach channel is obtained by Equation (4.10) and the distances of the projections by Equations (4.12) and (4.13). The influence factor in piping is the same as in overtopping, but instead of using the ratio of zone area it is applied the ratio $DIST_{zone}$ and $DIST_{dam}$:

$$y_{intersection} = \frac{1}{1-\lambda}[(H_c - H_l) + \tan(\pi - \arctan(S_{breach}))(H_{zone}(ZU + ZD_{zone}) - (WC - XP) - (H_c - H_l)ZU)], \tag{4.10}$$

$$\lambda = \frac{\tan(\pi - \arctan(S_{breach}))}{\tan\left(\pi - \arctan\left(\frac{1}{ZD_{zone}}\right)\right)}, \tag{4.11}$$

$$DIST_{zone} = WC_{zone} + [(H_{zone} - H_l) - y_{intersection}](ZU + ZD_{zone}), \tag{4.12}$$

$$DIST_{dam} = WC + [(H_u - H_l) - y_{intersection}](ZU + ZD). \tag{4.13}$$

Where:

$DIST_{zone}$ is the distance of horizontal projection of breach channel within the zone [ft];

$DIST_{dam}$ is the distance of horizontal projection of breach channel over entire dam [ft];

S_{breach} is the slope of the breach channel [-];

$y_{intersection}$ is the intersection height between the breach channel and downstream face of the zone [ft];

H_{zone} is the top elevation of the zone [ft];

H_c is the bottom elevation of the breach [ft];

H_l is the river bed elevation [ft];

ZD_{zone} is the slope of the downstream face of the zone [1 ft : ZD_{zone}];

ZU is the slope of the upstream face of the dam [1 ft : ZU];

ZD is the slope of the downstream face of the dam [1 ft : ZD];

WC_{zone} is the width of the zone [ft];

WC is the width of the dam [ft];

λ is an auxiliary variable [-].

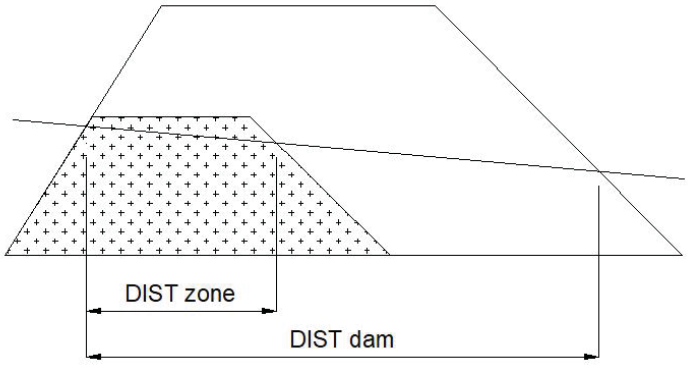

FIGURE 18 – Schematic of breach channel position in piping (The author, 2019).

The routine was tested with the case of Teton dam, USA, a composite dam that failed due to piping. Teton was used to validate the original BREACH model and its main inputs and outputs are listed in Table 2.

TABLE 2 – Main inputs and outputs of Teton dam simulation (The author, 2019).

INPUT			
El. Water surface [m]	79.86	El. Spillway [m]	0
El. Top dam [m]	79.86	Crest width [m]	10.67
El. Bottom dam [m]	0	Upstr. face slope [1V:x]	2.5
Dam height [m]	79.9	Downstr. face slope [1V:x]	2
El. Piping [m]	48.77		
OUTER CORE			
D50 [mm]	1	D_{90}/D_{30}	8
Unit weight [kg/m^3]	1,601.52	Porosity [%]	35
Internal friction angle [°]	40	Cohesion [kg/m^2]	1,220.36
INNER CORE			
D50 [mm]	0.03	Porosity [%]	35
Unit Weight [kg/m^3]	1,601.52	Cohesion [kg/m^2]	1,220.36
Internal friction angle [°]	35	Mean face slope [1V:x]	1.8
D_{90}/D_{30}	8		
OUTPUT			
Total time [h]	4.02	Breach depth [m]	79.86
Peak outflow [m^3/s]	60,944.88	El. Bottom breach [m]	0
Time to peak [h]	2.21	El. Water surface [m]	26.01

Although it was breached due to piping, it was overtopped as well after the material above the piping channel collapsed. This transition of failure modes is one of the capabilities

of the BREACH explained in Chapter 3 and it is marked by an abrupt reduction of the outflow in the hydrographs to be presented. This sudden change dos not necessarily reflects the real event of transition between failure modes and it may or not occur according to the breaching conditions.

In all analyses the zone had a downstream slope of 1:2 and a crest width of 60 m. The resulting percentage differences of the analyzed parameters are presented in Appendix E and some of the results are shown bellow.

Figure 19 shows the impact of a zone with fixed porosity of 35%, a D_{90}/D_{30} of 8, a height of 60% of the dam height and D_{50} of 25, 50, 75 and 100 mm. The increase in the time to peak is a result of the zone affecting the erosion right since the piping. As observed in Section 4.1, there was no expressive in the time to peak when in overtopping.

In general, the increase of the D_{50} corresponded to a lesser smoothing of the hydrograph while the breach remained practically the same. In average, the breach reduced in 1.24%. For a D_{50} of 25 mm the peak outflow reduced in 20.25% and the time to peak increased in 76.3%, while for 100 mm the peak outflow reduced 9.44% and the time to peak increased 63.17%.

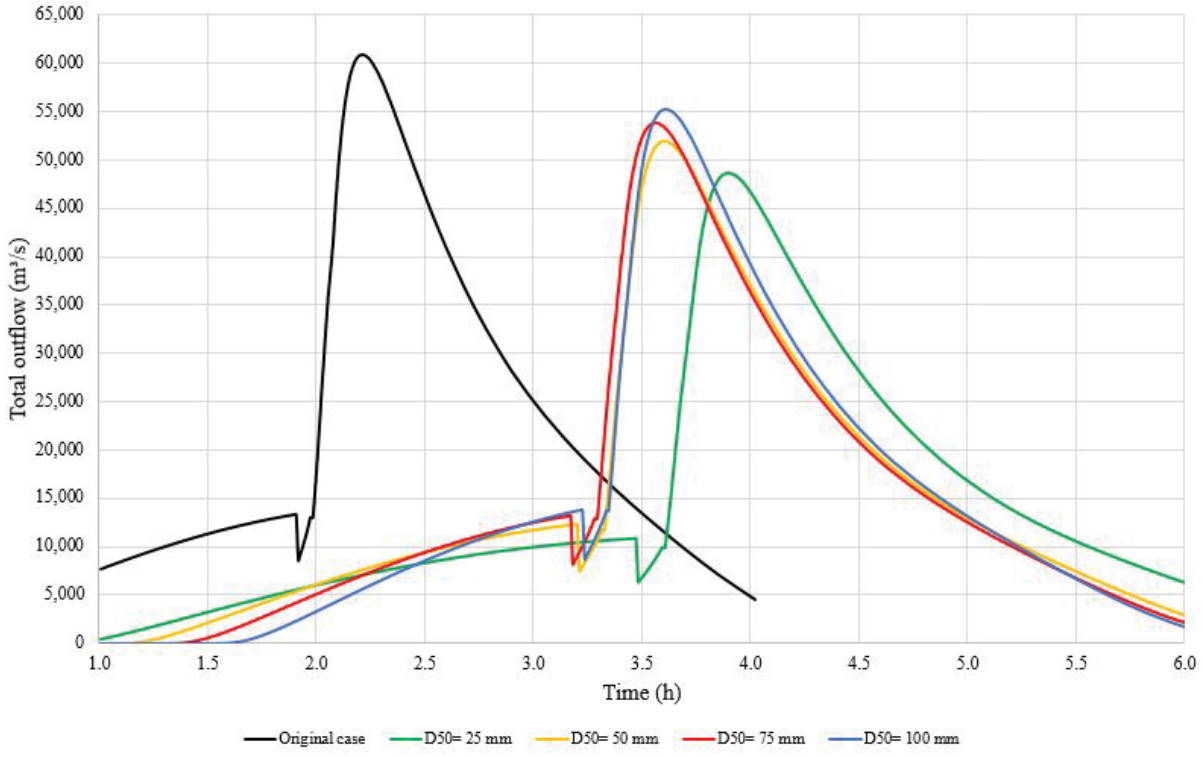

FIGURE 19 – Sensitivity analysis of Teton dam for different D_{50} and zone height of 60% dam height (The author, 2019).

In piping, it seems to have an inverse relation between the mean diameter of the zone and the hydrograph smoothing, behavior contradictory to what it was expected. The greater the material, the heavier it becomes and thus, the more difficult it is to be carried away.

To test if this odd behavior was indeed a coding error of the new routine, a sensibility

study was done with the original BREACH model. With the Teton case two types of simulations were performed: variating either the D_{50} of the inner or outer core while the other remained fixed. The same behavior was observed in both cases, revealing that the new routine was not the source of error. The Figure 20 shows that as the D_{50} increased so did the peak outflow and the sooner it happened. The Figure 21 shows the behavior when changing the outer core, except that for D_{50} greater than the original (1 mm) the time to peak started to increase. This performance of the model is consistent with the effect of percolation due to the space between the grains, although the model was not written to do such.

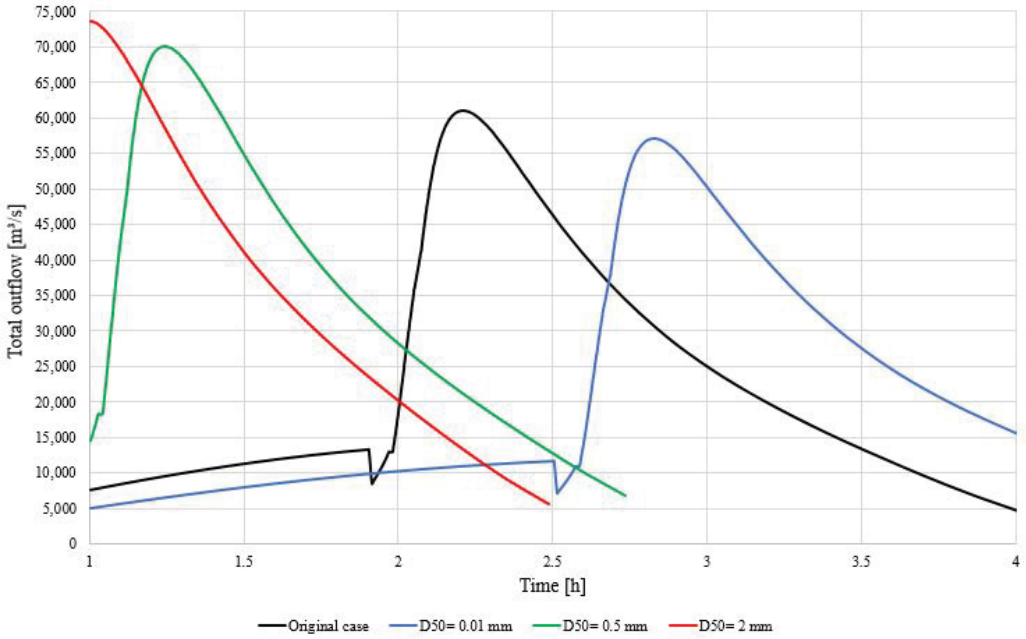

FIGURE 20 – Sensitivity analysis of Teton dam for different D_{50} of the inner core performed with the original BREACH model (The author, 2019).

Returning to the analysis of the zoned dam routine, the Figure 22 shows the impact of a zone with fixed porosity of 35%, a height of 50% of the dam height, a D_{50} of 25 mm and a D_{90}/D_{30} of 1, 4, 8 and 40. Turning the zone material more uniform diminished the peak outflow and breach and increased the time to peak and total time. For a theoretical material of D_{90}/D_{30} equals to 1, the peak outflow and breach reduced in 31.35% and 2%, respectively, and increased the time to peak in 125.19%. A zone material of D_{90}/D_{30} of 40, a wider grain curve than the original Teton dam, had no relevant effect on the peak outflow and breach, but increased the time to peak in 19.66%.

Figure 23 shows the impact of a zone with fixed porosity of 35%, a D_{50} of 25 mm, a D_{90}/D_{30} of 8 and a height of 30%, 40%, 50% and 60% of the dam height. It is noticed that only for the heights of superior to 40% the time to peak was increased, when the zone started being eroded while in piping. As commented before, the transition to overtopping is marked by a sudden decreased in the outflow which remained unchanged for zone heights up to 40% and it took longer to occur and to be over for superior heights. Moreover, according to the original

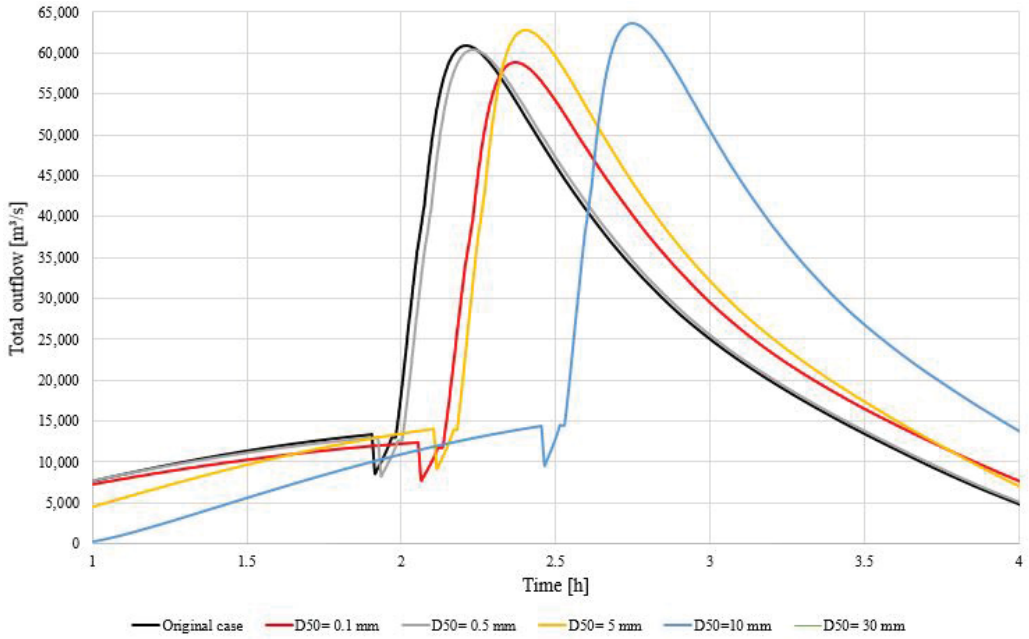

FIGURE 21 – Sensitivity analysis of Teton dam for different D_{50} of the outer core performed with the original BREACH model (The author, 2019).

simulation of Teton dam failure, the piping starts at a height of 48.77 m (60% of dam height) and it ceases at 36.42 m (45% of dam height) thus, still not affecting the zone with its fixed crest width and downstream slope and height of 30% and 40% of dam height.

For a zone height of 60%, the peak outflow was reduced in 20.25% and the time to peak increased in 76.30%. For a height of 30%, the peak outflow reduced in 5.63% and the time to peak remained practically unchanged. In average, the breach reduced in 1%.

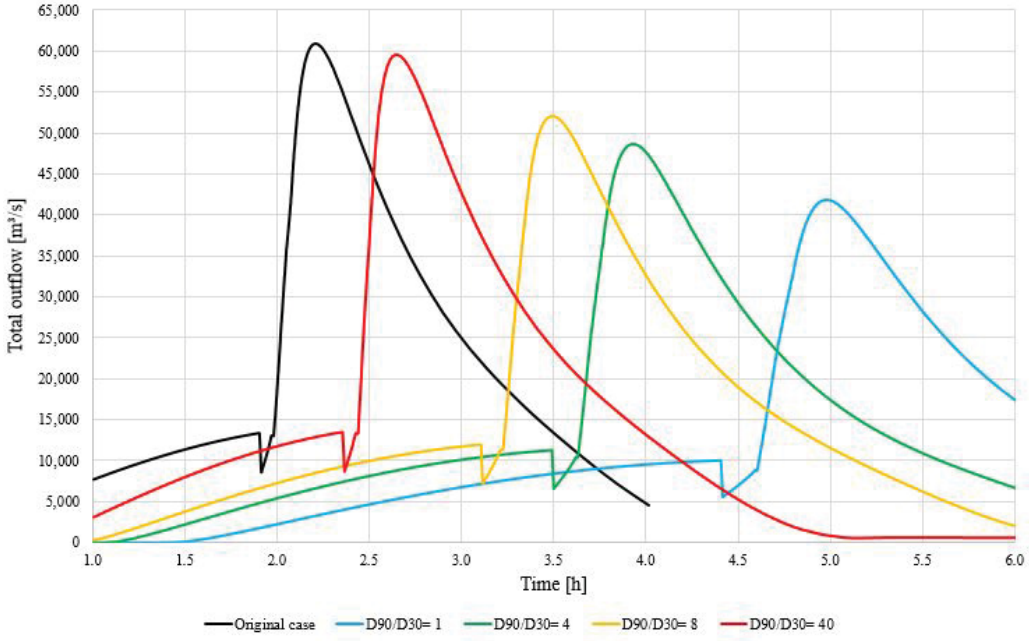

FIGURE 22 – Sensitivity analysis of Teton dam for different D_{90}/D_{30} (The author, 2019).

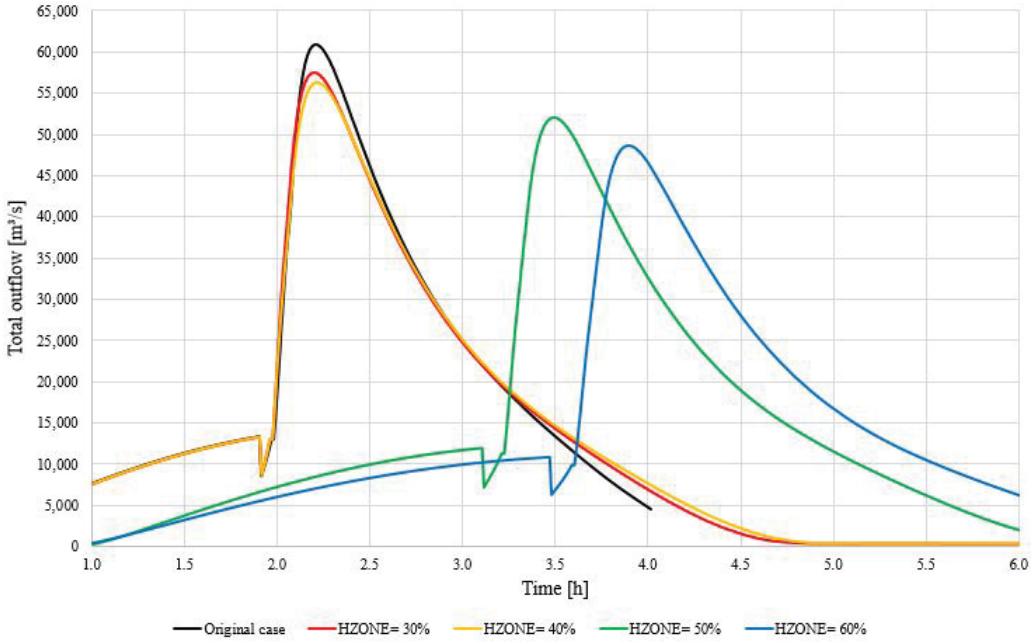

FIGURE 23 – Sensitivity analysis of Teton dam for different zone heights (The author, 2019).

Figure 24 shows the impact of a zone with fixed D_{50} of 25 mm, a D_{90}/D_{30} of 8, a height of 50% the dam height and porosity of 40%, 35% and 30%. Even though the presence of a zone affected the breaching process, changing the porosity revealed little effect on the hydrograph, reducing the peak outflow in 14.74% and the breach in 1.13% and increasing the time to peak in 58%, all in average.

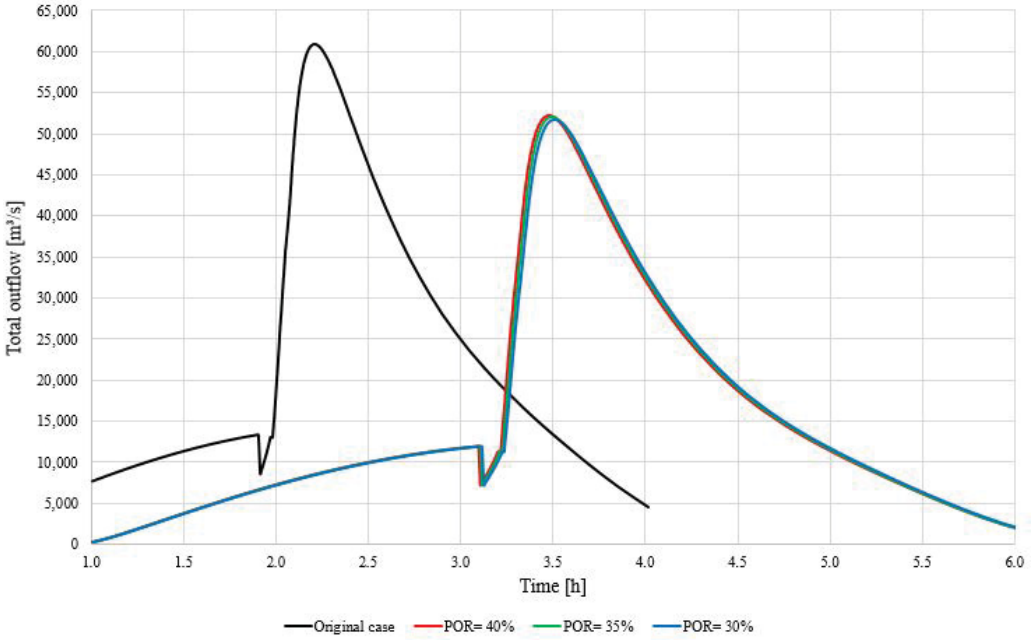

FIGURE 24 – Sensitivity analysis of Teton dam for different porosities (The author, 2019).

As discussed when analyzing the Figure 19, zone heights of 30% and 40% only affected the breaching when it transitioned to overtopping due to the zone dimensions and

initial and final conditions of the piping. To show better what happens for a zone only eroded in overtopping, it was modeled a zone with fixed porosity of 35%, a height of 40% the dam height, a D_{90}/D_{30} of 8 and a D_{50} of 25, 50, 75 and 100 mm. As observed in Figure 25, in overtopping the D_{50} had little effect, reducing the peak outflow in 7.80%, in average, and practically not changing the time to peak and breach dimensions.

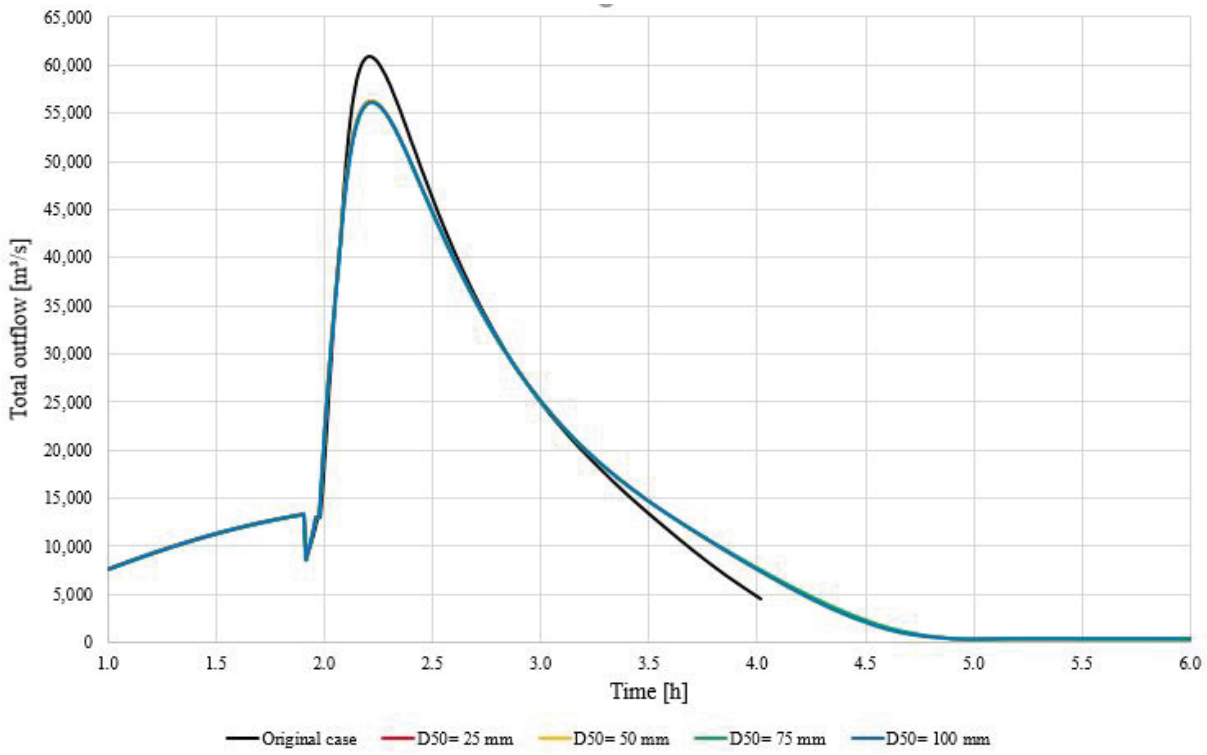

FIGURE 25 – Sensitivity analysis of Teton dam for different D_{50} and zone height of 40% the dam height (The author, 2019).

5 CASE STUDY

The new BREACH was tested against a real case of dam breaching. Due to legal reasons, no names or specific informations are herein presented.

Briefly, an upstream cofferdam was breached by piping during a flood event. The Figure 26 shows a topview of the incident site and Figure 27 a cross-section. The piping started close to the amendment of the embankment to the soil (elevation 47 m) and it developed to a breach around 150 m wide after 10 hours and reached a bottom elevation around 45 m. As for the peak outflow through the breach, it was estimated close to 1,000 m^3/s.

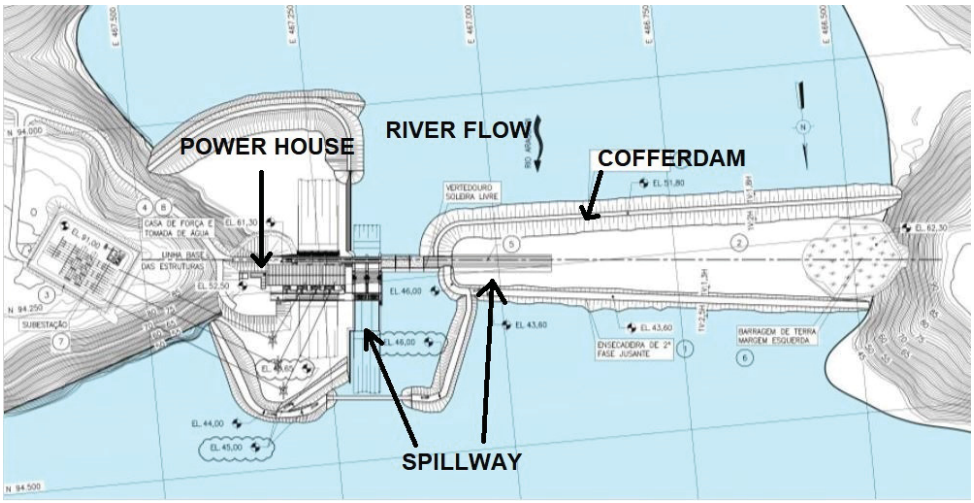

FIGURE 26 – Topview of cofferdam site (The author, 2019).

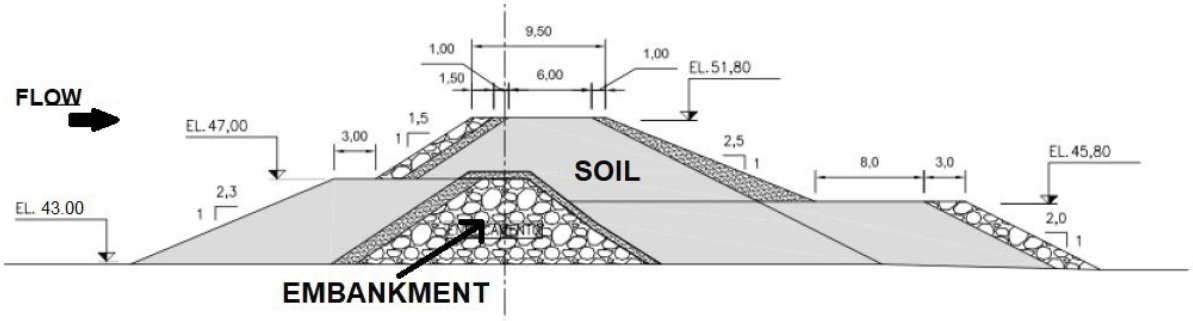

FIGURE 27 – Cross-section of cofferdam (The author, 2019).

The analysis of the incident, named here as Report, was done with the original BREACH model considering the cofferdam as dual cored: inner core of soil and outer core of embankment. The main inputs can be seen in Table 3 and a remark is done about the spillway elevation, which had to be lowered in order to obtain an outflow consistent with its discharge curve. Moreover, in order to obtain a result closer to the actual event, the Report altered the properties of the materials by adding a porosity (not known previously) and reducing

the friction angle and cohesion. Hence, the cofferdam was weakened, allowing it to reach the width observed on the field. Furthermore, the bottom elevation of the cofferdam, i.e the river bed, was fixed in 47 m, thus not allowing it to be eroded downward beyond that point. The maximum breach width was also fixed in 156 m. The Table 4 shows the inputs and outputs used by the Report to obtain a best fit simulation with all these modifications.

TABLE 3 – Main original inputs of the cofferdam (The author, 2019).

INPUT			
El. Water surface [m]	51.35	El. Spillway [m]	36.30
El. Top dam [m]	51.80	Width crest [m]	9.50
El. Bottom dam [m]	43.00	Upstr. face slope [1 ft:x]	2.0
El. Piping [m]	49.18	Downstr. face slope [1 ft:x]	1.5
River bed slope [%]	0.50		
OUTER CORE			
D50 [mm]	300	D90/D30	2.5
Unit weight [ton/m^3]	2.037	Porosity [%]	-
Internal friction angle [°]	40	Cohesion [kg/m^2]	-
INNER CORE			
D50 [mm]	0.04	Porosity [%]	-
Unit Weight [ton/m^3]	1.833	Cohesion [kg/m^2]	1018.26
Internal friction angle [°]	25	Mean face slope [1 ft:x]	2.0
D90/D30	110		

TABLE 4 – Main inputs and outputs of the Report for the best fit (The author, 2019).

INPUT			
El. Water surface [m]	51.35	El. Spillway [m]	22.43
El. Top dam [m]	51.80	Width crest [m]	9.50
El. Bottom dam [m]	47.00	Upstr. face slope [1 ft:x]	2.0
El. Piping [m]	49.18	Downstr. face slope [1 ft:x]	1.5
River bed slope [%]	0.25		
OUTER CORE			
D50 [mm]	300	D90/D30	2.5
Unit weight [ton/m^3]	2.037	Porosity [%]	70
Internal friction angle [°]	10	Cohesion [kg/m^2]	-
INNER CORE			
D50 [mm]	0.04	Porosity [%]	70
Unit Weight [ton/m^3]	1.833	Cohesion [kg/m^2]	509.13
Internal friction angle [°]	12.5	Mean face slope [1 ft:x]	2.0
D90/D30	110		
OUTPUT			
Breach top width [m]	156	Breach depth [m]	4.80
Peak outflow [m^3/s]	930.24	El. Bottom breach [m]	47.00
Time to peak [h]	4.88	El. Water surface [m]	48.25

As observed in from Figure 27, the cofferdam is similar to a homogeneous dam with an inner embankment core close to its upstream face, a perfect candidate for the use of the new BREACH. However, the Report modeled it as an embankment dam with an inner core as

in Figure 9. Using the routine for zoned dams the incident was simulated to compared it with the Report, to see if a better result could be obtained without forcing the inputs to get a best fit as in Table 4.

All analyses are presented bellow and the inputs were based in Table 3, resulting in a simplified design of the cofferdam as demonstrated in Figure 28. On each one it was observed the convergence of the breach outflow to the Report's, the reservoir's water level and breach evolution, these last two with field data for comparison additional to the Report's results.

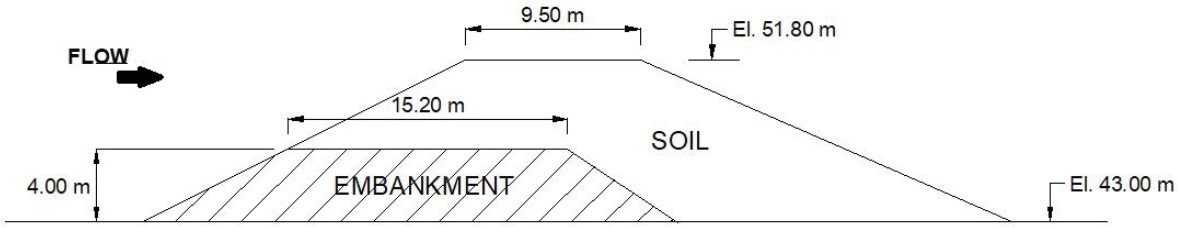

FIGURE 28 – Adopted design of the cofferdam for simulations (The author, 2019).

5.1 SIMULATION 1

The Table 5 presents the inputs, without any change, and outputs for the first run. In Figure 29 it can be seen that the obtained peak outflow (Spill. modified) is greater than the Report's while the breach's top width is 50 m shorter than it should be, as shown in Figure 30. Thus, three more simulations were done with slight changes to the inputs.

TABLE 5 – Main inputs and outputs of the new BREACH for the case study (The author, 2019).

INPUT			
El. Water surface [m]	51.35	El. Spillway [m]	36.30
El. Top dam [m]	51.80	Width crest [m]	9.50
El. Bottom dam [m]	43.00	Upstr. face slope [1 ft:x]	2.0
El. Piping [m]	49.18	Downstr. face slope [1 ft:x]	2.3
OUTER CORE			
D50 [mm]	0.04	D90/D30	110
Unit weight [ton/m^3]	1.833	Porosity [%]	-
Internal friction angle [°]	25	Cohesion [kg/m^2]	1018.26
ZONE			
D50 [mm]	300	El. Zone top [m]	47.00
Unit Weight [ton/m^3]	1.833	Width [m]	15.20
Internal friction angle [°]	40	Downstr. face slope [1 ft:x]	1.5
Cohesion [kg/m^2]	-	D90/D30	110
Porosity [%]	-		
OUTPUT			
Breach top width [m]	109.88	Breach depth [m]	8.80
Peak outflow [m^3/s]	1,227.56	El. Bottom breach [m]	43.00
Time to peak [h]	7.27	El. Water surface [m]	45.54

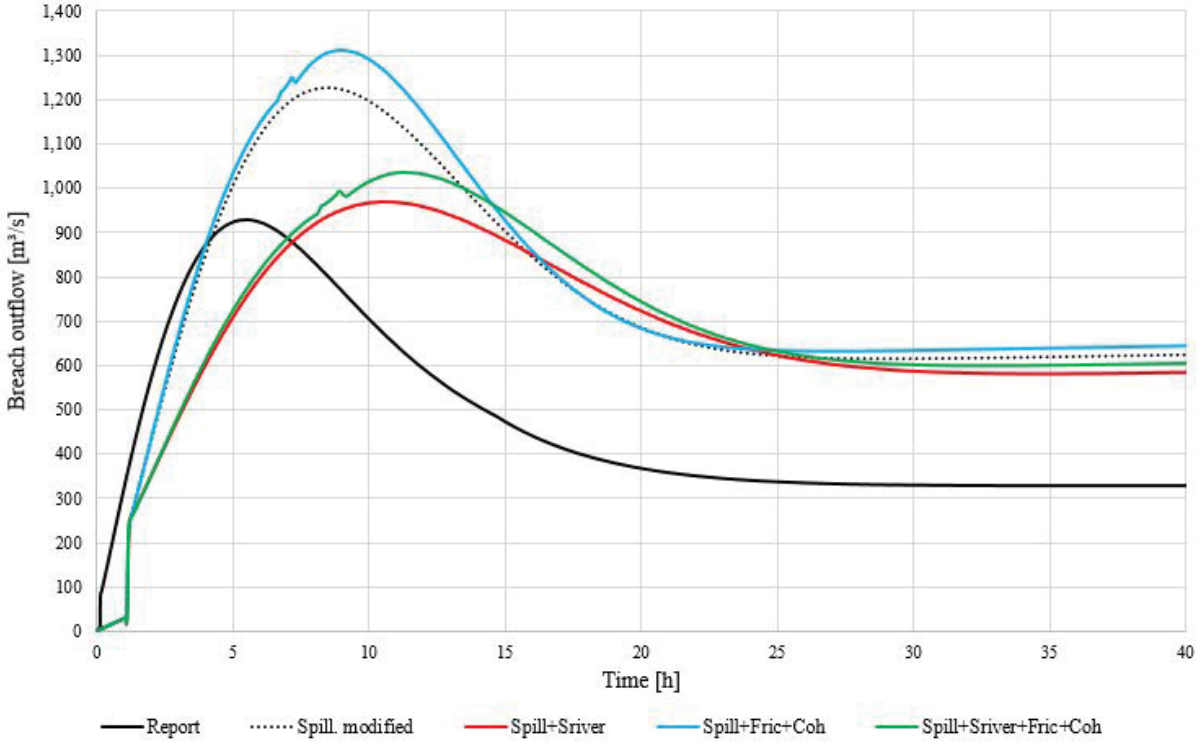

FIGURE 29 – Breach outflows for the Simulation 1 (The author, 2019).

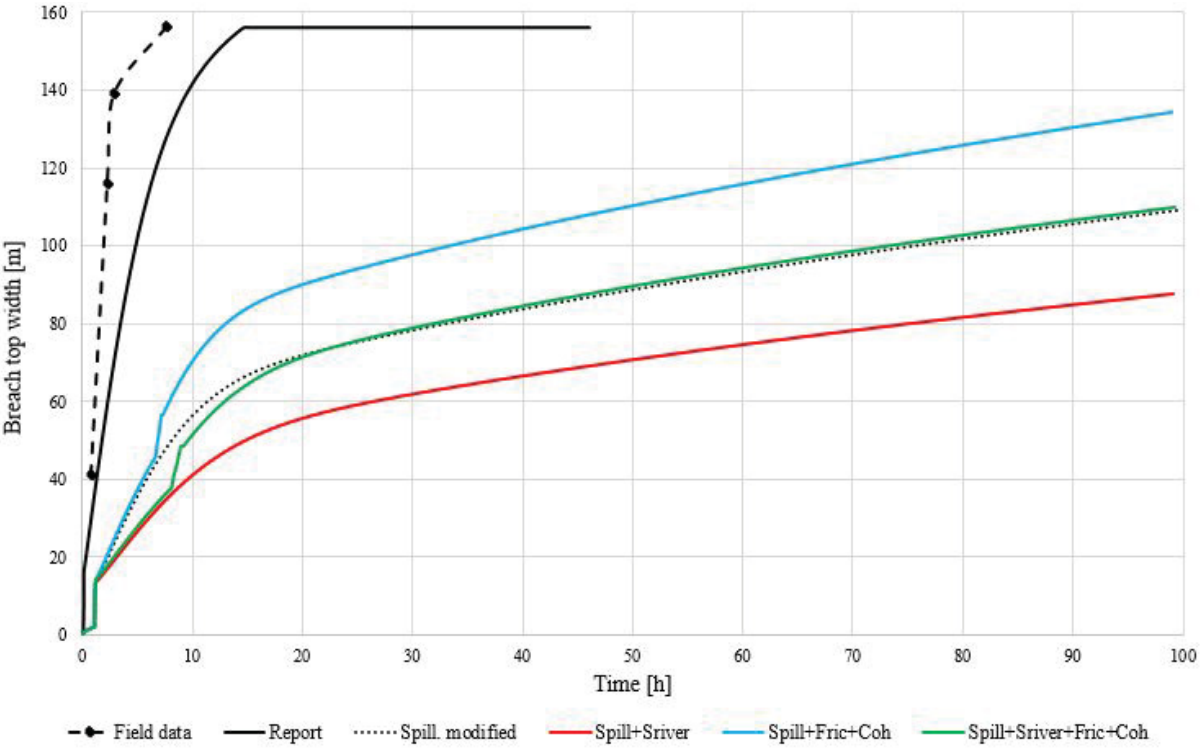

FIGURE 30 – Breach widths for the Simulation 1 (The author, 2019).

The first rerun (Spill+Sriver) was with a smoother river bed's slope reduced in 5%. The second (Spill+Fric+Coh) was with weakened materials, reducing the friction angles in 8% and the cohesion in 5%. The last test (Spill+Sriver+Fric+Coh) was a combination of the

previous two.

Smoothing the river bed's slope reduced the peak outflow to around 960 m^3/s, since it increased the influence of the tailwater, which corresponded also to a smaller breach around 90 m. Weakening the cofferdam's erosion resistance increased the outflow around 1,300 m^3/s, but it came closer to the actual breach reaching almost 140 m. Combining both variations gave a mid-term result where the peak outflow was of 1,030 m^3/s and the breach 109 m wide. These results for outflow and breach width are presented in Figures 29 and 30.

Besides all, the simulations ended up breaching the entire cofferdam. This happened because of the conditions set to terminate the program and explained in Chapter 3, before listing all subroutines. Recalling here these conditions based on the simulations, the following was the trigger:

- Estimated simulation time (input of 100 hours) is reached $\longrightarrow$ **YES**;
- Reservoir is entirely depleted $\longrightarrow$ **NO**;
- Dam is entirely breached (**YES**) and breach outflow is less than 10% of its peak (**NO**) $\longrightarrow$ **NO**;
- Simulation surpassed the imposed limit of 5,000 iterations $\longrightarrow$ **NO**.

Even though the erosion rate would start to decrease at some point of the simulation, it would never cease and the breach would continue to develop. Thus, it was thought on how to get around this problem which will be detailed on the sequence.

5.2 SIMULATION 2 - LIMITED BOTTOM ELEVATION OF BREACH

In order to avoid the total breaching, the model started to keep track of the greatest erosion rate and to compared it to the current rate at each time-step. Whenever the current erosion was equal to or less than 5% of the greatest recorded value, it would be considered as if the breach reached the river bed and it would only be further enlarged sideways. As described in Chapter 3, whenever the breach's side slopes collapse the erosion is interrupted until the removal of the collapsed material. So, it was set a condition to avoid limiting the breach's bottom elevation during these instants. This condition is informed together with the inputs of the zoned dam routine, as specified in Appendix B.

The inputs were the same as in Table 5. The first run (HC+Spill) had a peak outflow around 880 m^3/s and the breach's top width reached 110 m as observed by Figures 31 and 32, while the bottom elevation was fixed in 44.46 m.

Even though the breach's bottom elevation reached a good mark, the other variables did not. Again some of inputs were altered in order to obtain more accurate results. A new

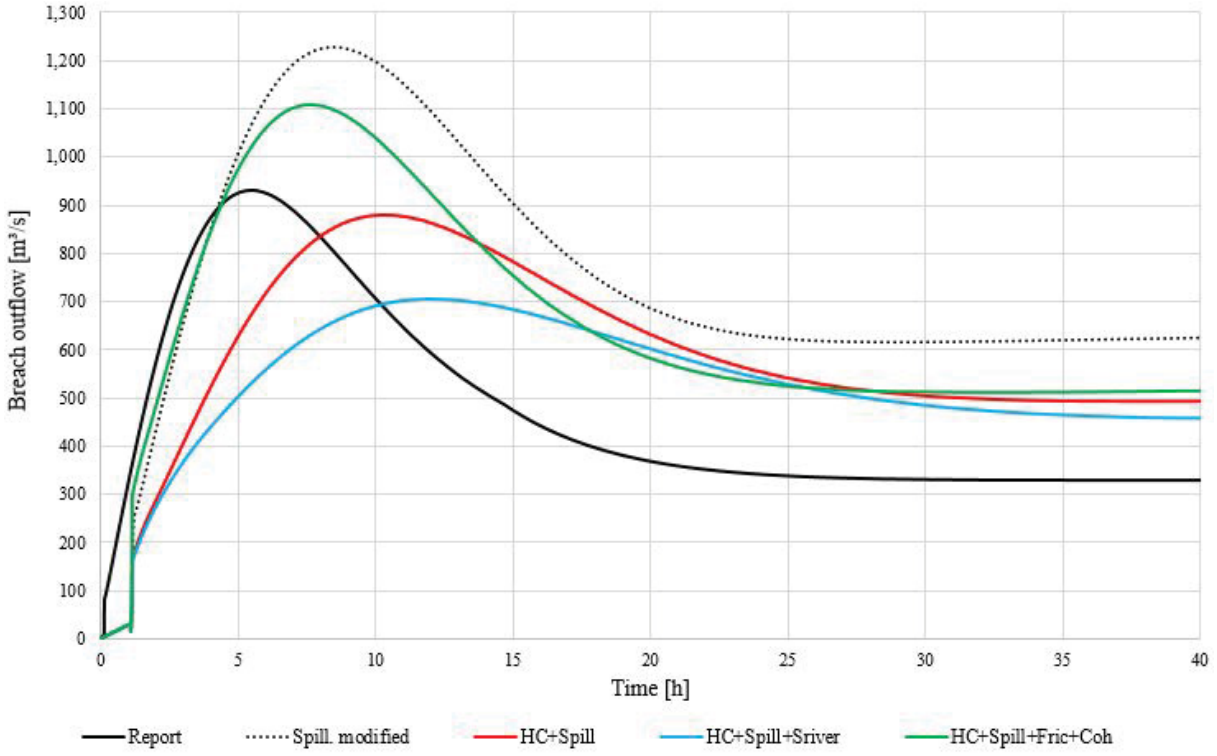

FIGURE 31 – Breach outflows for the Simulation 2 (The author, 2019).

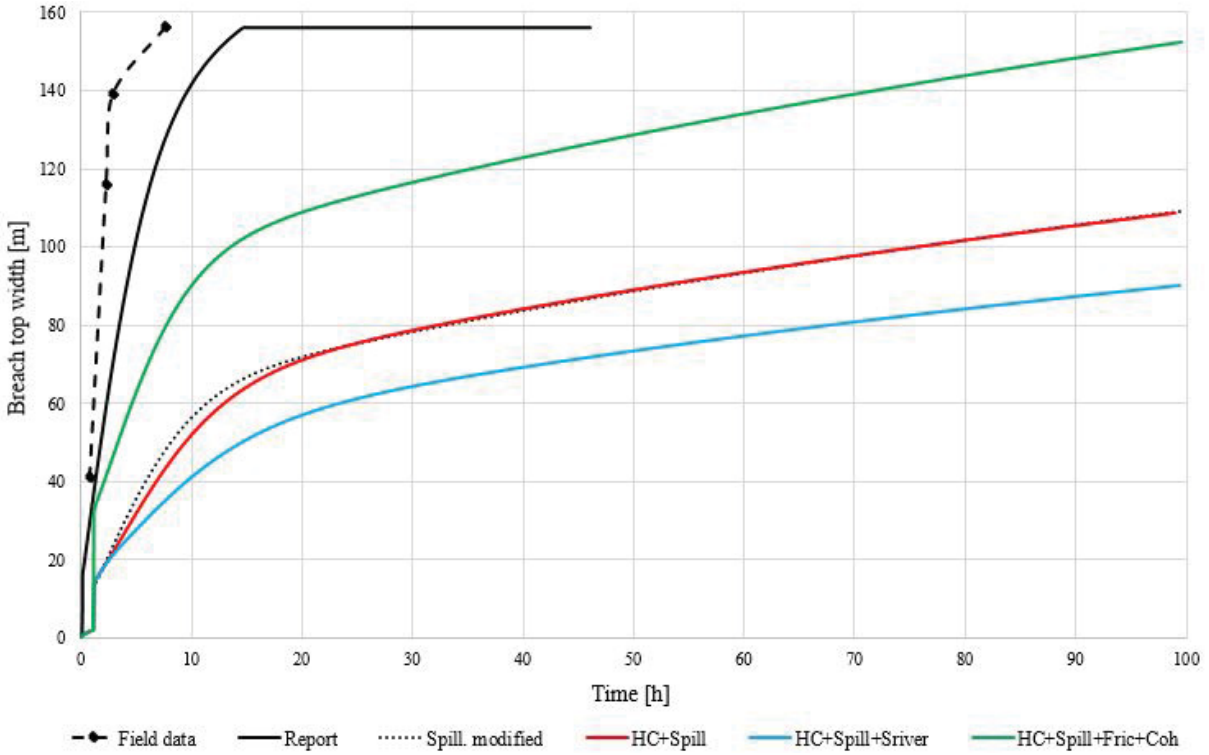

FIGURE 32 – Breach widths for the Simulation 2 (The author, 2019).

test (HC+Spill+Fric+Coh) was performed with the cohesion reduced in 5% and the friction angles in 8%. Weakening the cofferdam's erosion resistance increased the outflow around 1,300 m^3/s, but it came closer to the actual breach reaching almost 140 m wide and eroded until the

elevation of 44.73 m. Another test (HC+Spill+Sriver) was also performed, this time reducing the river slope in 5%. The results were an outflow around 700 m^3/s and a breach 90 m wide at the elevation of 44.79 m. These results are presented in Figures 31 for outflow and 32 for breach width.

5.3 SIMULATION 3 - CONTROL SECTION AT DOWNSTREAM

Another set of tests was thought to account the existence of spillway, still under construction, between the up- and downstream cofferdam as seen in Figure 26. To do so, a new routine was implemented to work together with the original model to determine the tailwater.

Recalling quickly what was described in Chapter 3 little before detailing the subroutines, the original BREACH compares the total outflow with an estimated outflow by Manning's equation from the tailwater level, which in turn is measured by a linear interpolation of a tailwater table (input). If there is a convergence of the outflows, it is known then the tailwater level.

In a similar manner, with this new feature the user can inform a discharge curve and the model uses it to determine the tailwater by linear interpolation until there is a convergence of the outflows. The Figures 33 and 34 show the downstream view of the spillway under construction at the time of the incident, composed of 30 blocks of 20 m each. The red line shows the topography at the site before the construction of the cofferdam and the yellow columns the stage of construction of each spillway block.

To determine whether or not the spillway is controlling the outflow, the tailwater is determined by both procedures. Then, the higher value is taken as the correct one.

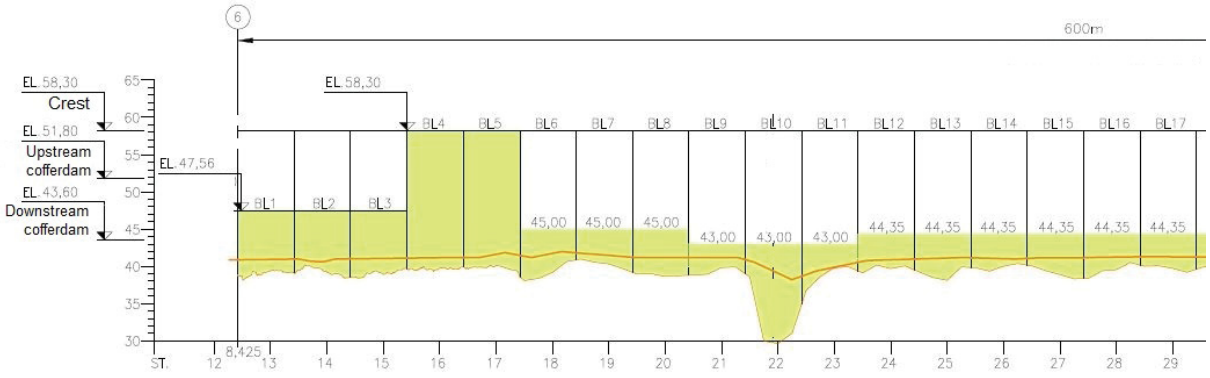

FIGURE 33 – Downstream view I of the spillway of the case study (The author, 2019).

The discharge curve can be observed in Figure 35 which was defined by a broad-crested weir equation like Equation (3.1). To do so, for a serie of tailwater levels it was determined the head of each constructed block of the spillway and its corresponding discharge. Then, the curve of defined by the mean of the discharges and heads to represented the spillway as a whole.

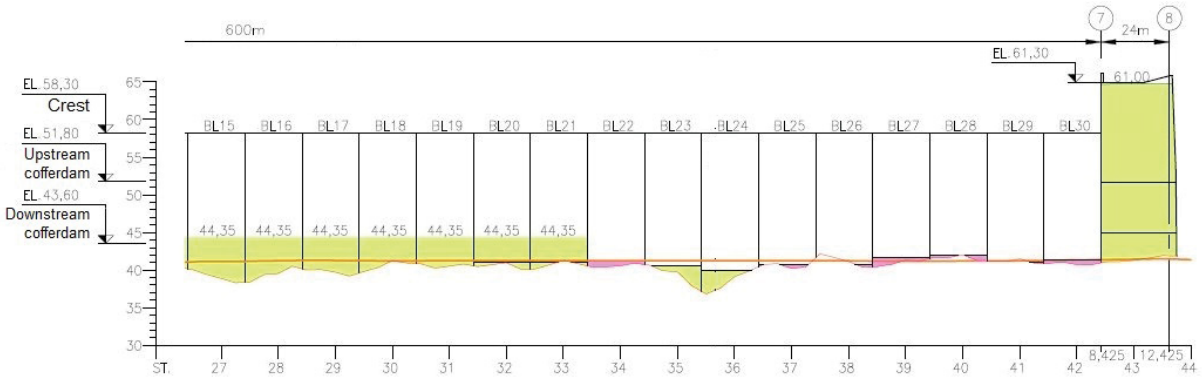

FIGURE 34 – Downstream view II of the spillway of the case study (The author, 2019).

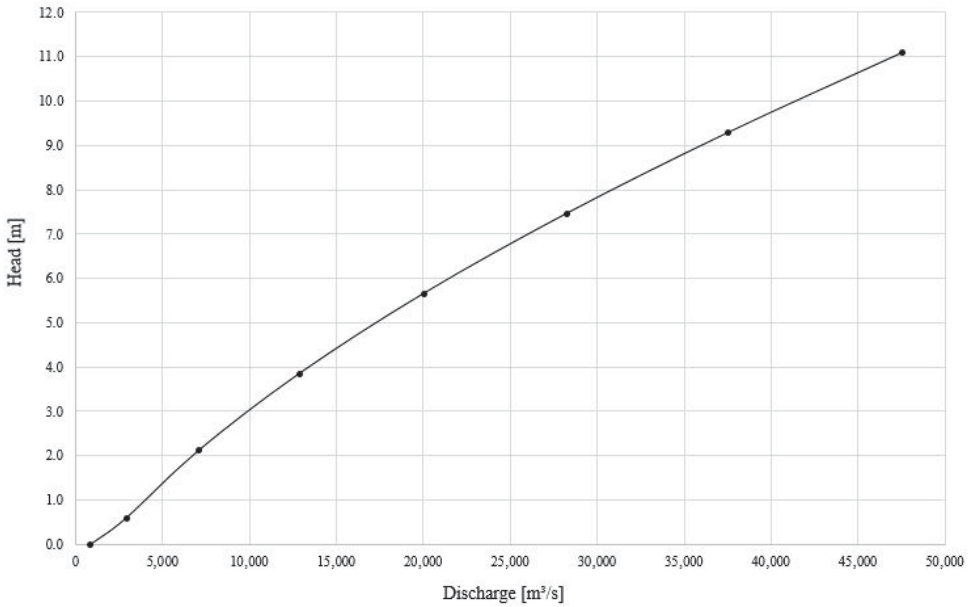

FIGURE 35 – Discharge curve of the spillway of the case study (The author, 2019).

Once this procedure was defined, a new simulation was done with the same inputs of Table 5 plus the discharge curve informed the same way as done for the dam's spillway, as listed in Appendix B. The first run (Control+Spill) showed no change from the original simulation (Spill. modified), even though it raised the tailwater level in about half meter to 45.21 m. The results are listed in Table 5 and the cofferdam was totally breached by the same reason presented in the end of Section 5.1.

To improve the simulation, variations to the test "Control+Spill"were performed. The first (Control+Spill+Fric+Coh) reduced the cohesion in 5% and the friction angles in 8%. The second (Control+HC+Spill) had no change to the inputs, but used the strategy of Section 5.2. The final test (Control+HC+Spill+Fric+Coh) was a combination of the previous two.

The test "Control+Spill+Fric+Coh"gave an outflow around 1,300 m^3/s and a breach of 133 m wide. The test "Control+HC+Spill"reduced the outflow to 750 m^3/s and the breach width to 101 m, while the breach eroded until the elevation of 45.09 m. The last test gave

the same outflow as "Control+HC+Spill", but with a wider breach of 103.5 m eroded until the mark of 45.14 m. The results for outflow and breach width are presented in Figures 36 for outflow and 37 for breach width.

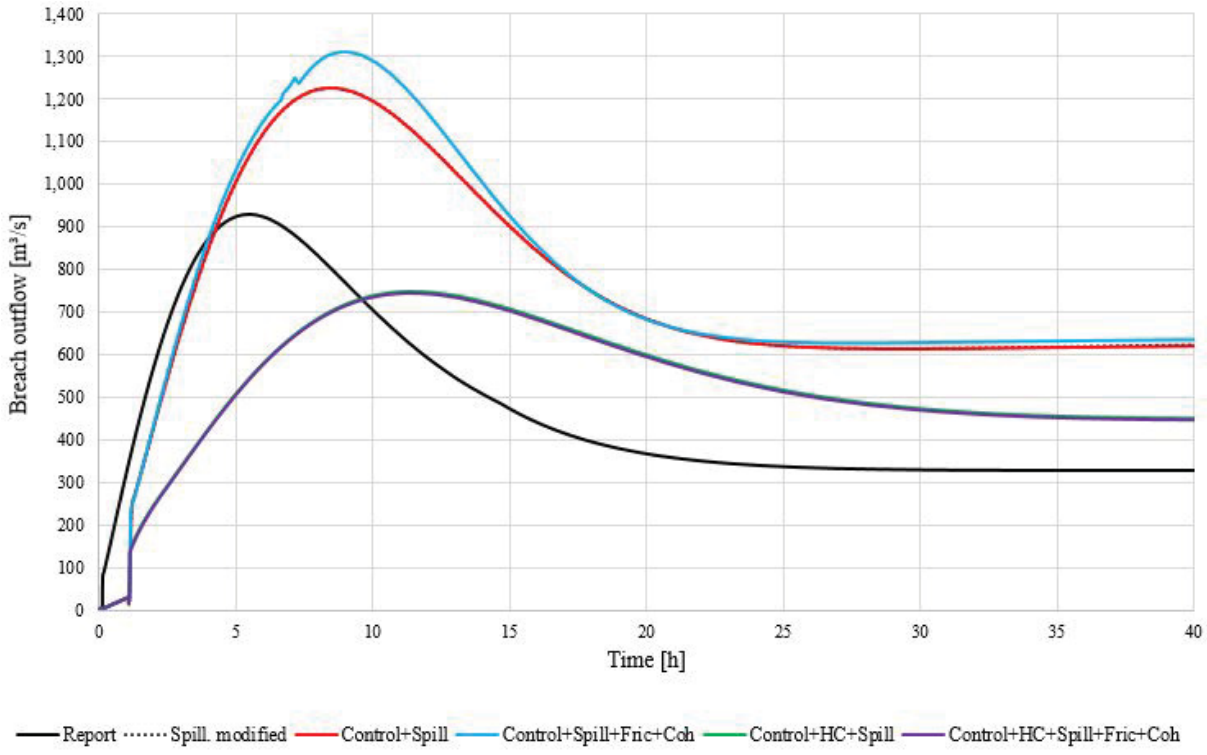

FIGURE 36 – Breach outflows for the Simulation 3 (The author, 2019).

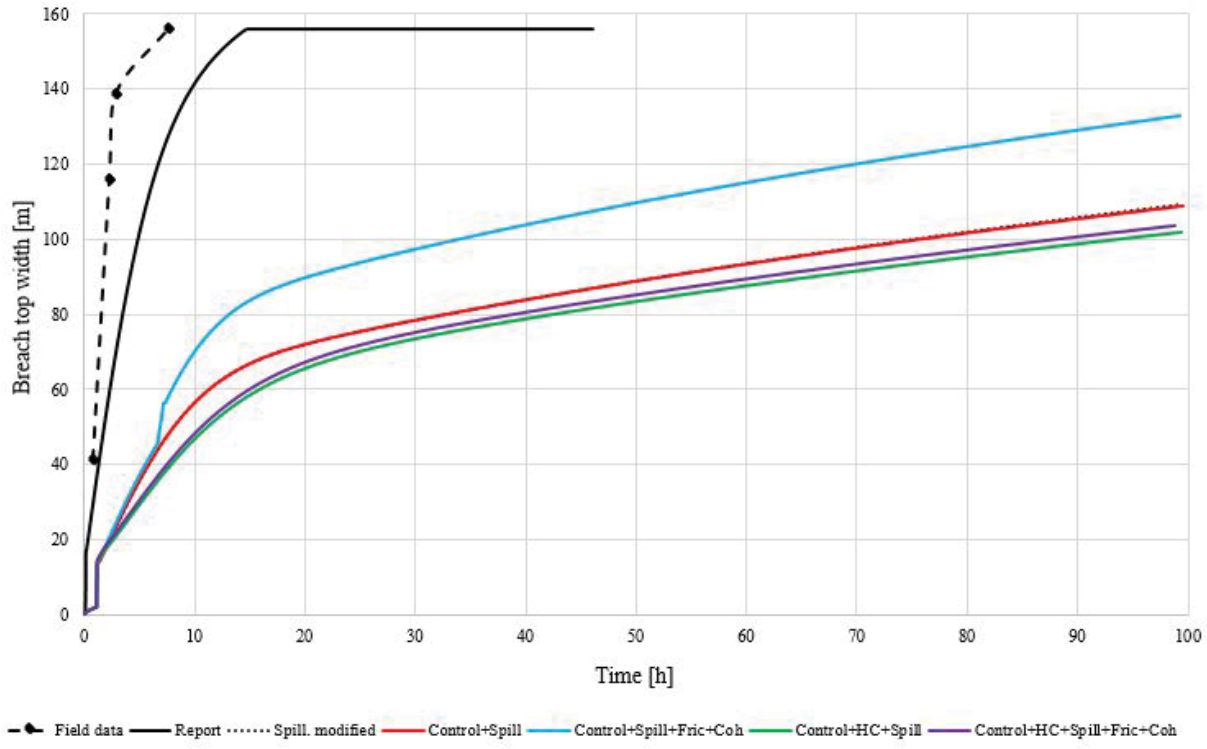

FIGURE 37 – Breach widths for the Simulation 3 (The author, 2019).

5.4 COMPARISON OF CORE SIMULATIONS

In short, without changing the materials of the cofferdam, the simulations were around the following main ideas:

- "Spill modified": simply with the new routine of zoned dam;
- "HC+Spill": limiting the breach's bottom elevation to the point where the erosion is 5% or less the maximum erosion;
- "Control+Spill": informing a discharge curve of a downstream structure or section that may control the tailwater level;
- "Control+HC+Spill": a combination of the previous two;
- "Spill+Sriver": reducing the slope of the river bed in 5%.

To better view the differences among them, the simulations results were plotted together as seen in Figures 38 for outflow and 39 and breach width. The "Spill modified"and "Control+Spill"gave the the same outflow of 1,227.11 m^3/s and breach width of 108.77 m, even though the control section at downstream raised the tailwater in half meter.

The "Spill+Sriver"presented the best fit to the outflow with 967.78 m^3/s, 5% higher than the Report's answer. However, the breach size of 87.72 m was the furthest from the 150 m measured at the field.

As for the "HC+Spill"it presented an outflow of 879.71 m^3/s, close to the Report, and a breach of 108.77 m. Combining this simulation with a control at downstream, the "Control+HC+Spill"reduced the outflow to 748.21 m^3/s and the breach to 99.39 m.

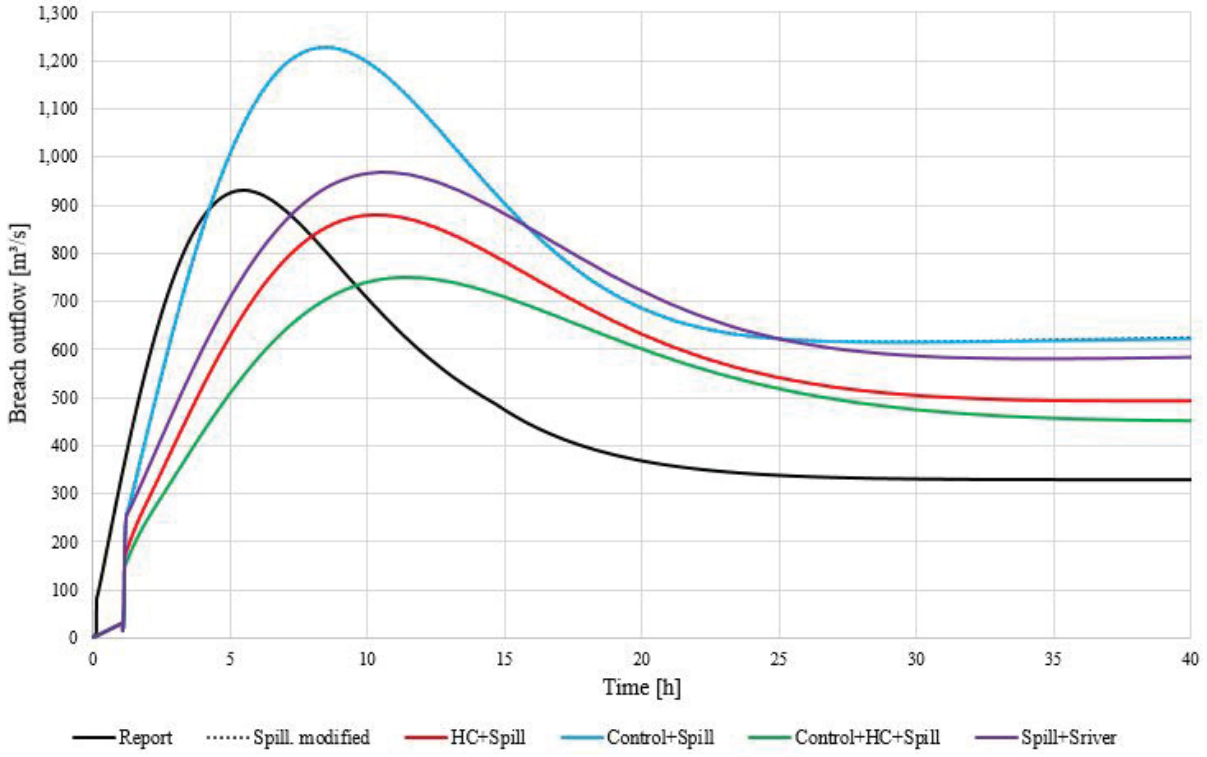

FIGURE 38 – Breach outflows for the core simulations (The author, 2019).

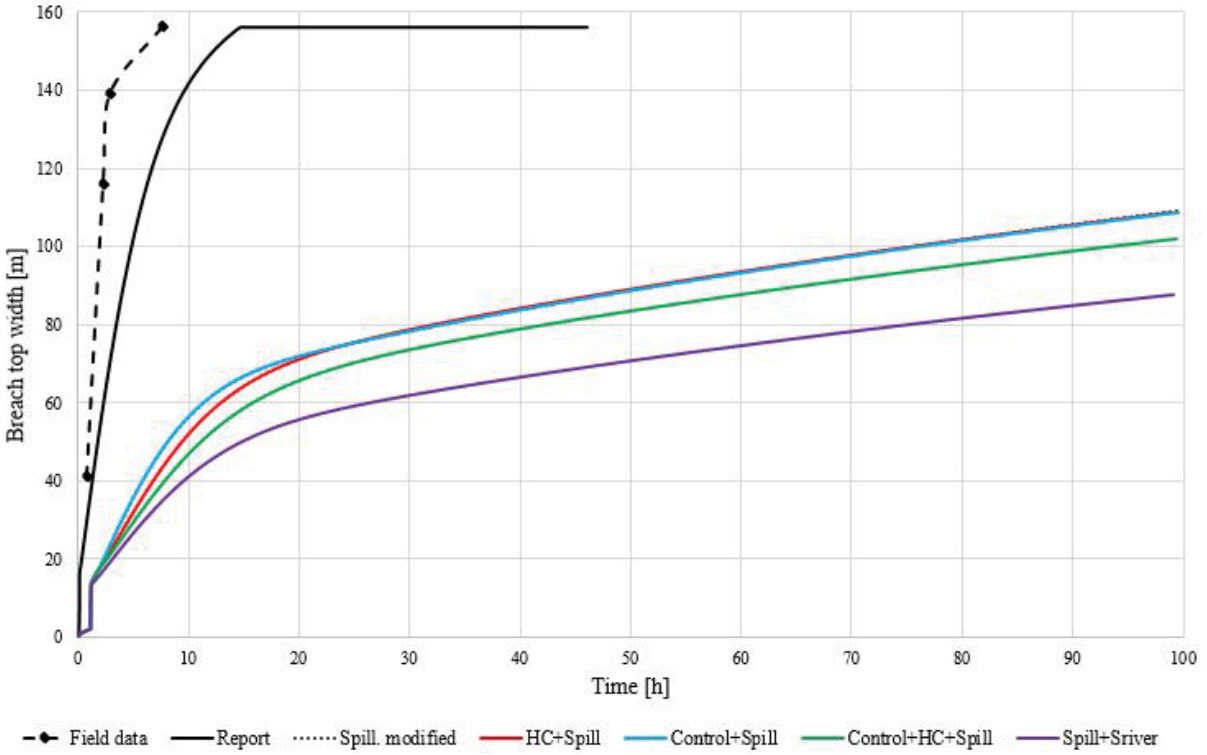

FIGURE 39 – Breach widths for the core simulations (The author, 2019).

5.5 BEST FIT SIMULATION

All simulations so far presented a good convergence either to breach outflow or size, usually with a little change to the materials' properties. Thus, it was sought a best fit simulation to see how far the inputs would need to be altered.

One of the possibles best fit was obtained using the simulation "HC+Spill+Fric+Coh", in Section 5.2, plus a smoother river bed. From the inputs of Table 5 the friction angles were reduced in 8%, the cohesion in 7% and the slope of the river bed in 9%.

The peak outflow was of 980.17 m^3/s while the breach width was of 150.74 m, as seen in Figures 40 and 41, and the breach's bottom elevation was in 45.34 m. The reservoir's water level over time was in good accord with the field data as in Figure 42, which it was expected by the similar hydrographs.

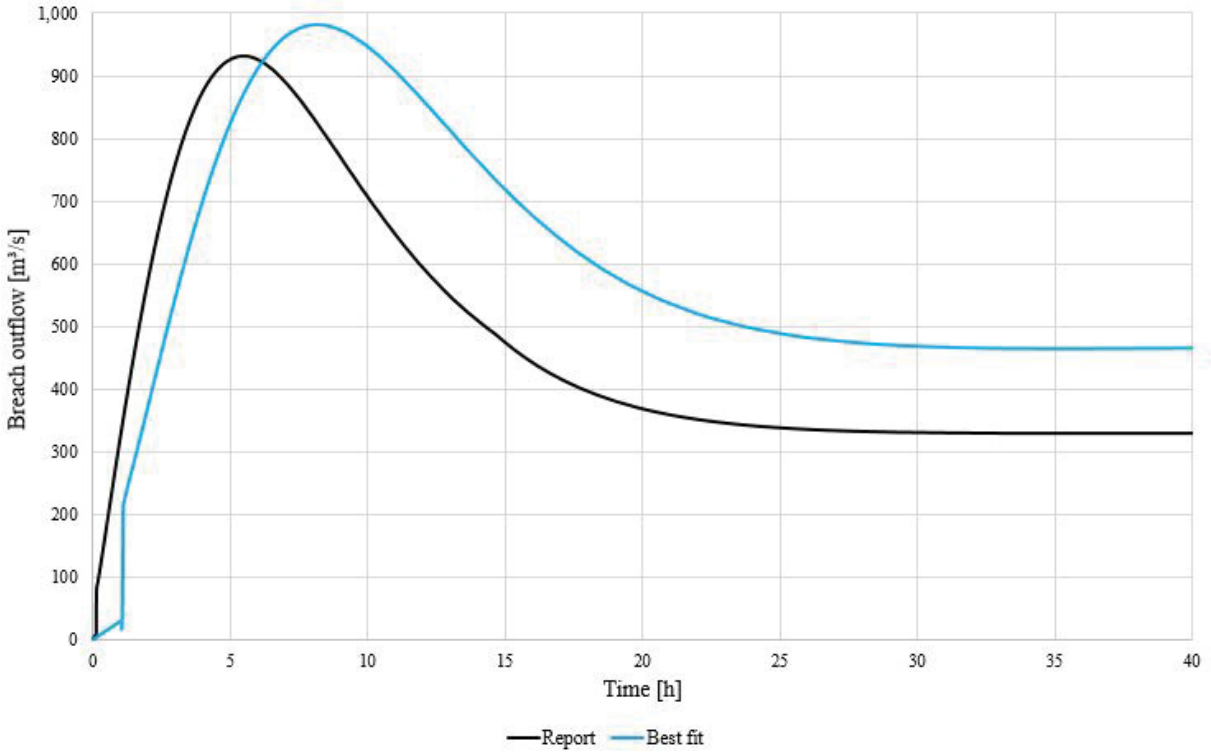

FIGURE 40 – Breach outflow for the best fit simulation (The author, 2019).

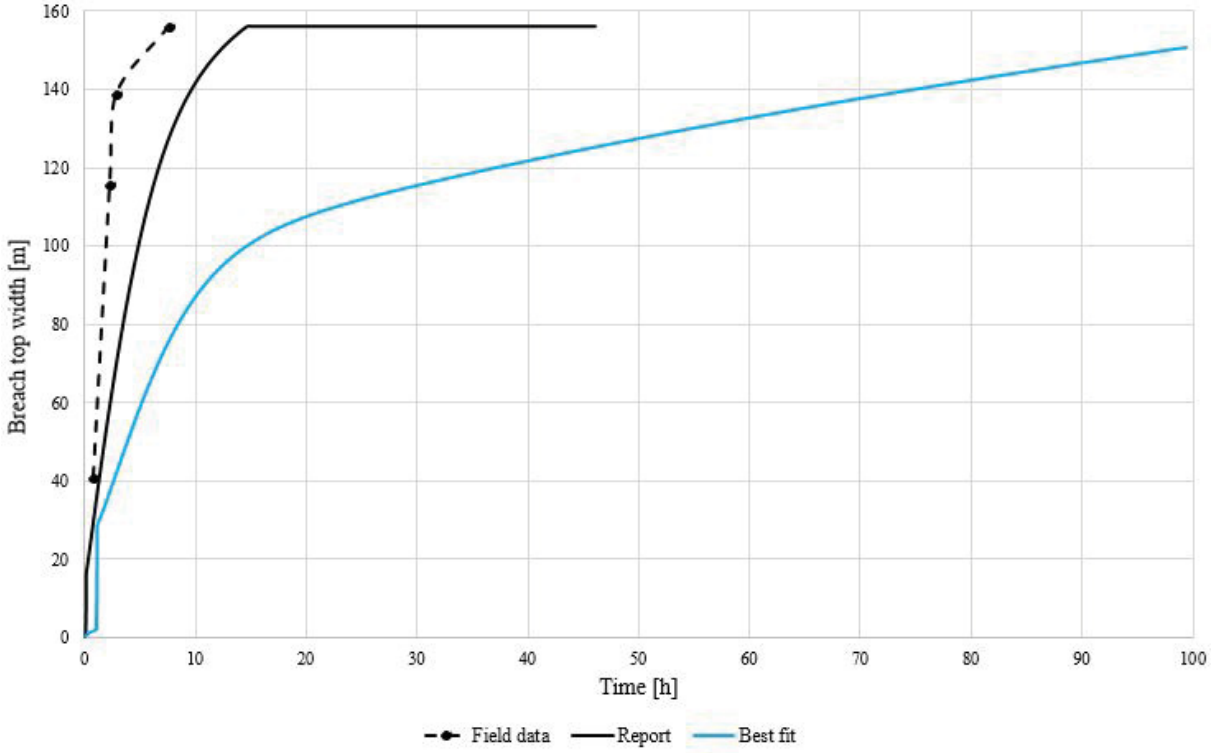

FIGURE 41 – Breach width for the best fit simulation (The author, 2019).

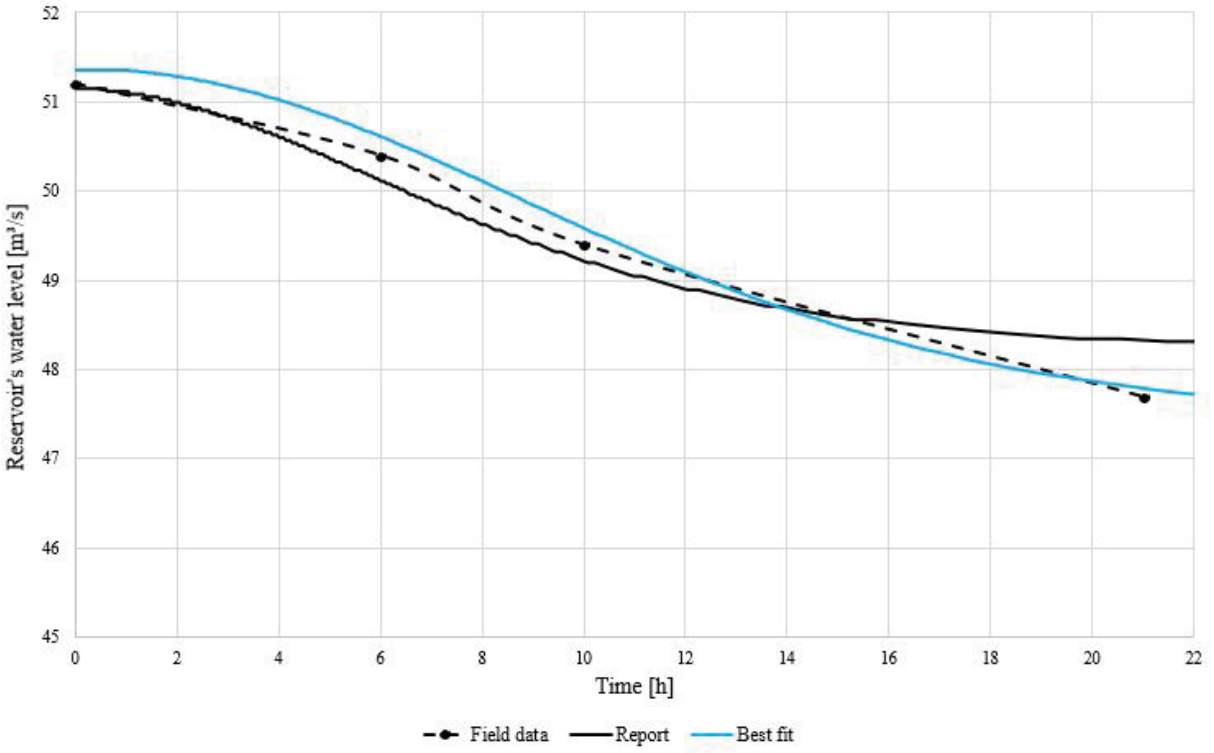

FIGURE 42 – Reservoir's water level for the best fit simulation (The author, 2019).

5.6 DISCUSSION OF RESULTS

Without altering the inputs, the model overestimated the outflow while underestimating the breach width, though the cofferdam was entirely breached. With small changes to the inputs, usually around 5%, the results came in part closer to the corrected answers. However, one of the variables of interest, either outflow or breach size, would still render the simulation as imprecise.

Adding new features to the BREACH model to work along the new routine helped improving the simulation. Moreover, the two additional features did not altered or corrected the zoned dam routine and that is important to emphasize. What they did was to consider a control section at downstream, as existed in the case study, and to avoid a total breached cofferdam caused by how the model was originally conceived - the erosion continues as long the reservoir is not empty or the dam is totally breach and the outflow is less than 10% of its peak.

Stopping the downward erosion when it became less than 5% its peak allowed to obtain a breach at a good final elevation, close to the 45 m as stated in the Report. Considering the ogee crest spillway between the up- and downstream cofferdams had two effects. The tailwater level was raised, some simulations showed no change in the outflow and the breach width because the cofferdam was totally breached by the ever ongoing erosion. However, when the erosion was limited the higher tailwater level halted the outflow and, in turn, reduced the final breach width as expected.

From the sensibility of the simulations to changes in the inputs, it can be seen that the simulation may give the correct breach outflow and width with the right input and without any extreme changes as done in the Report. For instance, with the feature to limit the breach elevation and reducing the friction angles in 8%, the cohesion in 7% and the slope of river bed in 9%, the peak outflow was 5.37% higher than the Report's while the breach width practically matched and the final elevation reached 45.34 m.

In comparison to the Report that did major changes (e.g. not defined porosity and cutting by half the remaining material properties), the best fit simulation resorted to reasonable ones to the point that it can be attributed to the normal variability of in site conditions and measurements of parameters.

A final remark is about the hydrographs. As observed in APPENDIX **??**, some of them shows sudden pattern changes. This occurs always with the transition from piping to overtopping or the second side slope collapse of the breach. This changes are present in the plotting of the breach top width as well.

6 CONCLUSION

Dam breaching is a complex phenomenon with great temporal variability. Several models exist and are still being developed nowadays, each one trying different strategies, computational grids and coupled differential equations to better describe the breaching. These models demand high computational time, what sometimes may not be interesting to assess potential risks at downstream in dam-break, are usually suitable only to homogeneous earthfill dams and, not so often, to embankment dams with an inner core. Thus, this thesis provides a way of analyzing the breaching of zoned dams, i.e. with a non-central inner core similar to cofferdams, through the open-source and free-of-use BREACH model.

The developed zoned dam routine performs well in modeling different zones to the dam body, similar to what is seen in cofferdams, and it does that in a similar fashion as the original model does already with embankment dams with an inner core.

The sensibility to the modeled zone is coherent with the observed results. Increasing the zone height makes it affect sooner the breaching and have a greater impact over it, reducing the peak outflow and, according to each case, increasing the time for it to happen. Reducing the D_{90}/D_{30} makes for a more uniform zone which reduces the peak outflow and increases the time to it, depending from the case. The reduction of the porosity presents the same effects, but with a smaller impact.

The only remark is regarding the D_{50}, since it raises the peak outflow along when mean diameter of the dam. According to the used equation of Meyer-Peter-Müller for sediment transport, a greater material corresponds to a lower sediment transport. However, this behavior exists also in the original BREACH which excludes the possibility of the new routine having any coding error that could be the cause of it. A possible reason seems to be that increasing the D_{50} corresponds to a greater space among the material grains that intensifies the outflow, in the same way as to what happens when we increase the D_{90}/D_{30}. Hence, the model accounts indirectly for a percolation.

Regarding the case study, the Report did great changes to the inputs in order to match the field data. As for the zoned dam routine, it provides a good match to the field data without any major variation, with the greatest change being to the slope of the river bed with a reduction of 9%. Plus, an additional feature works along the new routine and stops the downward erosion once it becomes less than 5% of its highest recorded value. As a result, the breach outflow is 5.37% higher while the breach width is matched to the Report.

Informing a discharge curve to work as a control section at downstream improves also the simulation of the case study, even though it does not take part in the best fit simulation.

Thus, the new BREACH is validated through this case study and it constitutes an one

of a kind model to assess the breaching of embankment dams, homogeneous or composite, and now zoned dams for both piping and overtopping. All the new features - zoned dams, limited bottom elevation of breach and downstream control section - are upon user's choice.

The BREACH model is a collection of empirical and analytical equations to describe a non-stationary and complex event that could be better defined by differential equations. So, for future researches we recommend the creation of a mathematical model for the zoned dam routine to improve the analyzes and to address the uncertainty around the sensibility to the D_{50}, found in the original BREACH. Moreover, the development of small-scaled models of composite and zoned dams would provide more data for validation.

Another recommendation is to study a sediment transport equation more suitable for cohesive materials, other than to adapt the measurement of the Shields parameter based only in the plasticity index as the BREACH model does. Thus, we could have a better modeling of clay-like materials without having to resort to equations for headcut erosion that need to estimate the erodibility of the material, which is difficult to do properly.

To further improve the BREACH model it would be interesting to consider the flow characteristics along the breach channel and the position where the breach's side slopes collapse. That's because if the control section, where the Froude number is one and there is the separation between the fluvial and torrential flows, is upstream of the collapse there will be no significant change to the flow kinematics. However, if the collapse occurs upstream it will cause a slight oscillation followed by an increase of the outflow.

Concerning the reservoir we recommend also that it is not treated anymore as a horizontal pool. Instead, the reservoir should be routed to better represent its variation in time.

A final recommendation is to rewrite the model. The code was written in 1988 and nowadays the Fortran language was improved in comparison to that time. Now some new functions are available that substitutes old ones and some old functions are no longer recommended for use. An example is the "GO TO"function that allows the program to freely jump back and forth in the code and it had the purpose of creating loops, making the code difficult to be studied for tending to lead to spaghetti codes. It would be helpful to exchange the "GO TO"to proper functions, creating a better structured and linear program. When rewritten the model, it could even be done with object oriented programming, making the model more flexible, modular and effective to solving problems.

REFERENCES

AMARAL, S. R. C. **Experimental characterization of the failure by overtopping of embankment dams**. 2017. Tese (Doutorado) – Instituto Superior Técnico - Universidade de Lisboa. Citado 2 vezes nas páginas 13, 30.

ANA. **Agência Nacional de Águas - Agência Nacional de Águas - 2017**. [S.l.], 2018. Citado 1 vez na página 12.

BENTO, A. M.; AMARAL, S.; VISEU, T.; CARDOSO, R.; FERREIRA, R. M. L. Direct Estimate of the Breach Hydrograph of an Overtopped Earth Dam. **Journal of Hydraulic Engineering**, v. 143, 2017. Citado 1 vez na página 31.

BOSS. **BOSS DAMBRK - Users manual**. [S.l.], 2003. Citado 1 vez na página 23.

BRASIL. **Lei n. 12.334 - Política Nacional de Segurança de Barragens**. [S.l.: s.n.], 2010. Presidência da República - Casa Civil. Citado 1 vez na página 12.

BRUNNER, G. **Using HEC-RAS for dambreak studies**. 1. ed. [S.l.], ago. 2014. Citado 3 vezes nas páginas 22, 29.

BUREAU. **U.S. Bureau of Reclamation - Design of Small Dams**. 3 ed. [S.l.], jan. 1987. Citado 4 vezes nas páginas 15–17.

CBDB. **Comitê Brasileiro de Barragens - Desvio de grandes rios brasileiros**. Edição: BCOLD Publications Committee. 1 ed. [S.l.]: BCOLD Publications Committee, 2009. Citado 1 vezes nas páginas 17, 18.

COSTA, W. D. **Geologia de barragens**. Edição: Oficina de Textos. 3 ed. [S.l.]: Oficina de Textos, 2012. Citado 2 vezes nas páginas 17, 18.

CRESPO, A. J. C.; DOMINGUEZ, J. M.; ROGERS, B. D.; GÓMEZ-GESTEIRA, M.; LONGSHAW, S.; CANELAS, R.; VACONDIO, R.; BARREIRO, A.; GARCÍA-FEAL, O. DualSPHYSICS: Open-source parallel CFD solver based on Smoothede Particle Hydrodynamics. **Computer Physics Communications**, 2015. Citado 1 vez na página 27.

CRUZ, P. T.; MATERÓN, B.; FREITAS, M. **Barragens de enrocamento com face de concreto**. Edição: Oficina de Textos. [S.l.]: Oficina de Textos, 2014. Citado 0 vez na página 16.

ENGEMOEN, W. C. **Embankment design - Design standards n. 13**. 10 ed. [S.l.], dez. 2012. Citado 5 vezes nas páginas 15–17.

FEMA. **Strategic Plan for the National Dam Safety Program Fiscal YEars 2012 - 2016**. [S.l.], out. 2012. Citado 1 vez na página 12.

FERREIRA, R. M. L.; FRANCA, M. J.; LEAL, J. G. A. B.; CARDOSO, A. H. Mathematical modeling of shallow flows: Closure models drawn from grain-scale mechanics of sediment transport and flow hydrodynamics. **Canadian Journal of Civil Engineering**, v. 36, p. 1605–1621, 2009. Citado 1 vez na página 28.

FREAD, D. L. **BREACH: An erosion model for earthen dam failures**. 2 ed. [S.l.], ago. 1991. Citado 5 vezes nas páginas 13, 23, 33–35, 39, 42.

GÓMEZ-GESTEIRA, M.; ROGERS, B. D.; C., CRESPO A. J.; DALRYMPLE, R. A.; NARAYANASWAMY, M.; DOMÍNGUEZ, J. M. SPHysics - Development of a free-surface fluid solver - Part 1: Theory and formulations. **Computer & Geosciences**, 2012. Citado 1 vez na página 27.

_____. SPHysics - Development of a free-surface fluid solver - Part 2: Efficiency and test cases. **Computer & Geosciences**, 2012. Citado 1 vez na página 27.

GRAF, Walter Hans. **Hydraulics of Sediment Transport**. Edição: Water Resources Publications. 1. ed. [S.l.]: Water Resources Publications, 1984. ISBN 0-918334-56-X. Citado 1 vez na página 39.

HANSON, G. J.; COOK, K. R.; HUNT, S. Prediction of Headcut Migration Using a Deterministic Approach. **American Society of Agricultural Engineers**, 2005. Citado 0 vez na página 20.

HENDERSON, F. **Open Channel Flow**. Edição: G. Nordby. 15 ed. [S.l.]: Macmilllan Publishing Co, 1966. ISBN 0309092930. Citado 1 vez na página 40.

ICOLD. **As Barragens e a Água do Mundo**. [S.l.], 2008. Citado 1 vez na página 15.

IMPACT. **Investigation of Extreme Flood Processes and Uncertainty - Breach formation (WP2) - Technical report: sections 4**. [S.l.], 2004. Citado 0 vez na página 20.

_____. **Investigation of Extreme Flood Processes and Uncertainty - Breach formation (WP2) - Technical report: sections 7 - 9**. [S.l.], 2004. Citado 1 vez na página 20.

_____. **Investigation of Extreme Flood Processes & Uncertainty - Final technical report**. [S.l.], 2005. Citado 1 vez na página 25.

_____. **Investigation of Extreme Flood Processes & Uncertainty - Risk and Uncertainty (WP5) - Technical report**. [S.l.], dez. 2004. Citado 1 vez na página 26.

KAHAWITA, R. **REPORT N. T032700-0207C: Dam Breach Modeling - A literature review of numerical models**. [S.l.], dez. 2007. Citado 3 vezes nas páginas 18, 19.

LOPES, A. F. P. **Numerical Modeling of Earth Dam Breaching by Overtopping**. 2015. Tese (Doutorado) – Instituto Superior Técnico de Lisboa. Citado 1 vez na página 28.

LUO, Y.; CHEN, L.; XU, M.; TONG, X. Review of dam-break research of earth-rock dam combining with dam safety management. **Procedia Engineering**, v. 28, p. 382–288, 2011. ISSN 18777058. Citado 1 vez na página 12.

MACHADO, N. C. **RETROANÁLISE DA PROPAGACÃO DECORRENTE DA RUPTURA DA BARRAGEM DE FUNDÃO COM DIFERENTES MODELOS NUMÉRICOS E HIPÓTESES DE SIMULACÃO**. 2017. Diss. (Mestrado) – Universidade Federal de Minas Gerais - Programa de Pós Graduacão em Saneamento, Meio Ambiente e Recursos Hídricos. Citado 1 vez na página 30.

MAGELA, G. **Projeto de usinas hidrelétricas - passo a passo**. Edição: Oficina de Textos. 1 ed. [S.l.]: Oficina de Textos, 2015. ISBN 978-85-7975-162-2. Citado 0 vez na página 16.

MORRIS, M. **Breaching of Embankments and Dams**. 2011. Tese (Doutorado) – Open University. Citado 11 vezes nas páginas 13, 18–21, 27, 58.

MORRIS, M. W.; HASSAN, M. A. A. M.; SAMUELS, P. G.; GHAHATAORA, G. S. **Development of the HR BREACH model for predicting breach growth through flood embankments and embankment dams**. [S.l.], 2008. Citado 1 vezes nas páginas 20, 21.

MORRIS, M.; GALLAND, J.-C.; BALABANIS, P. Proceedings of the CADAM meeting in Milan, Italy, 6 and 7 May 1999. In: _____. **CADAM: Concerted Action on Dam-Break Modeling**. [S.l.]: European Communities, 2000. European Comission. Citado 1 vez na página 25.

_____. Proceedings of the CADAM meeting in Munich, Germany, 8 and 9 October 1998. In: _____. **CADAM: Concerted Action on Dam-Break Modeling**. [S.l.]: European Communities, 1999. European Comission. Citado 1 vez na página 25.

_____. Proceedings of the CADAM meeting in Zaragoza, Spain, 18 and 19 November 1999. In: _____. **CADAM: Concerted Action on Dam-Break Modeling**. [S.l.]: European Communities, 2000. European Comission. Citado 1 vez na página 25.

MORRIS, M.; HASSAN, M. **FLOODsite Project Report T06-08-11 - Breach Initiation & Growth: Physical Processes**. [S.l.], mar. 2009. Citado 1 vez na página 20.

MORRIS, M.; J.-C., GALLAND; BALABANIS, P. Proceedings of the CADAM meeting in Wallingford, United Kingdom, 2 and 3 March 1998. In: _____. **CADAM: Concerted Action on Dam-Break Modeling**. [S.l.]: European Communities, 1999. European Comission. Citado 3 vezes nas páginas 12, 24.

MORRIS, M.; SAMUELS, P. Final Report. In: HR WALLINGFORD. CADAM: Concerted Action on Dambreak Modelling. [S.l.]: European Communities, 2000. Citado 1 vez na página 25.

NOGUEIRA, V. **A mathematical model of progressive earth dam failure**. 1984. Tese (Doutorado) – Colorado State University. Citado 1 vez na página 22.

SMART, G. M. Sediment Transport Formula for Steep Channels. **Journal of Hydraulic Engineering**, v. 110, n. 3, p. 267–276, 1984. ISSN 0733-9429. Citado 3 vezes nas páginas 21, 39.

VAN EMELEN, S.; ZECH, Y.; SOARES-FRAZAO, S. Impact of sediment transport formulations on breaching modelling. **Journal of Hydraulic Research**, v. 53, n. 1, p. 60–72, 2015. ISSN 00221686. Citado 1 vez na página 21.

WAHL, T. L. Dam Breach Modeling: An Overview of Analysis Methods. In: JOINT Federal Interagency Conference on Sedimentation and Hydrologic Modeling. [S.l.: s.n.], jun. 2010. Citado 2 vez na página 12.

_____. Predicting Embankment Dam Breach Parameters - A Needs Assessment. **XXVII IAHR Congress**, p. 48–53, 1997. Citado 1 vez na página 13.

_____. **Prediction of Embankment Dam Breach Parameters - A literature Review and Needs Assessment**. [S.l.], jul. 1998. Citado 2 vez na página 18.

WEST, M.; MORRIS, M.; HASSAN, M. **A guide to breach prediction**. [S.l.], jan. 2018. Citado 3 vezes nas páginas 13, 19.

WU, W. Earthen Embankment Breaching. **Journal of Hydraulic Engineering**, v. 137, p. 1549–1564, 2011. Citado 1 vez na página 21.

_____. **Introduction to DLBreach - A Simplified Physically-Based Dam/Levee Breach Model**. 4 ed. [S.l.], abr. 2016. Citado 1 vez na página 28.

XU, Y.; ZHANG, L. Breaching Parameters for Earth and Rockfill Dams. **Journal of Geotechnical and Geoenvironmental Engineering**, v. 135, p. 1957–1970, 2009. ISSN 1090-0241. Citado 1 vez na página 20.

ZHU, Y.; VISSER, P.; VRIJLING, J. Review on embankment dam breach modeling. **New Developments in Dam Engineering**, p. 1189–1196, 2004. Citado 2 vez na página 19.

APPENDICES

APPENDIX A – FLOWCHART OF ORIGINAL NWS BREACH MODEL

The description of the variables is listed bellow.

Q_{wr} is the flow over dam crest;

Q_{sp} is the flow over spillway;

Q_s is the sediment outflow;

Q_b is the breach outflow;

i is the time-iteration counter;

t is the simulation time;

dt is the time-step;

$t_{max.simulation}$ is the maximum simulation time;

j is the convergence-iteration counter;

S is the channel slope;

V is the flow velocity;

h is the flow depth;

DH is the estimated erosion;

DHH is the measured erosion;

H is the breach height;

Error is the accepted error between estimates and measurements (input);

FTH is a factor with its first value equal to 1;

DY is the variation of reservoir's water level;

DYE is the corrected value of DY based on previous iterations;

YC is the wedge height that causes collapse due to hydrostatic force;

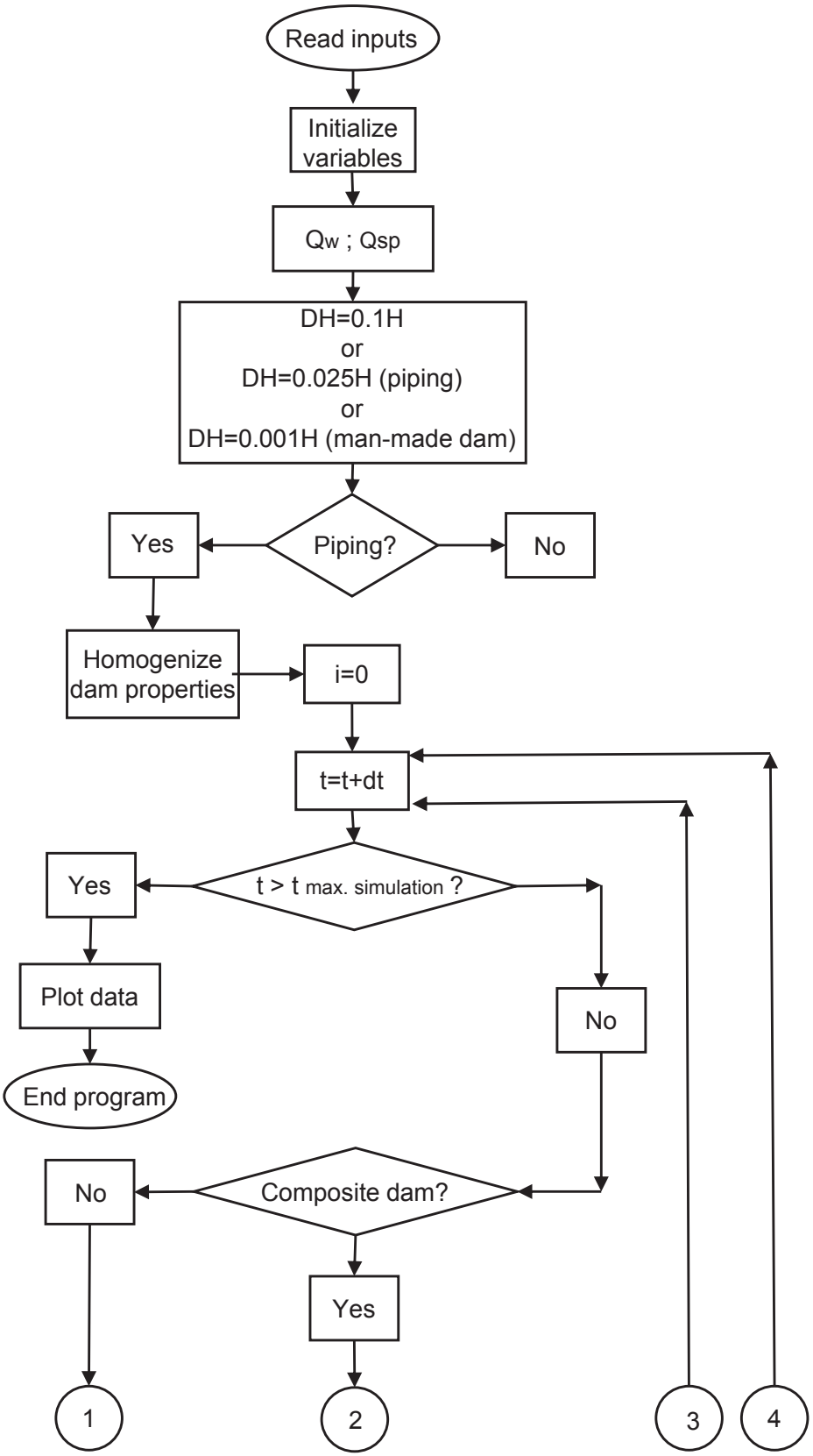
Read inputs
Initialize variables
Qw ; Qsp
DH=0.1H
or
DH=0.025H (piping)
or
DH=0.001H (man-made dam)
Piping?
Yes
No
Homogenize dam properties
i=0
t=t+dt
t > t max. simulation ?
Yes
No
Plot data
End program
Composite dam?
No
Yes
1
2
3
4

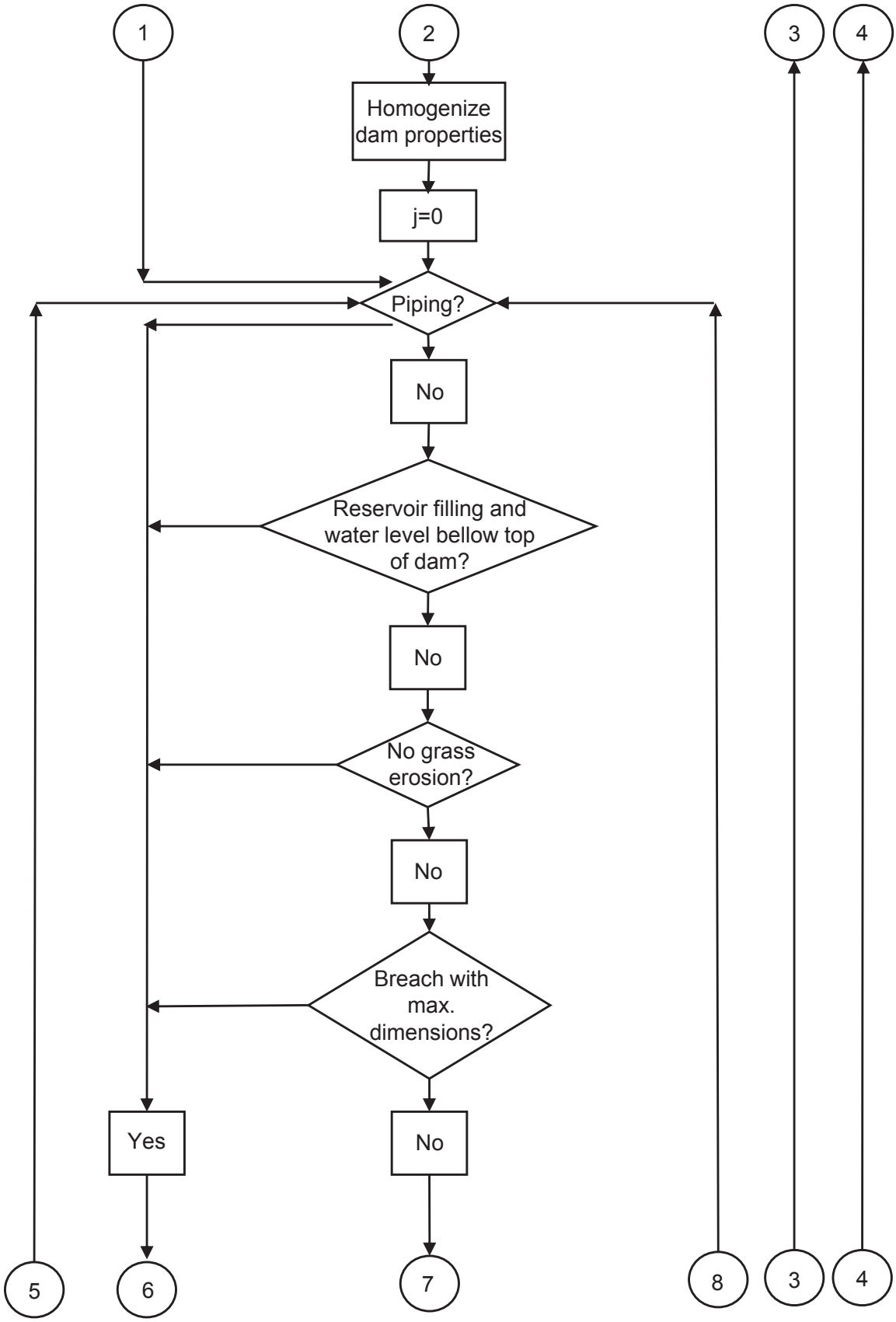
1
2
3
4
Homogenize dam properties
j=0
Piping?
No
Reservoir filling and water level bellow top of dam?
No
No grass erosion?
No
Breach with max. dimensions?
Yes
No
5
6
7
8
3
4

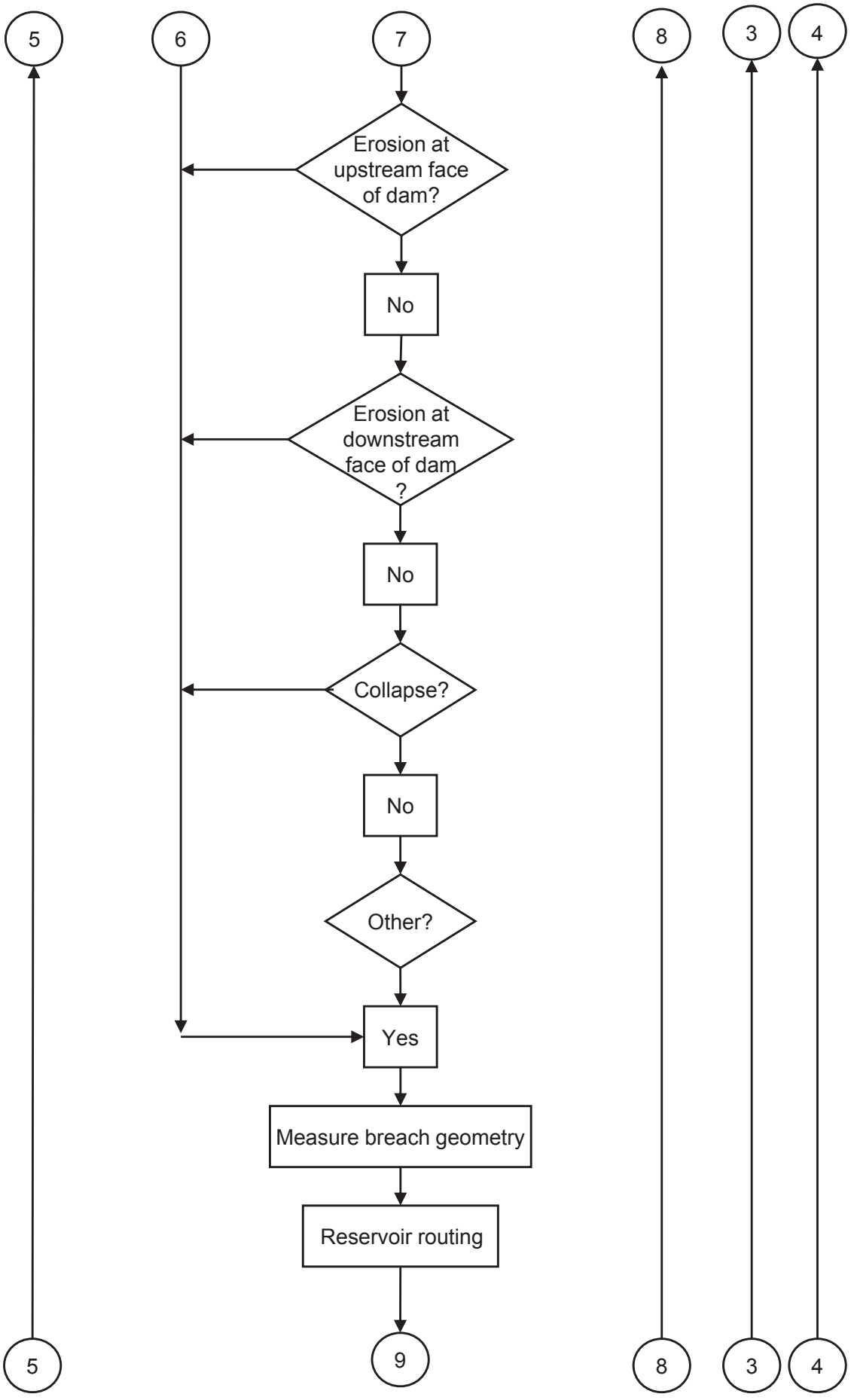
5
6
7
8
3
4
Erosion at upstream face of dam?
No
Erosion at downstream face of dam ?
No
Collapse?
No
Other?
Yes
Measure breach geometry
Reservoir routing
9
5
8
3
4

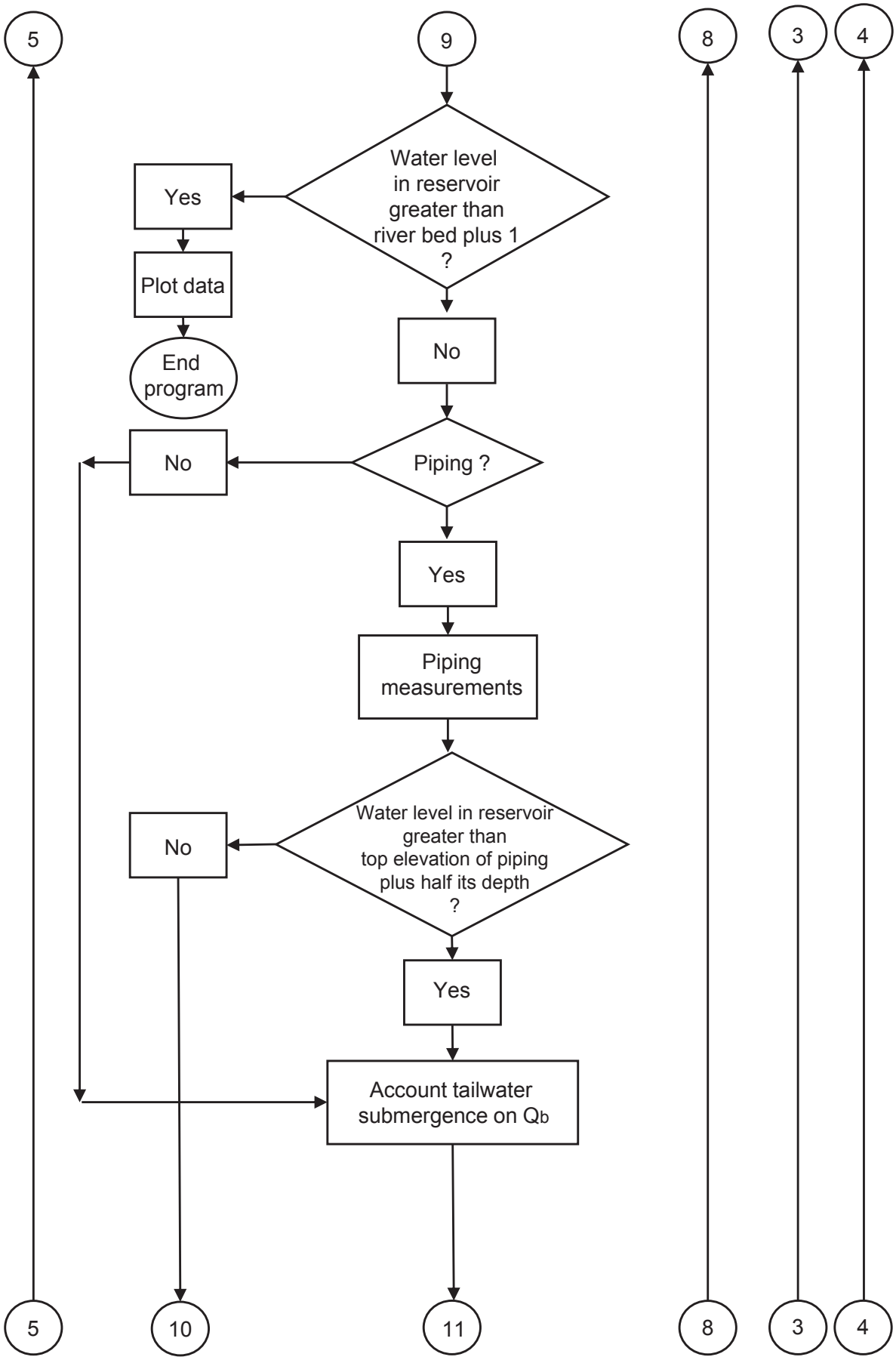
5
9
8
3
4
Water level in reservoir greater than river bed plus 1 ?
Yes
Plot data
End program
No
Piping ?
No
Yes
Piping measurements
Water level in reservoir greater than top elevation of piping plus half its depth ?
No
Yes
Account tailwater submergence on Qb
5
10
11
8
3
4

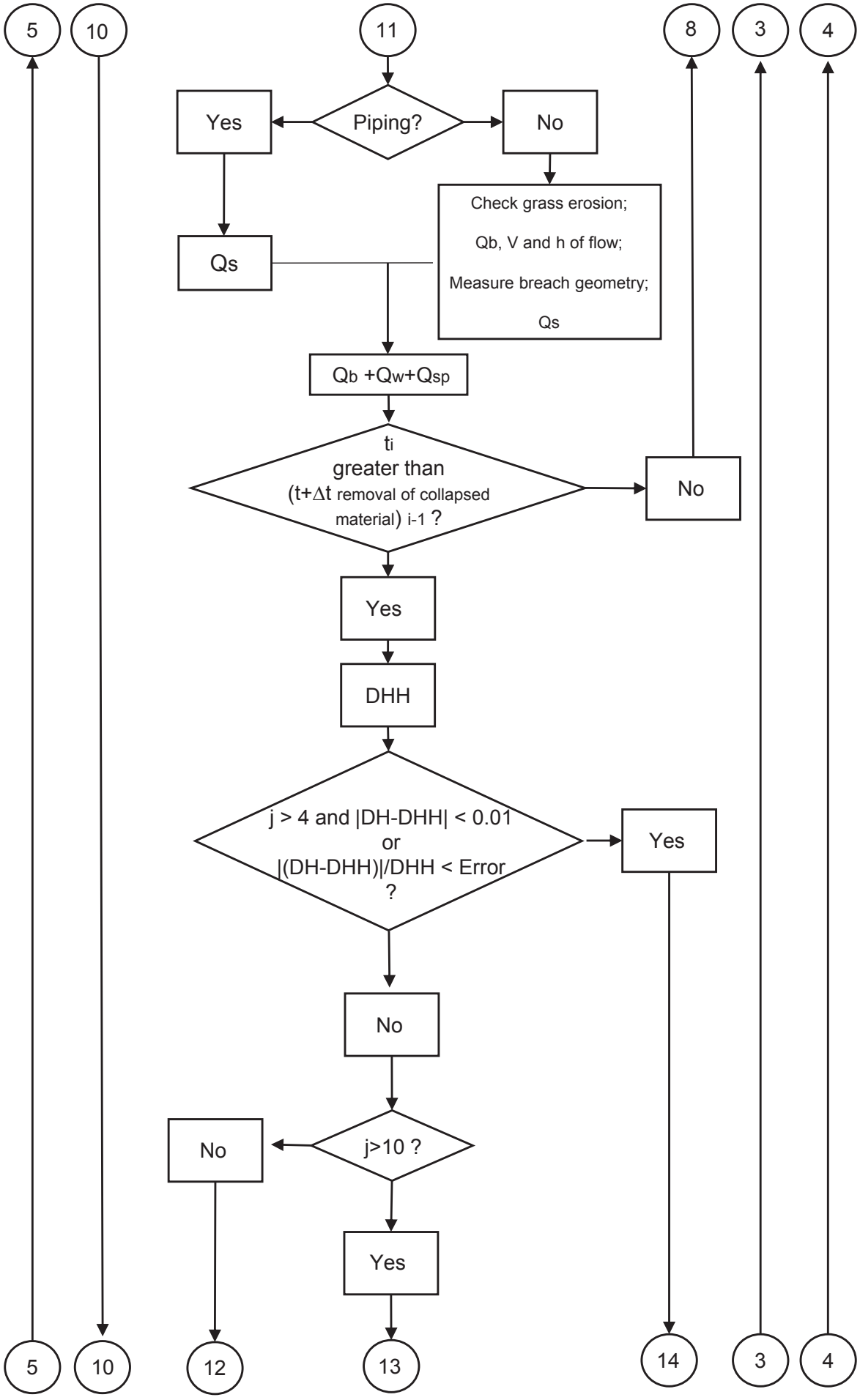
5
10
11
8
3
4
Yes
Piping?
No
Check grass erosion;
Qb, V and h of flow;
Measure breach geometry;
Qs
Qs
Qb +Qw+Qsp
ti
greater than
(t+Δt removal of collapsed material) i-1 ?
No
Yes
DHH
j > 4 and |DH-DHH| < 0.01
or
|(DH-DHH)|/DHH < Error
?
Yes
No
No
j>10 ?
Yes
5
10
12
13
14
3
4

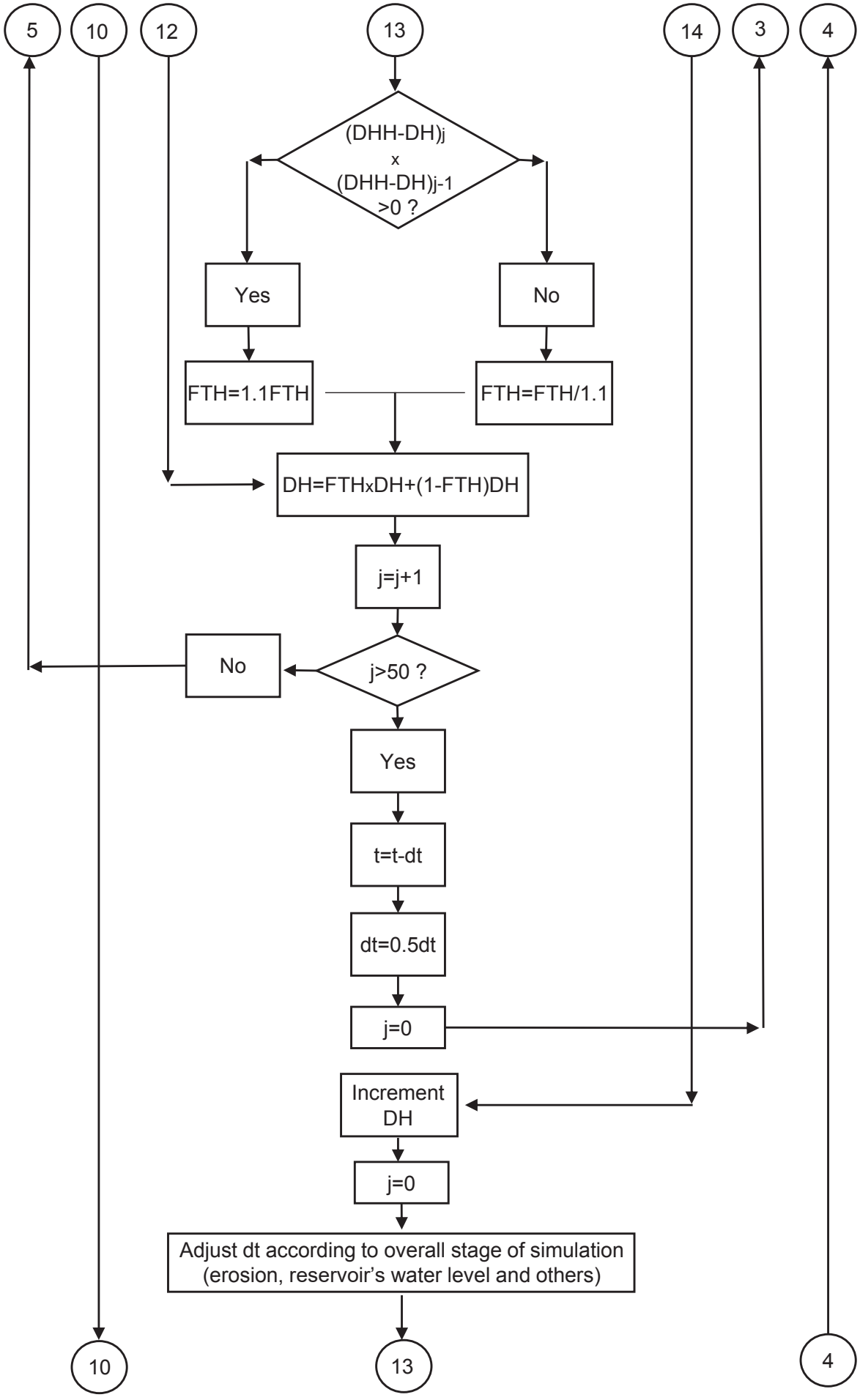
5
10
12
13
14
3
4
(DHH-DH)j
x
(DHH-DH)j-1
>0 ?
Yes
No
FTH=1.1FTH
FTH=FTH/1.1
DH=FTHxDH+(1-FTH)DH
j=j+1
No
j>50 ?
Yes
t=t-dt
dt=0.5dt
j=0
Increment
DH
j=0
Adjust dt according to overall stage of simulation
(erosion, reservoir's water level and others)
10
13
4

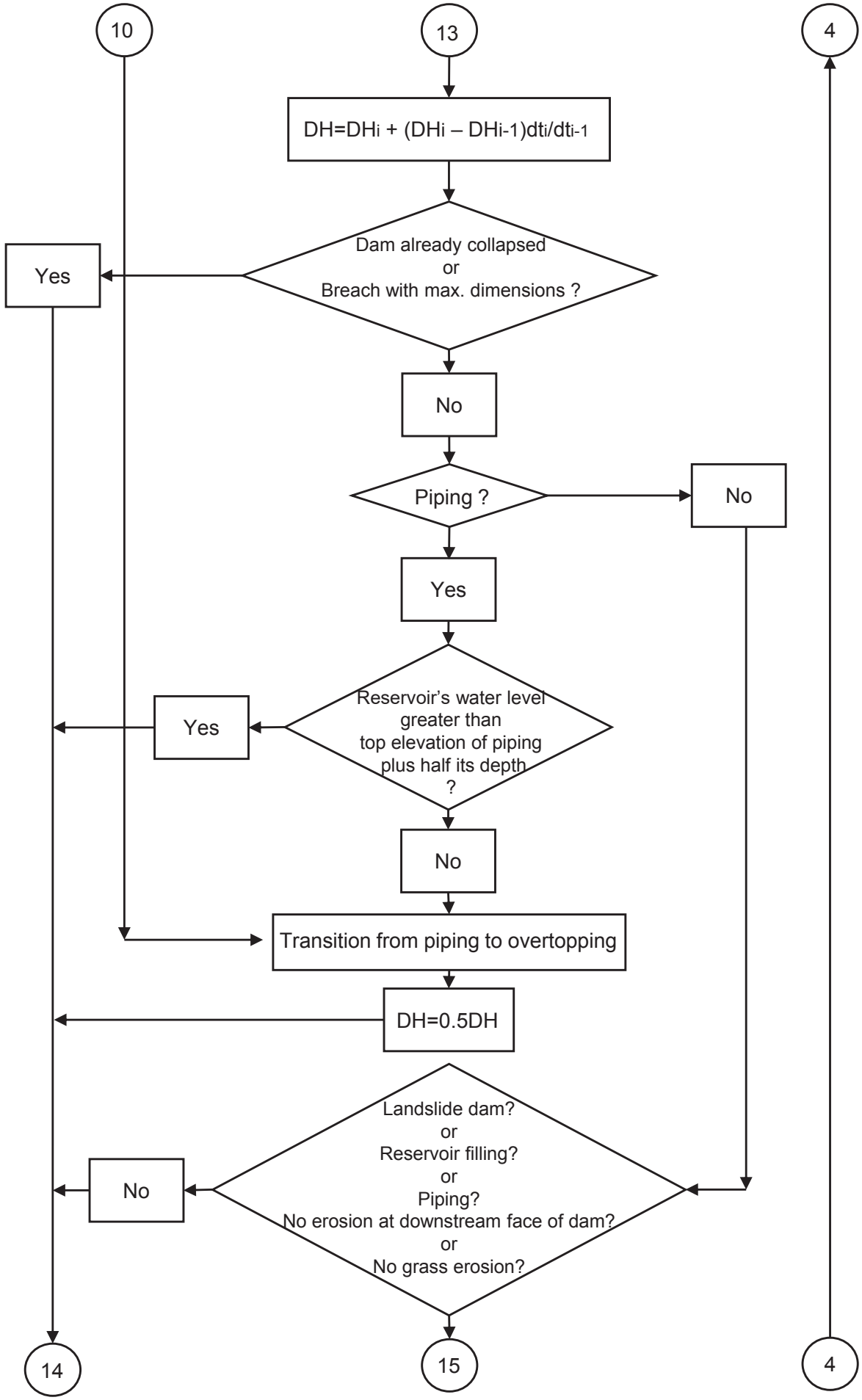
10
13
4
DH=DHi + (DHi – DHi-1)dti/dti-1
Dam already collapsed
or
Breach with max. dimensions ?
Yes
No
Piping ?
No
Yes
Reservoir's water level
greater than
top elevation of piping
plus half its depth
?
Yes
No
Transition from piping to overtopping
DH=0.5DH
Landslide dam?
or
Reservoir filling?
or
Piping?
No erosion at downstream face of dam?
or
No grass erosion?
No
14
15
4

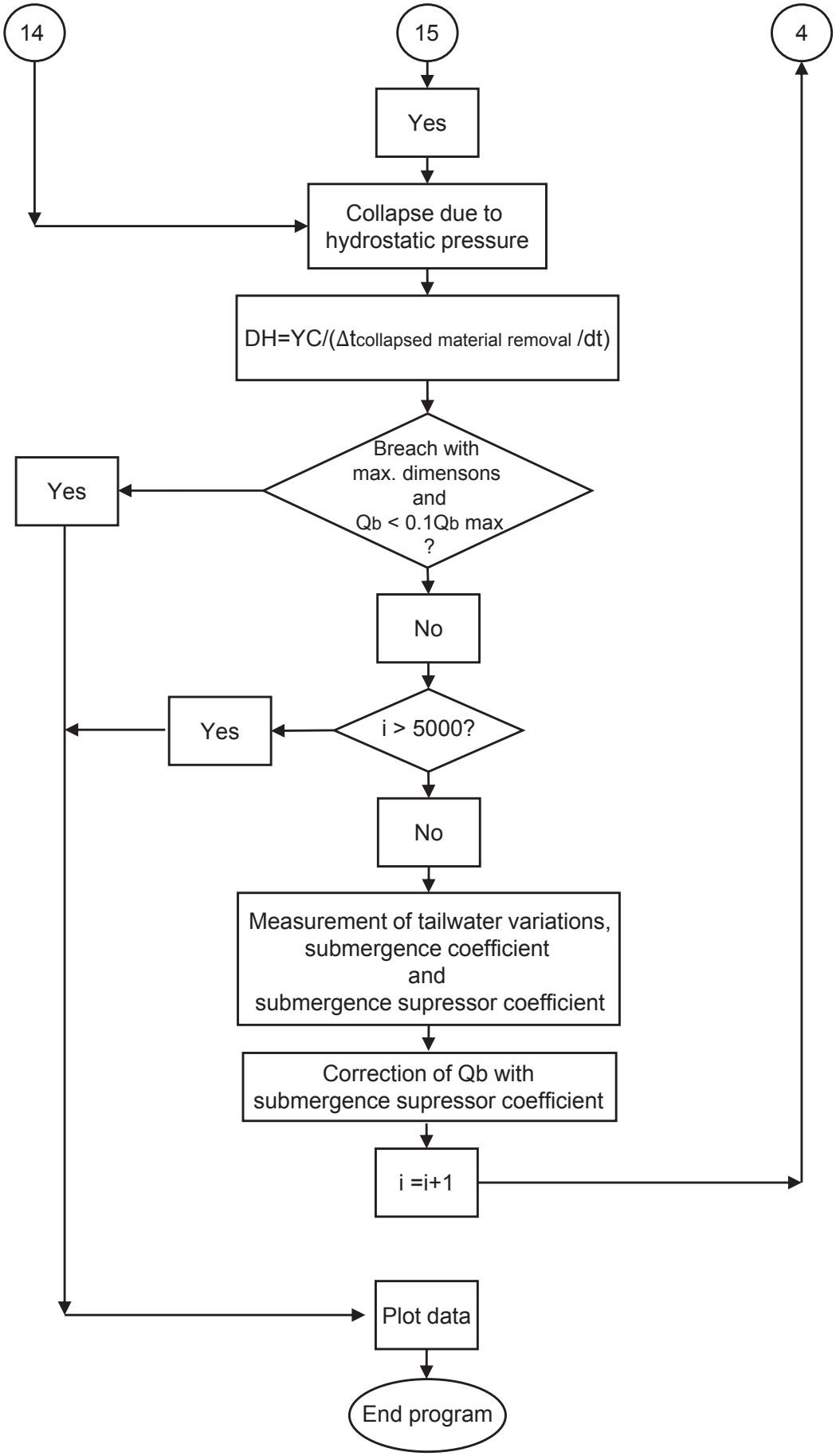
14
15
4
Yes
Collapse due to hydrostatic pressure
DH=YC/(Δtcollapsed material removal /dt)
Breach with max. dimensons and Qb < 0.1Qb max ?
Yes
No
i > 5000?
Yes
No
Measurement of tailwater variations, submergence coefficient and submergence supressor coefficient
Correction of Qb with submergence supressor coefficient
i =i+1
Plot data
End program

APPENDIX B – INPUTS OF THE NEW BREACH MODEL

The following inputs are named as presented and used in the own source code. For the program to read them, they need to be written in a text file (.txt) in which each line contains the informations of each following item. When an item contains more than one information, separate them with a single space.

To make it more user friendly, all inputs are converted to the Imperial System of Units, since the original BREACH model works with such.

1. MESSAGE: Any message such as name of dam, message may be up to 80 characters;
2. HI: Initial elevation of water surface in reservoir at t=0 [m];

   HU: Elevation of top of dam [m];

   HL: Elevation of bottom of dam (usually original stream-bed elevation) [m];

   HPI: Elevation at which piping failure commences (if no piping failure is simulated, leave blank) [m];

   HSP: Elevation of spillway crest (if no spillway, leave, blank) [m];

   PI: Average plasticity index for clay of predominately clay dams [m];

   CA: Coefficient for clay critical shear stress recommended between 0.004 <CA< 0.02 [-];

   CB: Coefficient for clay critical stress recommended between 0.58 < CB < 0.84 [-].
3. QIN(I): Inflow to reservoir [m^3/s]. I subscript goes from 1 to 8. Inflow hydrograph may be defined with from 2 to 8 values.
4. TIN(I): Time associated with QIN(I) reservoir inflow [h].
5. RSA(I): Surface area of reservoir [km^2]. I subscript goes from 1 to 8. Surface area is defined using 2 to 8 elevations starting at the highest elevation and proceeding to the reservoir bottom.
6. HSA(I): Elevation associated with RSA(I) surface area [m].
7. HSTW(I): Elevation associated with top widths of tailwater cross-section [m]. Elevations start at invert. I goes from 1 to maximum of 8.
8. BSTW(I): Top widths of tailwater cross-section [m].
9. CMTW(I): Manning's coefficient associated with each top width of the tailwater cross-section.

10. ZU: Slope of upstream face of dam [1 (vertical) : ZU (horizontal)];

    ZD: Slope of downstream face of dam [1 (vertical) : ZD (horizontal)];

    ZC: Average slope of upstream and downstream faces of inner core of dam [1 (vertical) : ZC (horizontal)]. If no inner core, leave blank;

    GL: Average length of grass [cm]. If no grass, leave blank;

    GS: Condition of stand of grass. If good GS=1, if poor stand or no grass exists GS=0;

    VMP: Maximum permissible velocity [m/sec] for grass-lined channel before grass cover is eroded away. Can vary from 3 to 6 [m/sec]. If no grass, leave blank;

    SEDCON: Maximum sediment concentrations (0.4 to 0.5) in breach flow. If left blank, default value of 0.5 is used.

11. D50C: D_{50} [mm] grain size of inner core material (50 percent finer). If no core, leave blank;

    PORC: Porosity ratio of inner core material [-]. If no core, leave blank;

    UWC: Unit weight [kg/m^3] of inner core material. If no core, leave blank;

    CNC: Manning's coefficient of inner core material. If left blank, it will be computed from the Strickler equation which is a function of the grain size. If a value greater than 0.99 is entered, it will be computed from a Moody diagram (Darcy f vs. D50 relationship). If no core, leave blank;

    AFRC: Internal friction angle [degrees] of inner core material. If no core, leave blank;

    COHC: Cohesive strength [kg/m^2] of inner core material. If no core, leave blank;

    UNFCC: Ratio of D_{90} to D_{30} grain sizes of inner core material. If no core, leave blank. If core exists and left blank, default value is 10.

12. D50S: D_{50} [mm] grain size of outer core material (50 percent finer). If no core, leave blank;

    PORS: Porosity ratio of outer core material [-]. If no core, leave blank;

    UWS: Unit weight [kg/m^3] of outer core material. If no core, leave blank;

    CNS: Manning's coefficient of outer core material. If left blank, it will be computed from the Strickler equation which is a function of the grain size. If a value greater than 0.99 is entered, it will be computed from a Moody diagram (Darcy f vs. D50 relationship). If no core, leave blank;

    AFRS: Internal friction angle [degrees] of outer core material. If no core, leave blank;

    COHS: Cohesive strength [kg/m^2] of outer core material. If no core, leave blank;

    UNFCS: Ratio of D_{90} to D_{30} grain sizes of outer core material. If no core, leave blank. If core exists and left blank, default value is 10.

- Note: If dam material is homogeneous, use the outer layer to represent the entire homogenous dam material.

13. BR: Ratio of breach width to flow depth for initial rectangular-shaped breach. Range of value are from 1 to 2. Usually use 2 for overtopping and 1 for a piping failure. If left blank, BR=2;

    WC: Width [m] of crest of dam (can be zero);

    CRL: Length [m] of crest of dam;

    SM: Bottom slope [m/km] of downstream river for first few thousand feet below the dam;

    D50DF: D_{50} [mm] grain size of material composing the top one-foot of the downstream face of the dam. If left blank, D50DF=D50S;

    UNFCDF: Ratio of D_{90} to D_{30} grain size of material of downstream face. If left blank, UNFCDF=3 when D50DF>0 or UNFCDF=UNFCS when D50F=0;

    BMX: Maximum allowable width [m] of breach bottom as restrained by valley cross-section;

    BTMX: Maximum allowable width [m] of breach top as restrained by valley cross-section.

    - Note: Omit items 15 and 16 if spillway crest elevation HSP (item 2) is blank or zero.

14. SPQ(I): Spillway flow [m^3/s]. I subscript goes from 1 to 8. Spillway flow is defined for from 2 to 8 heads starting at the spillway crest elevation and proceeding upwards until maximum spillway.

15. SPH(I): Head [m] associated with SPQ(I) spillway flow.

    - Note: Zoned dam routine - inputs.

16. MODE: Equal to 1 if a zone is within the dam, otherwise equal to 0;

    HCLIM: Equal to 1 if the downward erosion is limited to 5% of its peak erosion;

    ZDZONE: Slope of the downstream face of the zone [1 m : ZDZONE];

    WCZONE: Width of zone [m];

    HZONE: Top elevation of the zone [m];

    D50ZONE: Grain size of zone material which 50% is finer [mm];

    UWZONE: Unit weight of zone material [kg/m^3];

    COHZONE: Cohesion of zone material [kg/m^2];

    AFRZONE: Internal friction angle of zone material [$^\circ$];

PORZONE: Porosity of zone material [%];

D90D30ZONE: Ratio of D_{90} to D_{30} grain size of zone material [-];

CNZONE: Manning's coefficient of zone material. If left blank, it is measured as a function of grain size.

- Note: Omit item 18 if there is no control section at downstream.

17. QCONTROL(I): Flow at the downstream control section [m^3/s]. I subscript goes from 1 to 8. Spillway flow is defined for from 2 to 8 heads starting at the spillway crest elevation and proceeding upwards until maximum spillway.

18. HCONTROL(I): Head [m] associated with SPQ(I) spillway flow.

APPENDIX C – OUTPUTS OF THE NEW BREACH MODEL

To make it more user friendly, the model converts all outputs to the International System of Units.

I: COUNTER;

T: Time [h];

DTH: Time-step [h];

KG: Code for region of failure:

-1 reservoir filling;

0 no erosion on grass;

1 erosion of downstream face;

2 erosion of upstream face;

3 draining of reservoir with breach size fixed at max dimensions;

4 piping mode;

5 collapse mode.

KC: Collapse height [m];

QTOT: total outflow [m^3/s];

QTS: Spillway outflow [m^3/s];

QB: Breach outflow [m^3/s];

SUB: Submergence correction factor bt top width of breach [m];

HY: Elevation of reservoir water surface, ft hc elev of bottom of breach [m];

BO: Bottom width of breach [m];

PPP:

Depth [m] of erosion perpendicular to downstream face (KREG=1);

Length [m] of breach along downstream face (KREG=2);

Breach width [m] increase (KREG=3);

Elevation [m] of top of pipe (KREG=4).

HP:

Distance [m] eroded across top of dam (KREG=1);

Vertical distance [m] eroded at upstream face (KREG=2);

Depth [m] of flow in breach (KREG=3);

Head [m] on pipe (KREG=4).

TWD: Tail water depth [m];

DH: Estimated erosion depth during time step [m];

DHH: Computed erosion depth during time-step [m];

KIT: Iteration counter;

AGL: Acute angle [degrees] that breach side makes with vertical;

QPB: Maximum outflow through breach [m^3/s];

TP: Time at which peak outflow occurs [h];

QP: Maximum total outflow occurring at time TP [m^3/s];

TRS: Duration of rising limb of hydrograph (TP-TB) [h];

TB: Time [h] at which failure starts (either KG=2 or KG=4);

BRD: Final depth [m] of breach;

BRW: Top width [m] of breach at time tp hu elev [m] of top of dam;

HY: Final elevation of reservoir water surface [m];

HC: Final elevation of bottom of breach [m];

QO: Outflow at t=0 [m^3/s];

Z: Side slope of breach at time tp [m/m];

TFH: Time of failure [h] determined by simplified dam-break equation from the SMPDBK model;

TFHI: Time of failure [h] determined by integration of discharge time series from TB to TP;

BO: Bottom width [m] of breach at time TP.

APPENDIX D – PERCENTAGE VARIATIONS OF A ZONE IN MANTARO LANDSLIDE DAM

HZONE is the height of implemented zone [-];

H is the dam height [-];

D_{90}/D_{30} is the ratio of grain diameter for which 90% and 30% of the sample is finer [-];

Qp is the peak outflow [-];

Tp is the time to peak outflow [-];

Tf is the simulation time [-];

Breach is the height of the breach [-].

TABLE D.1 – Percentage variations for an implemented zone of porosity of 65% - Part I.

25 mm						
D90/D30	HZONE = 0.3H			HZONE = 0.4H		
	Qp	**Tp**	**Breach**	**Qp**	**Tp**	**Breach**
1	-0.40%	-3.03%	-27.41%	-29.02%	-25.09%	-35.93%
100	0.31%	1.01%	-10.59%	-3.54%	-5.08%	-16.17%
200	3.67%	5.68%	-7.35%	5.83%	-4.01%	-12.60%
300	6.69%	7.55%	-5.39%	11.98%	-4.71%	-10.45%
400	9.30%	8.75%	-3.94%	16.62%	-3.86%	-8.89%
D90/D30	HZONE = 0.5H			HZONE = 0.6H		
	Qp	**Tp**	**Breach**	**Qp**	**Tp**	**Breach**
1	-61.07%	-3.69%	-42.82%	-72.29%	42.46%	-47.47%
100	-16.39%	-8.29%	-21.49%	-31.01%	-5.94%	-26.47%
200	-5.76%	-10.21%	-17.79%	-21.31%	-10.24%	-22.72%
300	1.06%	-11.07%	-15.58%	-15.03%	-13.34%	-20.38%
400	6.21%	-11.22%	-13.97%	-10.35%	-15.22%	-18.75%

TABLE D.2 – Percentage variations for an implemented zone of porosity of 65% - Part II.

50 mm						
D90/D30	HZONE = 0.3H			HZONE = 0.4H		
	Qp	**Tp**	**Breach**	**Qp**	**Tp**	**Breach**
1	-0.40%	-3.03%	-27.78%	-29.02%	-25.09%	-36.38%
100	0.10%	0.29%	-10.98%	-4.54%	-4.92%	-16.52%
200	3.17%	5.19%	-7.72%	4.70%	-4.23%	-12.94%
300	6.07%	8.06%	-5.74%	10.76%	-4.67%	-10.76%
400	8.58%	8.51%	-4.30%	15.38%	-4.08%	-9.20%
D90/D30	HZONE = 0.5H			HZONE = 0.6H		
	Qp	**Tp**	**Breach**	**Qp**	**Tp**	**Breach**
1	-61.80%	-3.70%	-43.20%	-73.08%	44.24%	-47.88%
100	-17.73%	-8.14%	-21.82%	-32.27%	-4.19%	-26.73%
200	-7.18%	-9.61%	-18.09%	-22.59%	-9.34%	-22.98%
300	-0.41%	-10.78%	-15.86%	-16.40%	-12.18%	-20.62%
400	4.72%	-11.22%	-14.24%	-11.70%	-14.10%	-19.06%
75 mm						
D90/D30	HZONE = 0.3H			HZONE = 0.4H		
	Qp	**Tp**	**Breach**	**Qp**	**Tp**	**Breach**
1	-0.40%	-3.03%	-28.19%	-29.02%	-25.09%	-36.89%
100	-0.02%	-0.19%	-11.47%	-5.22%	-5.14%	-16.96%
200	2.84%	4.71%	-8.19%	3.94%	-4.45%	-13.35%
300	5.64%	7.82%	-6.18%	9.94%	-4.41%	-11.17%
400	8.09%	8.27%	-4.72%	14.55%	-4.30%	-9.59%
D90/D30	HZONE = 0.5H			HZONE = 0.6H		
	Qp	**Tp**	**Breach**	**Qp**	**Tp**	**Breach**
1	-62.25%	-4.29%	-43.78%	-73.83%	47.56%	-48.51%
100	-18.58%	-7.72%	-22.24%	-33.23%	-2.73%	-27.11%
200	-8.09%	-9.53%	-18.47%	-23.61%	-8.00%	-23.32%
300	-1.35%	-10.49%	-16.21%	-17.43%	-11.06%	-21.03%
400	3.76%	-11.22%	-14.59%	-12.78%	-12.14%	-19.38%
100 mm						
D90/D30	HZONE = 0.3H			HZONE = 0.4H		
	Qp	**Tp**	**Breach**	**Qp**	**Tp**	**Breach**
1	-0.40%	-3.03%	-28.58%	-29.02%	-25.09%	-37.38%
100	-0.13%	-0.67%	-11.93%	-5.89%	-5.31%	-17.43%
200	2.53%	4.50%	-8.66%	3.19%	-4.64%	-13.78%
300	5.25%	7.34%	-6.65%	9.14%	-4.38%	-11.59%
400	7.62%	8.03%	-5.19%	13.71%	-4.52%	-9.99%
D90/D30	HZONE = 0.5H			HZONE = 0.6H		
	Qp	**Tp**	**Breach**	**Qp**	**Tp**	**Breach**
1	-62.69%	-2.15%	-44.37%	-74.38%	49.95%	-49.14%
100	-19.43%	-7.35%	-22.69%	-34.05%	-0.65%	-27.55%
200	-8.99%	-9.22%	-18.89%	-24.51%	-7.08%	-23.63%
300	-2.28%	-10.23%	-16.61%	-18.34%	-9.95%	-21.40%
400	2.81%	-10.94%	-14.96%	-13.66%	-11.68%	-19.73%

TABLE D.3 – Percentage variations for an implemented zone of porosity of 55% - Part I.

25 mm						
D90/D30	HZONE = 0.3H			HZONE = 0.4H		
	Qp	**Tp**	**Breach**	**Qp**	**Tp**	**Breach**
1	-0.40%	-3.03%	-30.40%	-29.02%	-25.09%	-39.61%
100	-0.40%	-3.03%	-14.46%	-16.54%	-7.11%	-20.01%
200	-0.40%	-3.03%	-11.31%	-9.32%	-5.25%	-16.35%
300	-0.07%	-0.43%	-9.31%	-4.34%	-3.74%	-14.12%
400	0.76%	2.19%	-7.85%	-0.50%	-3.93%	-12.43%
D90/D30	HZONE = 0.5H			HZONE = 0.6H		
	Qp	**Tp**	**Breach**	**Qp**	**Tp**	**Breach**
1	-67.06%	-8.17%	-46.37%	-77.93%	60.02%	-50.40%
100	-30.48%	-3.76%	-24.92%	-41.67%	4.74%	-29.17%
200	-21.14%	-4.73%	-21.09%	-32.90%	-1.19%	-25.36%
300	-15.07%	-6.58%	-18.78%	-27.18%	-3.06%	-23.03%
400	-10.48%	-7.17%	-17.10%	-22.84%	-6.55%	-21.36%
50 mm						
D90/D30	HZONE = 0.3H			HZONE = 0.4H		
	Qp	**Tp**	**Breach**	**Qp**	**Tp**	**Breach**
1	-0.40%	-3.03%	-30.74%	-29.02%	-25.09%	-40.07%
100	-0.40%	-3.03%	-14.98%	-17.34%	-7.61%	-20.44%
200	-0.40%	-3.03%	-11.65%	-10.29%	-5.28%	-16.74%
300	-0.21%	-0.94%	-9.73%	-5.39%	-4.39%	-14.50%
400	0.48%	1.49%	-8.25%	-1.63%	-4.08%	-12.87%
D90/D30	HZONE = 0.5H			HZONE = 0.6H		
	Qp	**Tp**	**Breach**	**Qp**	**Tp**	**Breach**
1	-67.60%	-9.42%	-46.91%	-78.62%	63.08%	-50.76%
100	-31.74%	-3.20%	-25.30%	-42.89%	6.73%	-29.50%
200	-22.50%	-5.13%	-21.43%	-34.16%	1.81%	-25.64%
300	-16.49%	-6.11%	-19.11%	-28.49%	-2.43%	-23.31%
400	-11.95%	-6.78%	-17.43%	-24.19%	-5.04%	-21.61%
75 mm						
D90/D30	HZONE = 0.3H			HZONE = 0.4H		
	Qp	**Tp**	**Breach**	**Qp**	**Tp**	**Breach**
1	-0.40%	-3.03%	-31.13%	-29.02%	-25.09%	-40.60%
100	-0.40%	-3.03%	-15.44%	-17.87%	-7.71%	-20.95%
200	-0.40%	-3.03%	-12.17%	-10.94%	-5.41%	-17.24%
300	-0.27%	-1.47%	-10.24%	-6.09%	-4.57%	-14.90%
400	0.31%	1.01%	-8.75%	-2.37%	-4.02%	-13.26%
D90/D30	HZONE = 0.5H			HZONE = 0.6H		
	Qp	**Tp**	**Breach**	**Qp**	**Tp**	**Breach**
1	-67.93%	-9.53%	-47.57%	-79.32%	69.28%	-51.49%
100	-32.54%	-2.87%	-25.79%	-43.87%	8.45%	-29.96%
200	-23.36%	-4.55%	-21.88%	-35.16%	2.60%	-26.04%
300	-17.40%	-5.64%	-19.55%	-29.54%	-1.32%	-23.69%
400	-12.86%	-5.78%	-17.84%	-25.30%	-3.70%	-21.99%

TABLE D.4 – Percentage variations for an implemented zone of porosity of 55% - Part II.

100 mm						
D90/D30	HZONE = 0.3H			HZONE = 0.4H		
	Qp	**Tp**	**Breach**	**Qp**	**Tp**	**Breach**
1	-0.40%	-3.03%	-31.48%	-29.02%	-25.09%	-41.09%
100	-0.40%	-3.03%	-15.95%	-18.39%	-8.11%	-21.40%
200	-0.40%	-3.03%	-12.70%	-11.57%	-5.51%	-17.74%
300	-0.32%	-2.00%	-10.68%	-6.79%	-4.69%	-15.39%
400	0.16%	0.53%	-9.19%	-3.10%	-3.10%	-13.74%
D90/D30	HZONE = 0.5H			HZONE = 0.6H		
	Qp	**Tp**	**Breach**	**Qp**	**Tp**	**Breach**
1	-68.25%	-10.59%	-48.21%	-79.86%	71.05%	-52.23%
100	-33.34%	-2.84%	-26.32%	-44.69%	10.24%	-30.42%
200	-24.23%	-4.26%	-22.38%	-36.04%	3.48%	-26.49%
300	-18.30%	-5.54%	-20.00%	-30.42%	0.06%	-24.11%
400	-13.78%	-6.00%	-18.21%	-26.20%	-2.35%	-22.39%

TABLE D.5 – Percentage variations for an implemented zone of porosity of 45% - Part I.

25 mm						
D90/D30	HZONE = 0.3H			HZONE = 0.4H		
	Qp	**Tp**	**Breach**	**Qp**	**Tp**	**Breach**
1	-0.40%	-3.03%	-32.59%	-29.02%	-25.09%	-42.56%
100	-0.40%	-3.03%	-17.92%	-24.08%	-11.98%	-23.56%
200	-0.40%	-3.03%	-14.84%	-19.07%	-8.11%	-19.86%
300	-0.40%	-3.03%	-12.87%	-15.31%	-6.46%	-17.61%
400	-0.40%	-3.03%	-11.42%	-12.30%	-4.37%	-15.96%
D90/D30	HZONE = 0.5H			HZONE = 0.6H		
	Qp	**Tp**	**Breach**	**Qp**	**Tp**	**Breach**
1	-70.43%	-16.70%	-49.54%	-81.92%	76.24%	-52.91%
100	-40.94%	0.01%	-28.15%	-50.18%	16.71%	-31.85%
200	-32.84%	-1.59%	-24.21%	-42.23%	8.09%	-27.94%
300	-27.51%	-1.51%	-21.86%	-37.03%	4.70%	-25.54%
400	-23.42%	-3.36%	-20.14%	-33.12%	2.15%	-23.84%

TABLE D.6 – Percentage variations for an implemented zone of porosity of 45% - Part II.

50 mm						
D90/D30	HZONE = 0.3H			HZONE = 0.4H		
	Qp	**Tp**	**Breach**	**Qp**	**Tp**	**Breach**
1	-0.40%	-3.03%	-32.89%	-29.02%	-25.09%	-43.01%
100	-0.40%	-3.03%	-18.39%	-24.62%	-12.79%	-24.04%
200	-0.40%	-3.03%	-15.31%	-19.82%	-8.41%	-20.33%
300	-0.40%	-3.03%	-13.33%	-16.17%	-6.65%	-18.03%
400	-0.40%	-3.03%	-11.88%	-13.22%	-4.93%	-16.39%
D90/D30	HZONE = 0.5H			HZONE = 0.6H		
	Qp	**Tp**	**Breach**	**Qp**	**Tp**	**Breach**
1	-70.80%	-17.77%	-50.10%	-82.54%	79.48%	-53.29%
100	-42.11%	-0.37%	-28.59%	-51.30%	17.30%	-32.19%
200	-34.10%	-0.38%	-24.63%	-43.45%	10.04%	-28.24%
300	-28.82%	-1.89%	-22.23%	-38.34%	6.35%	-25.88%
400	-24.82%	-2.87%	-20.52%	-34.40%	4.64%	-24.15%
75 mm						
D90/D30	HZONE = 0.3H			HZONE = 0.4H		
	Qp	**Tp**	**Breach**	**Qp**	**Tp**	**Breach**
1	-0.40%	-3.03%	-33.22%	-29.02%	-25.09%	-43.53%
100	-0.40%	-3.03%	-18.94%	-24.96%	-13.02%	-24.64%
200	-0.40%	-3.03%	-15.78%	-20.28%	-7.85%	-20.87%
300	-0.40%	-3.03%	-13.88%	-16.73%	-6.94%	-18.58%
400	-0.40%	-3.03%	-12.43%	-13.83%	-5.59%	-16.91%
D90/D30	HZONE = 0.5H			HZONE = 0.6H		
	Qp	**Tp**	**Breach**	**Qp**	**Tp**	**Breach**
1	-71.02%	-18.21%	-50.83%	-83.19%	85.34%	-54.12%
100	-42.85%	0.10%	-29.14%	-52.28%	19.32%	-32.71%
200	-34.91%	-0.59%	-25.16%	-44.48%	12.28%	-28.72%
300	-29.68%	-2.02%	-22.73%	-39.37%	7.94%	-26.33%
400	-25.71%	-2.51%	-20.99%	-35.49%	5.55%	-24.57%
100 mm						
D90/D30	HZONE = 0.3H			HZONE = 0.4H		
	Qp	**Tp**	**Breach**	**Qp**	**Tp**	**Breach**
1	-0.40%	-3.03%	-33.53%	-29.02%	-25.09%	-43.99%
100	-0.40%	-3.03%	-19.48%	-25.28%	-13.58%	-25.20%
200	-0.40%	-3.03%	-16.34%	-20.75%	-8.25%	-21.45%
300	-0.40%	-3.03%	-14.37%	-17.28%	-7.25%	-19.13%
400	-0.40%	-3.03%	-12.99%	-14.43%	-5.96%	-17.46%
D90/D30	HZONE = 0.5H			HZONE = 0.6H		
	Qp	**Tp**	**Breach**	**Qp**	**Tp**	**Breach**
1	-71.23%	-19.72%	-51.50%	-83.68%	88.93%	-54.97%
100	-43.58%	0.34%	-29.74%	-53.06%	21.19%	-33.25%
200	-35.71%	-0.66%	-25.71%	-45.33%	15.29%	-29.23%
300	-30.53%	-1.58%	-23.26%	-40.25%	10.60%	-26.79%
400	-26.59%	-2.46%	-21.49%	-36.37%	6.73%	-25.03%

APPENDIX E – PERCENTAGE VARIATIONS OF A ZONE IN TETON DAM

HZONE is the height of implemented zone [-];

H is the dam height [-];

D_{90}/D_{30} is the ratio of grain diameter for which 90% and 30% of the sample is finer [-];

Qp is the peak outflow [-];

Tp is the time to peak outflow [-];

Breach is the height of the breach [-].

TABLE E.1 – Percentage variations for an implemented zone of porosity of 40% - Part I.

25 mm						
D90/D30	HZONE = 0.3H			HZONE = 0.4H		
	Qp	**Tp**	**Breach**	**Qp**	**Tp**	**Breach**
1	-13.30%	1.68%	-1.56%	-16.13%	2.80%	-1.75%
4	-7.76%	-0.03%	-1.04%	-10.08%	0.71%	-1.20%
8	-5.17%	-0.54%	-0.84%	-7.23%	0.01%	-0.97%
40	0.57%	-2.11%	-0.45%	-0.99%	-1.78%	-0.53%
D90/D30	HZONE = 0.5H			HZONE = 0.6H		
	Qp	**Tp**	**Breach**	**Qp**	**Tp**	**Breach**
1	-30.83%	124.18%	-2.01%	-36.34%	148.51%	-2.18%
4	-19.85%	77.04%	-1.38%	-25.34%	97.30%	-1.53%
8	-14.36%	57.22%	-1.11%	-19.98%	75.97%	-1.25%
40	-1.91%	19.16%	-0.63%	-7.56%	34.19%	-0.73%

TABLE E.2 – Percentage variations for an implemented zone of porosity of 40% - Part II.

50 mm						
D90/D30	HZONE = 0.3H			HZONE = 0.4H		
	Qp	**Tp**	**Breach**	**Qp**	**Tp**	**Breach**
1	-13.42%	1.74%	-1.57%	-16.22%	3.00%	-1.77%
4	-7.93%	-0.08%	-1.06%	-10.16%	0.86%	-1.20%
8	-5.26%	-0.50%	-0.84%	-7.30%	-0.03%	-0.97%
40	0.45%	-2.13%	-0.45%	-1.07%	-1.74%	-0.54%
D90/D30	HZONE = 0.5H			HZONE = 0.6H		
	Qp	**Tp**	**Breach**	**Qp**	**Tp**	**Breach**
1	-25.69%	119.25%	-2.01%	-31.19%	133.90%	-2.18%
4	-14.33%	71.00%	-1.37%	-19.91%	83.46%	-1.52%
8	-8.77%	50.67%	-1.10%	-14.41%	62.75%	-1.23%
40	3.52%	12.88%	-0.62%	-1.76%	22.46%	-0.71%
75 mm						
D90/D30	HZONE = 0.3H			HZONE = 0.4H		
	Qp	**Tp**	**Breach**	**Qp**	**Tp**	**Breach**
1	-13.66%	1.79%	-1.56%	-16.41%	2.96%	-1.77%
4	-8.07%	-0.04%	-1.07%	-10.31%	0.84%	-1.21%
8	-5.44%	-0.52%	-0.85%	-7.39%	0.10%	-0.98%
40	0.36%	-1.99%	-0.46%	-1.15%	-1.71%	-0.54%
D90/D30	HZONE = 0.5H			HZONE = 0.6H		
	Qp	**Tp**	**Breach**	**Qp**	**Tp**	**Breach**
1	-22.72%	128.52%	-2.00%	-28.27%	133.31%	-2.19%
4	-11.28%	77.10%	-1.37%	-16.80%	81.87%	-1.51%
8	-5.78%	55.83%	-1.12%	-11.19%	60.40%	-1.23%
40	6.63%	15.54%	-0.62%	1.40%	19.95%	-0.71%
100 mm						
D90/D30	HZONE = 0.3H			HZONE = 0.4H		
	Qp	**Tp**	**Breach**	**Qp**	**Tp**	**Breach**
1	-13.83%	1.84%	-1.57%	-16.55%	2.99%	-1.78%
4	-8.22%	0.15%	-1.06%	-10.43%	1.29%	-1.21%
8	-5.58%	-0.50%	-0.85%	-7.50%	0.09%	-0.97%
40	0.24%	-1.96%	-0.45%	-1.23%	-1.53%	-0.54%
D90/D30	HZONE = 0.5H			HZONE = 0.6H		
	Qp	**Tp**	**Breach**	**Qp**	**Tp**	**Breach**
1	-20.78%	148.82%	-2.02%	-26.32%	138.52%	-2.18%
4	-9.37%	92.09%	-1.36%	-14.76%	85.04%	-1.50%
8	-3.73%	68.59%	-1.11%	-9.05%	62.86%	-1.22%
40	8.54%	24.27%	-0.62%	3.42%	20.83%	-0.70%

TABLE E.3 – Percentage variations for an implemented zone of porosity of 35% - Part I.

25 mm						
D90/D30	HZONE = 0.3H			HZONE = 0.4H		
	Qp	**Tp**	**Breach**	**Qp**	**Tp**	**Breach**
1	-13.89%	1.89%	-1.57%	-16.73%	3.12%	-1.78%
4	-8.33%	0.24%	-1.05%	-10.59%	1.36%	-1.21%
8	-5.63%	-0.48%	-0.85%	-7.66%	0.14%	-0.98%
40	0.15%	-2.00%	-0.45%	-1.36%	-1.50%	-0.54%
D90/D30	HZONE = 0.5H			HZONE = 0.6H		
	Qp	**Tp**	**Breach**	**Qp**	**Tp**	**Breach**
1	-31.35%	125.19%	-2.04%	-36.68%	149.51%	-2.21%
4	-20.25%	77.88%	-1.38%	-25.72%	97.90%	-1.53%
8	-14.67%	58.18%	-1.13%	-20.25%	76.30%	-1.25%
40	-2.26%	19.66%	-0.63%	-7.82%	34.53%	-0.72%
50 mm						
D90/D30	HZONE = 0.3H			HZONE = 0.4H		
	Qp	**Tp**	**Breach**	**Qp**	**Tp**	**Breach**
1	-14.08%	1.94%	-1.58%	-16.82%	3.28%	-1.77%
4	-8.43%	0.27%	-1.05%	-10.67%	1.05%	-1.22%
8	-5.73%	-0.29%	-0.86%	-7.73%	0.14%	-0.98%
40	0.08%	-1.63%	-0.46%	-1.41%	-1.44%	-0.54%
D90/D30	HZONE = 0.5H			HZONE = 0.6H		
	Qp	**Tp**	**Breach**	**Qp**	**Tp**	**Breach**
1	-26.17%	119.92%	-2.02%	-31.58%	134.58%	-2.21%
4	-14.83%	72.04%	-1.39%	-20.31%	84.19%	-1.53%
8	-9.19%	51.68%	-1.11%	-14.70%	63.12%	-1.24%
40	3.23%	13.26%	-0.63%	-2.04%	22.93%	-0.71%
75 mm						
D90/D30	HZONE = 0.3H			HZONE = 0.4H		
	Qp	**Tp**	**Breach**	**Qp**	**Tp**	**Breach**
1	-14.24%	2.02%	-1.59%	-16.95%	3.25%	-1.79%
4	-8.57%	0.32%	-1.06%	-10.78%	1.09%	-1.21%
8	-5.92%	-0.25%	-0.86%	-7.83%	0.31%	-0.97%
40	-0.02%	-1.86%	-0.45%	-1.50%	-1.67%	-0.54%
D90/D30	HZONE = 0.5H			HZONE = 0.6H		
	Qp	**Tp**	**Breach**	**Qp**	**Tp**	**Breach**
1	-23.26%	129.67%	-2.03%	-28.67%	134.13%	-2.19%
4	-11.74%	78.00%	-1.39%	-17.24%	82.64%	-1.51%
8	-6.25%	56.65%	-1.12%	-11.58%	60.96%	-1.23%
40	6.30%	16.31%	-0.61%	1.00%	20.25%	-0.71%

TABLE E.4 – Percentage variations for an implemented zone of porosity of 35% - Part II.

100 mm						
D90/D30	HZONE = 0.3H			HZONE = 0.4H		
	Qp	**Tp**	**Breach**	**Qp**	**Tp**	**Breach**
1	-14.42%	2.13%	-1.59%	-17.10%	3.32%	-1.80%
4	-8.73%	0.40%	-1.07%	-10.90%	1.54%	-1.22%
8	-6.07%	-0.24%	-0.87%	-7.98%	0.40%	-0.99%
40	-0.20%	-1.85%	-0.46%	-1.59%	-1.30%	-0.54%
D90/D30	HZONE = 0.5H			HZONE = 0.6H		
	Qp	**Tp**	**Breach**	**Qp**	**Tp**	**Breach**
1	-21.28%	150.08%	-2.03%	-26.60%	139.20%	-2.20%
4	-9.80%	92.99%	-1.38%	-15.17%	85.60%	-1.51%
8	-4.18%	69.54%	-1.12%	-9.44%	63.17%	-1.23%
40	8.19%	24.96%	-0.62%	3.05%	21.51%	-0.71%

TABLE E.5 – Percentage variations for an implemented zone of porosity of 30% - Part I.

25mm						
D90/D30	HZONE = 0.3H			HZONE = 0.4H		
	Qp	**Tp**	**Breach**	**Qp**	**Tp**	**Breach**
1	-14.53%	2.04%	-1.60%	-17.27%	3.43%	-1.80%
4	-8.85%	0.28%	-1.06%	-10.98%	1.32%	-1.22%
8	-6.08%	-0.24%	-0.87%	-8.05%	0.48%	-0.99%
40	-0.24%	-1.84%	-0.46%	-1.71%	-1.26%	-0.54%
D90/D30	HZONE = 0.5H			HZONE = 0.6H		
	Qp	**Tp**	**Breach**	**Qp**	**Tp**	**Breach**
1	-31.92%	126.64%	-2.05%	-37.06%	150.35%	-2.22%
4	-20.73%	78.88%	-1.41%	-26.09%	98.60%	-1.54%
8	-15.18%	58.64%	-1.14%	-20.65%	77.10%	-1.27%
40	-2.64%	20.60%	-0.64%	-8.08%	34.92%	-0.72%

TABLE E.6 – Percentage variations for an implemented zone of porosity of 30% - Part II.

50 mm						
D90/D30	HZONE = 0.3H			HZONE = 0.4H		
	Qp	**Tp**	**Breach**	**Qp**	**Tp**	**Breach**
1	-14.66%	2.05%	-1.60%	-17.36%	3.50%	-1.80%
4	-8.95%	0.35%	-1.07%	-11.14%	1.40%	-1.23%
8	-6.24%	-0.24%	-0.87%	-8.19%	0.45%	-0.98%
40	-0.32%	-1.82%	-0.46%	-1.77%	-1.21%	-0.54%
D90/D30	HZONE = 0.5H			HZONE = 0.6H		
	Qp	**Tp**	**Breach**	**Qp**	**Tp**	**Breach**
1	-26.73%	121.23%	-2.04%	-31.98%	135.28%	-2.21%
4	-15.30%	72.84%	-1.40%	-20.60%	84.67%	-1.51%
8	-9.59%	52.32%	-1.11%	-15.10%	63.88%	-1.24%
40	2.84%	13.94%	-0.63%	-2.31%	23.18%	-0.71%
75 mm						
D90/D30	HZONE = 0.3H			HZONE = 0.4H		
	Qp	**Tp**	**Breach**	**Qp**	**Tp**	**Breach**
1	-14.83%	2.18%	-1.61%	-17.50%	3.62%	-1.81%
4	-9.10%	0.56%	-1.07%	-11.25%	1.45%	-1.23%
8	-6.37%	-0.21%	-0.87%	-8.29%	0.47%	-0.99%
40	-0.47%	-1.73%	-0.46%	-1.85%	-1.50%	-0.54%
D90/D30	HZONE = 0.5H			HZONE = 0.6H		
	Qp	**Tp**	**Breach**	**Qp**	**Tp**	**Breach**
1	-23.90%	130.93%	-2.03%	-29.14%	134.99%	-2.21%
4	-12.20%	79.20%	-1.39%	-17.62%	83.22%	-1.53%
8	-6.61%	57.31%	-1.12%	-11.87%	61.36%	-1.24%
40	5.93%	16.82%	-0.62%	0.73%	20.87%	-0.71%
100 mm						
D90/D30	HZONE = 0.3H			HZONE = 0.4H		
	Qp	**Tp**	**Breach**	**Qp**	**Tp**	**Breach**
1	-15.01%	2.21%	-1.62%	-17.65%	3.67%	-1.79%
4	-9.26%	0.63%	-1.08%	-11.38%	1.80%	-1.23%
8	-6.53%	0.01%	-0.88%	-8.41%	0.50%	-1.00%
40	-0.59%	-1.72%	-0.46%	-1.94%	-1.15%	-0.55%
D90/D30	HZONE = 0.5H			HZONE = 0.6H		
	Qp	**Tp**	**Breach**	**Qp**	**Tp**	**Breach**
1	-21.88%	151.59%	-2.05%	-27.18%	140.15%	-2.20%
4	-10.23%	93.84%	-1.40%	-15.57%	86.31%	-1.52%
8	-4.62%	70.40%	-1.13%	-9.83%	63.76%	-1.23%
40	7.78%	25.80%	-0.62%	2.83%	21.80%	-0.71%